Journal of Thermal Analysis, Vol. 48 (1997) 1143-1227

PHASE DIAGRAMS FOR THE $YBa_2Cu_3O_7$ FAMILY – ANNO 1996

P. Karen and A. Kjekshus

Department of Chemistry, University of Oslo, Blindern, N-0315 Oslo, Norway

Abstract

Phase diagrams for cuprates of alkaline earth and rare earth elements are presented, covering binary to quintenary oxides and including selected solid solution series with other elements. Elementary crystal chemical data are included for identification of the occurring phases. Chemical stability is discussed with respect to the high-temperature reactions with Lewis acids like CO_2, protons, etc. Particularly the occurrence of oxide carbonates is consistently pointed out as one of the possible reasons for contradictory results in phase diagrams which comprise oxides with high basicity.

Keywords: phase diagrams, $YBa_2Cu_3O_7$

I. Introduction

Phase diagrams represent an extremely efficient way of displaying thermodynamic information for practical use in solid-state chemistry. Multitudes of complex chemical equilibria, experimental, calculated or estimated data, can be combined into a clear and fairly precise picture of the chemical situation, regardless its intricacy. Particularly in the vastly expanded research on high-T_c superconductors there is a need for unambiguous chemical information. In these systems superconductivity often depends on a delicate balance on the edge of the chemical stability of the compound, while the practical application would often require the proverbial step beyond.

Owing to the sheer volume of data, any comprehensive survey on chemical phase diagrams which involves high-T_c superconductors must be limited in scope. The rapid increase of the information calls for frequent updates. In the present review, which is a completely reorganized follow-up and update of a previous report [1], only subsystems and systems closely related to $YBa_2Cu_3O_7$ are treated. A short information on crystal structure is listed for each phase, giving it its identity, as well as the concise chemical information which gives it its character. Some of the data included in this review are obtained by the authors, and this first-hand knowledge has hopefully contributed to an improved consistency.

A. Scope delimitation, units and symbols

Specification of scope

1. All rare earths (REs) are treated systematically except Sc.
2. Ba-rich regions are sometimes omitted due to the unclear identity of possible oxide carbonates.
3. High-temperature data for refractory oxides will be limited.
4. Illustrations are often simplified in order to convey the overall message, and the readers may have to consult the original papers for details. Formulae on illustrations always specify the metal content whereas only a principal oxygen content is often provided.
5. Phase-identifying X-ray data were, when appropriate, tested by indexing and crystal structure drawing to confirm suggested implications.

0368–4466/97/ $ 5.00

John Wiley & Sons Limited
Chichester

Specification of units and symbols

1. Chemical inorganic nomenclature is used in accordance with the IUPAC recommendations (1990) and consistency for formulae of cuprates concerning the sequence of rare earth (RE) and alkaline earth (AE) elements is reached by following the said order. This conforms with the alphabetically incorrect, but traditional way for the formula $YBa_2Cu_3O_7$, and the consequent Y → Ba → Cu anticlockwise orientation of the apices in ternary diagrams. Formulae for non-cuprate multicomponent oxides follow the electronegativity order, e.g., $SrDy_2O_4$. When necessary for distinction, the crystal system symbol (c cubic, t tetragonal, o orthorhombic, etc.) precedes the formulae.

2. Short-hand symbols of the type 123 (as for $YBa_2Cu_3O_7$) will be used when the relative cationic proportions of a phase rather than its complete formula is of importance.

3. When general compositional variables are used in chemical formulae, x relates to the RE host site in the structure, y to AE, z to Cu, w to oxygen and u to all other anions.

4. Symbols for physical variables are printed in italics, partial and relative values in lower case, absolute values in capitals.

5. Physical units follow the SI system. However, the absolute temperature unit (K) will be used only when the information is based or expressed in a thermodynamic connection. Centigrades are used for melting points, reaction temperatures, etc.

6. Standard deviations appear in parenthesis ( ), in units of the last decimal.

7. Crystal structure data are given when known, in a condensed form comprising some or all of the following information in a pair braces: {formula; space group or crystal system with (optional) Bravais centering (e.g., cI, cF, etc.); unit-cell parameters (r in h setting) in the order: a, b, c, α, β, γ (always in units of pm or °, but not specified)}. The data appear as given by the authors, i.e., the conversion into the standard crystallographic settings is not attempted when applicable. References to overall structure data will be given at the word structure, crystallize, or at the crystal system, whereas the reference at the braces refers to unit-cell data. (When more than one source of data are available, attempts have been made to select the best.)

8. Phase diagrams include phase identifiers like L liquid, AF antiferromagnetic, SC superconducting. When shorthand symbols are (exceptionally) used also to identify chemical phases, the explanation appears in the caption. Square brackets placed around a chemical formula indicate a specific composition, not the chemical phase. A formula in quotation marks refers to an approximate and/or uncertain composition with respect to the metal atoms. The diagrams' frame lines are drawn as solid lines. In areas where the enclosed information is not available, the frame lines are thin. In tetrahedral diagrams, the hidden frame line may appear dashed for better contrast. Mol fractions are used as composition units throughout, and the appropriate mol-unit formulae are printed in larger letters at the corners of the diagrams even when identical with the phase actually present (in smaller letters). The composition scales are omitted for all isothermal sections. Phase boundary lines are drawn as solid lines. Dashed lines are used for uncertain and/or speculative boundaries. Single-phase fields are shaded black and solid solutions in (pseudo)binary systems are hence drawn by thick lines. Uncertain boundaries of these single-phase fields are serrated. Tie lines are drawn thin. Chain lines are used for auxiliary lines or planes (the latter being drawn as non-transparent in order to improve the visual perception). Dotted lines then appear at intersections of these auxiliary planes with phase boundaries and tie lines.

9. Abbreviations for common solid-state chemistry techniques are used throughout the text: DTA differential thermal analysis, TG thermogravimetric analysis, SIMS secondary-ion mass-spectrometry, EDAX energy dispersive analysis by X-rays, EMP electron microprobe, HREM high-resolution (transmission) electron microscopy, TEM transmission elec-

tron microscopy, NQR nuclear quadrupole resonance, NMR nuclear magnetic resonance, SEM scanning electron microscopy, PND powder neutron diffraction, PXD powder X-ray diffraction, EXAFS extended X-ray absorption fine structure, EMF electromotive force (measurement).

II. Binary and pseudobinary systems

A. Oxides, peroxides and carbonates of AE metals

Oxides. The melting points of AE oxides decrease from CaO, 2576°C through SrO, 2430°C to BaO, 1923°C [2]. An analogous trend is observed for vapour pressures [3]. As an example, a partial pressure of 1 Pa of CaO, SrO and BaO in synthetic air is reached at ~2350, ~2100 and 1450°C, respectively. The crystal structures are of the NaCl-type; CaO {481} [4], SrO {514} [5] and BaO {552} [5].

Mixed oxides. SrO and BaO have unlimited solid solubility above 1083(4)°C [6]. At lower temperatures, segregation of the solid solutions occurs [6, 7]. However, the precipitation of the two components is hindered kinetically, and solid solutions in the complete region are readily obtained upon cooling [8]. A similar situation occurs in the Ca(O)–Sr(O) system [9, 10].

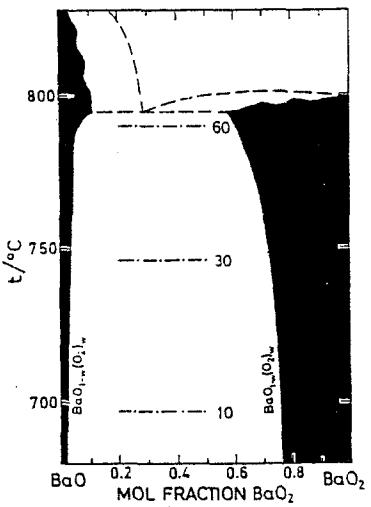

Fig. 1 A *w–t* diagram for the BaO–BaO_2 system with some equilibrium O_2 pressures (in kPa) indicated; after Ref. [13]

Peroxides. At relatively low temperatures, peroxides of AEs are stable. The equilibrium oxygen pressure for CaO_2 is estimated [11] to reach 100 kPa at around ambient temperature, at ~350°C for SrO_2 [12], and at ~820°C for BaO_2 [13]. A significant miscibility is expected in the AE oxide–peroxide systems, as indicated in Fig. 1 for the Ba case [13]. This should be taken into consideration in the evaluation of the oxygen dissociation pressure, which will vary with the content of peroxide in the solid-solution phase [13]. To illustrate rough trends, equilibrium oxygen pressures for $SrO_{1.97}$ [12], and for the oxide-saturated barium peroxide are expressed (p in Pa, T in K) [12, 13]:

$$SrO_{1.97(s)} \leftrightarrow SrO_{(s)} + \frac{0.97}{2} O_{2(g)} \quad (1a)$$

$$\log_{10} p_{O_2} = 11.4 - 4050/T \quad (1b)$$

$$BaO_{1-w}(O_2)_{w(s)} \leftrightarrow BaO_{(s)} + \frac{w}{2} O_{2(g)} \quad (2a)$$

$$\log_{10} p_{O_2} = 11.83 - 7500/T \quad (2b)$$

$$\log_{10}(1 - w) = 0.975 - 1552/T \quad (2c)$$

The peroxides crystallize [14, 15] with the CaC_2-type structures: CaO_2 {*P4/mmm*; 356, 596} [16], SrO_2 {355, 655} [17] and BaO_2 {381.14(6), 682.15(11)} [15].

Carbonates. As intermediate precursors in many preparation routes, AE carbonates must be considered. The temperature when the CO_2 pressure of the carbonate dissociation reaches 100 kPa increases from 897(1)°C for $CaCO_3$ [18] to 1250°C for $SrCO_3$ [19]. The corresponding temperature for $BaCO_3$ (expectedly, some 1600°C) is not directly measured, since strong sintering hampers the kinetics. For the temperature dependence of the equilibrium CO_2 pressures of the AE carbonates see Sec. V A.

The thermodynamically stable modification of calcium carbonate is calcite [20, 21] {$CaCO_3$; $R\bar{3}c$; 499.00(2), 1700.2(1)}, whereas the structures [22] of strontium and barium carbonate are of the aragonite-type: $SrCO_3$ {(7% Ca, 4% Ba); *Pmcn*; 509.0(2), 835.8(2), 599.7(4)}, $BaCO_3$ {531.26(5), 889.58(5), 642.84(5)}.

B. Oxides of RE elements

Trivalent REs. The oxides are typical refractory materials with melting points above 2300°C. Several polymorphic modifications occur, depending on temperature, pressure and atom size [23]. At ambient pressure, the sesquioxides of the larger (lighter) lanthanoids, La–Nd, form hexagonal structures [24] when subject to free cooling from any temperature up to the melting point, e.g., La_2O_3 {$P6_3/mmc$; 393.7, 613.0}. The sesquioxides of the small (heavier) lanthanoids Dy–Lu have the cubic [25] bixbyite-type structure {Lu_2O_3; $Ia\bar{3}$; 1039.07} and this also applies [26] to Y_2O_3 {1060.3}. In the intermediate size region, a monoclinic structure is preferred for Sm, Eu and Gd: {Sm_2O_3; *C2/m*; 1418, 363.3, 884.7, 99.96} [27].

Tetravalent REs. Since Ce, Pr, and Tb can also take a tetravalent state in the oxides, the situation becomes more complex. In line with the close structural relationship between the bixbyite (for the sesquioxides) and the fluorite (for the dioxides) structure types [28], a sequence of related intermediate phases occurs, with a formula $2RE_2O_3 \cdot nRE'O_2$. Symbols have been assigned to the occurring phases: $n=0$, θ phase (hexagonal RE_2O_3); $n=0$, σ phase (cubic RE_2O_3); $n=3$, ι phase (RE_7O_{12}); $n=4$, (RE_8O_{14}); $n=5$, ζ phase (RE_9O_{16}); $n=6$, ε phase ($RE_{10}O_{18}$); $n=7$, δ phase ($RE_{11}O_{20}$); $n=8$, β phase ($RE_{12}O_{22}$); $n=\infty$, α phase (REO_2). The pseudocubic parameter a generally increases with increasing oxygen content [28]. The most oxygen-rich CeO_2 {$Fm\bar{3}m$; 541.1} [29] is formed virtually stoichiometric up to some 1300°C in 100 kPa O_2 [30]. At room temperature, CeO_2 is a well defined stoichiometric compound, whereas above some 600°C it broadens into an appreciable range of homogeneity with oxygen vacancies (e.g., to a composition of $CeO_{1.72}$ at 1000°C). However, the equilibrium oxygen pressures of these solid solutions are very low (at 1000°C, ~10^{-15} Pa for $CeO_{1.72}$ and ~10^{-5} Pa for $CeO_{1.99}$) [30]. At ambient temperature, three phases (δ, ζ and ι) [30, 31] occur between CeO_2 and Ce_2O_3. Similar compositional

features are found among the praseodymium oxides, but here the dissociation pressures are much higher [28, 32]. The most oxygen-rich praseodymium dioxide {$Fm\bar{3}m$; 539.3(1)} [33] is formed when $p_{O_2} > 100$ kPa and it decomposes above 310°C in 100 kPa oxygen into the β phase, with a subsequent decomposition into lower oxides above some 480°C [33]. At ambient temperature, four phases (β, ε, ζ and ι) [28, 32] are considered stable between PrO_2 and Pr_2O_3, the fifth, δ phase, emerging only in a limited temperature region. Oxygen dissociation pressures of 1 to 100 kPa between 800 and 1300°C are reported for the range between Pr_2O_3 and Pr_7O_{12} [34].

Similar dissociation pressures are measured for the largely analogous terbium oxides. TbO_2 {$Fm\bar{3}m$; 521.9(1)} [35] is formed only on disproportionation in acidic solutions [35] (similarly to PbO_2) and decomposes above 340°C in 100 kPa O_2 into the δ phase [36]. The δ phase is the most oxygen-rich terbium oxide which can be obtained by oxidation with O_2 (TbO_2 forms in atomic oxygen [37]) and decomposes into the ι phase at ~450°C ($p_{O_2} = 1.3$ kPa) and subsequently into $Tb_2O_{3+\delta}$ (σ) at ~800°C for $p_{O_2} = 1.3$ kPa [38]. However, the most common preparation route for RE oxides, which involves thermal decomposition of oxalate in air at 600 to 1000°C gives reproducibly Tb_4O_7. This composition is, moreover, invariably obtained during various synthesis reactions in O_2 at ambient and reduced pressures [37, 39, 40]. Correspondingly, distinct plateaus at the Tb_4O_7 composition are observed [41, 42] by TG. However, diffraction methods failed to reveal any specific superstructure for the Tb_4O_7 composition which accordingly is suggested to be a consequence of the sluggish kinetics [38, 43]. Oxygen dissociation pressures for the terbium oxides up to 100 kPa between 500 and 1000°C are reported [44].

Mixed oxides. With the exception of the most different pairs of REs by size, which form a 1:1 ternary oxide, no further ternary compounds are found, but wide ranges of solid solubility occur for the RE sesquioxides. The structure of these solid solutions follows the behaviour of the binary oxides as a function of temperature and ionic size [23].

As may be expected for these refractory oxides, the solid-state diffusion rate is rather low and the formation of the 1:1 ternary oxides requires temperatures above 1600°C, long sintering times and the use of pressure [45]. It has therefore been suggested [46] that they in fact are metastable under ambient conditions. Structurally, these oxides are perovskite-related {$LaYO_3$; *Pnam*; 587.7, 849.3, 608.7} [47–49]. When based on La, they occur for Ho (or Y) and smaller REs [45, 49], but they are only found for Lu and Sc when based on Pr [49]. Scandium, on the other hand, forms $ScREO_3$ with all larger REs than Y [50].

The fluorite-type CeO_2 phase forms (at say 1600°C) an almost continuous series of solid solutions with trivalent REs, maximum extent being found between Sm and Ho (or Y) [51–53]. These elements of similar size are able (or nearly able) to form the cubic sesquioxide, the structure of which is closely related to fluorite. A nearly continuous conversion occurs from the fluorite-type CeO_2 phase through a (related vacant) cI solid-solution oxide, followed by a narrow ($\Delta x \approx 0.1$) miscibility gap into the regime of either a cF or monoclinic sesquioxide [53]. These trends are subject to alterations when equilibrium is established at lower temperature than 1600°C [23] or low O_2 pressures are used. The latter specification is particularly important for the otherwise analogous systems with RE(IV) = Pr [54, 55] and Tb [56].

Oxide carbonates. As intermediate products of thermal decomposition of hydrated RE carbonates or oxalates, oxide carbonates $RE_2O_2CO_3$ are obtained for practically all REs [57, 58]. Several metastable phases with defined crystal structures are formed as a function of temperature, before hexagonal (also type-II) $RE_2O_2CO_3$ appears, with crystal structure [59, 60] {$La_2O_2CO_3$; $P6_3/mmc$; 407.55(6), 1595.7(1)} related to that of the hexagonal ox-

ides of the early lanthanides. For RE=La, Pr, Nd, Sm, and Gd, these oxide carbonates are relatively stable and can be isolated as single phases [58].

C. Copper oxides

Thermodynamics of the copper-oxygen system has been recently assessed [61]. Only two copper oxides CuO and Cu_2O are normally encountered. CuO is monoclinic [62] {*C2/c*; 468.37(5), 342.26(5), 512.88(6), 99.54(1)} and Cu_2O is cubic [63] {$Pn\bar{3}m$; 425.7} [64]. Both have very narrow homogeneity ranges [65–67]. Recently, a metastable oxidized "extension" of the latter structure is reported [68] synthesized {Cu_3O_2; $Pn\bar{3}m$; 431(1)}. A true intermediate Cu(I), Cu(II)-oxide has been known for a long time as the mineral paramelaconite, Cu_4O_3. The phase is tetragonal [69] {$I4_1/amd$; 582, 988} and has been considered metastable before the recent successful synthesis by a long-term air-oxidation of metallic copper in boiling concentrated aqueous ammonia [70]. Under exotic conditions [71], condensed CuO_2 molecules can be obtained.

In line with the noble nature of copper, also the common Cu_2O and CuO oxides have somewhat limited thermal stability and the Cu–O system depends strongly on the partial pressure of oxygen in the surrounding atmosphere. The situation [72] for $p_{O_2}=100$ kPa is shown in Fig. 2, where also additional O_2 isobars are indicated. At $p_{O_2}=100$ kPa, Cu_2O melts at 1229°C, whereas CuO at some 1100°C [65, 73]. In air, however, dissociation of CuO into Cu_2O and O_2 at 1030°C precedes the melting of the monoxide. The temperature dependence of the dissociation pressure for CuO has been obtained by mass spectrometry [74] ($679<T<1033$ K) and by direct measurements [65] at higher temperatures ($1173<T<1373$ K). The latter are expressed as follows (in Pa, K):

$$2CuO_{(s)} \leftrightarrow Cu_2O_{(s)} + \frac{1}{2} O_{2(g)} \tag{3a}$$

$$\log_{10} p_{O_2} = 14.53 - 13260/T \tag{3b}$$

The analogous relation for Cu_2O can be expressed from data in Ref. [61] (in Pa, K; $800<T<1300$ K):

$$Cu_2O_{(s)} \leftrightarrow 2Cu_{(s)} + \frac{1}{2} O_{2(g)} \tag{4a}$$

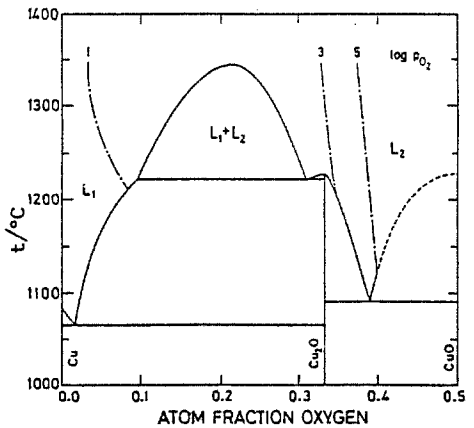

Fig. 2 A *w–t* diagram for the Cu–O system with some equilibrium O_2 pressures (in Pa) indicated; after Ref. [72]

$$\log_{10} p_{O_2} = 12.485 - 17449/T \quad (4b)$$

Of near precursors to the copper oxides, the metallic $Cu_7O_{8-w}NO_3$ {$Fm\bar{3}m$; 948} is worth mentioning as the last intermediate product of the thermal decomposition of copper nitrate [75].

III. Ternary and pseudoternary systems

A. Systems AE(O)–RE(O)

A general note. The refractory character of the components suggests low rates of diffusion and problems with the establishment of equilibrium. Experimental data are sometimes accompanied by a note that "phase-pure samples could not be obtained" or "a variety of other phases seem to appear if other conditions are applied". The AE(O)–RE(O) systems are also very sensitive to moisture [76]. Due to the presence of the very electropositive AE elements, these ternary oxides will tend to react with CO_2 (and other Lewis acids as well for that matter). At high temperatures, the first step of such a reaction leads to a formation of oxide carbonates [77–79].

Ca(O)–RE(O)

No stable ternary compounds are reported [80] at ambient temperature for the largest REs, but some solid solubility in (hexagonal) RE_2O_3 is found [80, 81], e.g., $x=0.08$ for RE=La [81]. Starting from Sm, the smaller REs form a high-temperature stable phase $CaRE_4O_7$. For the even smaller RE=Dy, a $CaFe_2O_4$-type phase is formed, and its analogue is still found in the $CaO–Sc_2O_3$ system [82] {$CaSc_2O_4$; *Pnma*; 946.1, 1112.2, 314.3} [83]. No ternary oxide has been found for RE=Ce(IV) [84].

Sr(O)–RE(O)

Trivalent REs. Compared to $CaRE_2O_4$, in the presence of the larger Sr, the structure can tolerate somewhat larger trivalent REs, however, smaller than RE=La [80]. Except for RE=Nd, where decomposition occurs before melting, all these phases {SrY_2O_4; *Pnam*; 1008, 1191, 340} [85] melt congruently at temperatures around 2100°C [80]. Analogous phases to (rhombohedral) $Ba_3RE_4O_9$ are not observed, but an equi-compositional series of phases forms for La, Pr and Nd; also metastable at ambient temperatures [80, 86]. The crystal structure [87–89] is monoclinic, {$Sr_3La_4O_9$; *Cc*; 1165.7, 734.8, 1347.1, 115.6} [87].

Tetravalent REs. Ce, Pr and Tb form two ternary oxides in this system, $SrREO_3$ and Sr_2REO_4, the latter being known only for Ce (stable up to ~1400°C, where it decomposes into $SrCeO_3$ and SrO [84]). The crystal structure [90] of the former is derived from perovskite {$SrCeO_3$; $P2_12_12_1$; 601.1, 858.8, 615.6}. Sr_2CeO_4 is reported [91] to be triclinic {607.0, 897.6, 1059.8, 94.7, 90.4, 95.8}, but the present authors have indexed 32 of the first 36 PXD reflections orthorhombically {1034.0(5), 612.4(2), 360.0(2)}. Under reducing conditions, phases typical for trivalent REs are formed, like $SrTb_2O_4$, which adopts the calcium ferrite-type structure [92].

Ba(O)–RE(O)

Trivalent REs. Compared to $SrRE_2O_4$, the presence of the larger Ba makes this calcium ferrite-type structure more attractive the largest trivalent REs. $BaRE_2O_4$ occurs for La to Er

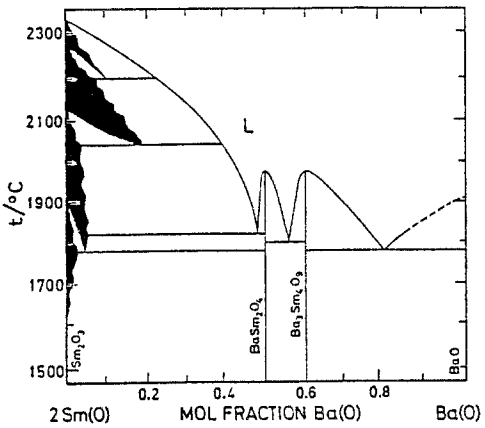

Fig. 3 An *x–t* diagram for the Sm(O)–Ba(O) system in air; after Ref. [80]

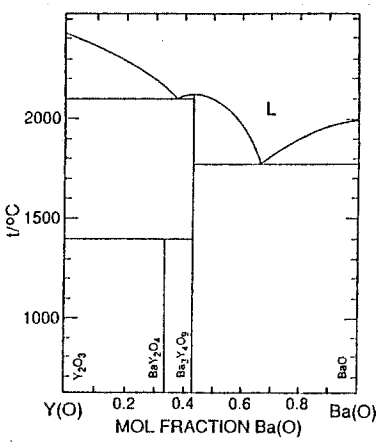

Fig. 4 An *x–t* diagram for the Y(O)–Ba(O) system in dry Ar/O_2 mixture with p_{O_2}=21 kPa; after Refs [95, 97]

and Y [80]. {$BaLa_2O_4$; *Pnam*; 1066.8(2), 1264.2(2), 370.4(1)} [93], {BaY_2O_4; *Pnam*; 1039.85(8), 1211.94(9), 345.06(2)} [94]. For RE=Nd and Sm, this phase melts congruently, whereas, for the larger and smaller REs, decomposition occurs before melting; between 1850°C for RE=La [80] and 1400°C for RE=Y [80, 95] (a markedly different value of ~1030°C being also reported [96]). The phase diagram for RE=Sm [80] is illustrated in Fig. 3 and for RE=Y [95, 97] in Fig. 4; for further diagrams, see Refs [80, 98, 99].

For Sm and smaller REs, another phase, $Ba_3RE_4O_9$ occurs as well. When its synthesis is attempted from RE oxides and $BaCO_3$, high temperatures are required, increasing with the electropositive character of the involved RE; from 1000°C for RE=Lu to 1550°C for RE=Sm [80]. The crystal structures [100] of the $Ba_3RE_4O_9$ phases are rhombohedral {$Ba_3Tm_4O_9$; *R3*; 605.56(4), 2495.7(2)}.

Tetravalent REs. In O_2 atmosphere, Ce, Pr and Tb form only one ternary oxide with BaO, viz., $BaREO_3$ [101], the crystal structures of which being slightly distorted variants of

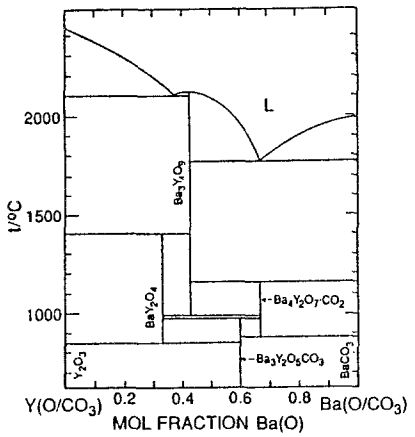

Fig. 5 A phenomenological *x–t* diagram for $BaCO_3$-based syntheses in the $Y(O/CO_3)$–$Ba(O/CO_3)$ system in air; after Ref. [95]

the perovskite (orthorhombic for RE=Ce and Pr, and rhombohedral for RE=Tb [102, 103]). Naturally, under reducing conditions, $BaRE_2O_4$ is obtained also for RE=Ce, Pr, Tb [80, 104].

Oxide carbonates. In the $Ba(O/CO_3)$–$Y(O/CO_3)$ system, at least two oxide carbonates occur. One has a triple-perovskite structure [94] with a (disordered) carbonate group at one of the three B-sites per unit cell {$Ba_3Y_2(CO_3)O_5$; *P4/mmm*; 438.63(4), 1185.9(2)} [78]. This phase has proved [78, 105] to be identical with $Y_2Ba_2O_5$ claimed in Refs [76, 106, 107]. Another oxide carbonate of composition $Ba_4Y_2O_7{\cdot}CO_2$ is suggested [77], corresponding to what was originally (with some caution due to unindexable PXD data) proposed as an oxide phase [76]. Like carbonates, also oxide carbonates release CO_2 at high enough temperatures, depending on the partial pressure of CO_2 in the reaction atmosphere. As an example, $Ba_3Y_2(CO_3)O_5$ decomposes [78] at 960°C in oxygen atmosphere with ~5 ppm CO_2 into the $Ba_3Y_4O_9$ phase and what can be identified (by PXD) as the uncertain $Ba_4Y_2O_7{\cdot}CO_2$. The formation and decomposition temperatures of oxide carbonates in the $Ba(O/CO_3)$–$Y(O/CO_3)$ system for an air atmosphere are studied in detail in Ref. [95]. A phenomenological chemical phase diagram [95] showing, inter alia, the observed lower temperature limits for formation from a $BaCO_3$-containing starting mixtures, is given in Fig. 5.

B. Systems AE(O)–Cu(O)

A general note. The AE(O)–Cu(O) systems have proved rather difficult to investigate. The variability of the Cu valence, combined with the strong basicity of the AE oxides, results in a tendency to form more oxidized cuprates when the AE content increases. At the same time, the reactivity towards CO_2 is more pronounced and higher temperatures for syntheses of pure oxides are required when CO_2 is present in the environment. The possibly formed oxide carbonate phases are difficult to identify. Occurrence of both oxide carbonates and highly oxidized cuprates intermingles in the picture of the redox equilibria, since the entropy of the liberated gaseous species is the main factor governing their thermodynamics. In addition, structural characterizations of these phases are often complicated by vacancies encountered in both the oxygen- and the AE-sublattices, and this leads to a variety of order-disorder phenomena.

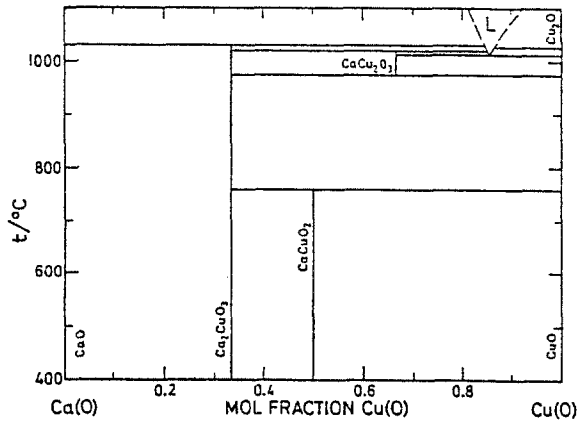

Fig. 6 A *y–t* diagram for the Ca(O)–Cu(O) system in air; after Refs [111, 112]

Ca(O)–Cu(O)

Due to the variable valence of Cu, the Ca(O)–Cu(O) phase system changes with varying partial pressure of oxygen. The occurring redox relationships have been examined [108] by means of EMF measurements in ZrO_2 solid-electrolyte cells. Functions of standard free energies of formation are evaluated and mapping of the phase relationships is attempted in a three-dimensional *y–p–t* phase diagram covering the interval $10^{-9} < p_{O_2} < 10^5$ Pa [108]. Thermodynamic assessment of this phase system which includes also solidus-liquidus and redox equilibria is attempted in Ref. [109]. An example for the *y–t* phase diagram is shown in Fig. 6, based on consensus data referring to an air atmosphere [110–112], and similar to what is seen for pure oxygen [110, 113]. Three ternary oxides are encountered:

Ca_2CuO_3, with orthorhombic crystal structure [114, 115] {*Immm*; 1220.8(6), 376.8(2), 324.9(2)} [116]. This phase has the highest thermal stability of these four intermediate phases, and melts incongruently at 1085(3)°C in oxygen [113]. In the same atmosphere at temperatures below some 700°C, this phase is not formed and CaO and $Ca_{1-y}CuO_2$ are seen instead [112, 117]. The oxygen content of Ca_2CuO_3 [118] does not vary significantly from what corresponds to $\nu_{Cu}=2$ and this is apparently the reason for the instability against the more oxidized phase at low temperatures.

$Ca_{1-y}CuO_2$, actually a structural series with superstructures or incommensurate orderings based on a $CaCuO_2$ subcell {*Fmmm*; 280.7(1), 635.1(2), 1059.7(3)} [119]. The crystal structure [119] contains linear edge-sharing chains of cuprate squares. Such an arrangement does not usually allow for any significant occurrence of oxygen vacancies, yet an oxygen content of 1.93(1) for $y=0.167$ has been measured, practically independent of temperature [117]. Since the Cu valence is high, the phase decomposes at the relatively low temperature of 835°C in oxygen, whereas in air already at 755°C [112]. The Ca deficiency is associated with various possibilities for superstructure ordering, such as in $Ca_4Cu_5O_{10}$ {*Pnca*; $a'=5a$} [119] or $Ca_5Cu_6O_{12}$. The latter was indexed on a monoclinic supercell {1680, 632, 1095, 75} [120]. The "homogeneity" range for AE depends somewhat on temperature and oxygen pressure, since, despite the fixed oxygen content, the Cu valence may still tend to vary through the change in the AE content.

$CaCu_2O_3$ {*Pmmm*; 985, 411, 347} has tetrahedrally distorted square Cu–O coordination, with each square (a flat tetrahedron) sharing three of its four corners to form double chains [121]. Probably as a result of the tetrahedral deformation, the oxygen content is fixed

(Cu(II)), and this contributes to the narrow range of thermal stability for this phase which occurs between 977(3) and 1045(5)°C in oxygen [113], or at somewhat lower temperatures in air. Recently, based on EDAX analysis, a composition $Ca_3Cu_7O_{10}$ is suggested {o; 994.2, 407.9, 345.9} [113], but a crystal structural confirmation of this claim is yet lacking.

Sr(O)–Cu(O)

Redox equilibria have been examined [122, 123] in the Sr(O)–Cu(O) phase system, by means of EMF measurements on ZrO_2 solid-electrolyte cells. Functions of standard free energies of formation are evaluated and mapping of the phase relationships is attempted in a three-dimensional x–p–t phase diagram covering the interval of $10^{-9} < p_{O_2} < 10^{11}$ Pa [122].

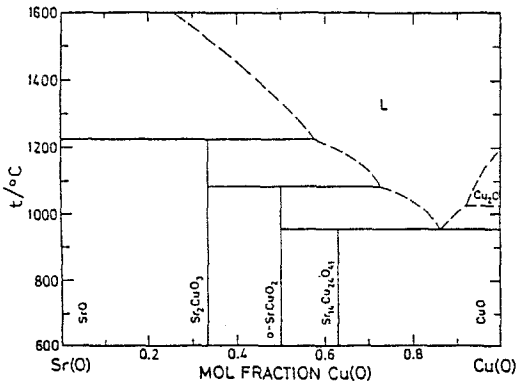

Fig. 7 A y–t diagram for Sr(O)–Cu(O) system in air; after Ref. [124]

Ambient partial pressures of oxygen. The y–t diagram [124] is shown in Fig. 7. Three ternary phases are encountered:

Sr_2CuO_3 {*Immm*; 1269, 391, 348}. The crystal structure [125], seen already for Ca_2CuO_3, contains chains of copper–oxygen coordination squares, and does not exhibit any significant variations in the oxygen content as a function of temperature [123]. However, at high pressures, the oxygen content may increase substantially.

o-$SrCuO_{2+w}$ {*Cmcm*; 357.7(1), 1634.2(1), 391.82(7)} [126]. The crystal structure [114, 126] contains edge sharing, slightly deformed, double-square cuprate anions, connected into zig-zag chains. Only minor variations in the oxygen content are allowed in this arrangement, $1.975 < w < 2.035$, as observed for $0.01 < p_{O_2} < 100$ kPa at 900°C 123].

$Sr_{14}Cu_{24}O_{41}$, with crystal structure [127, 128] described as being incommensurate, {$Sr_2Cu_2O_3$; *Fmmm*, 1145.7(5), 1340.9(9), 393.5(3); $+10/7CuO_2$; *Amma*; 1145.7(5), 1340.9(9), 274.0(2)} [128] and it is nearly compatible with a $7c = 10c'$ superstructure [124, 127]. The oxygen content is almost independent of temperature ($\Delta w < 0.002$ per Cu between 670 and 970°C), and the relatively high Cu valence $\nu_{Cu} \approx 2.24$ is preserved until decomposition.

Low partial pressures of oxygen. The y–t diagram [122] at $p_{O_2} = 10$ Pa, calculated from EMF-based thermodynamic data is shown in Fig. 8. The diagram is nearly identical with the diagram in Ref. [123] which is based on direct observations. One new ternary phase is seen, compared with the ambient-pressure situation:

$SrCu_2O_2$ {$I4_1amd$; 548, 982}, has crystal structure [129] with a typical linear coordination at each monovalent Cu, which is in turn located tetrahedrally around each oxygen atom. This phase is the last ternary oxide appearing upon reduction of the more oxidized phases. As an example of the redox reactions, $Sr_{14}Cu_{24}O_{41}$ decomposes [123] at 920°C and

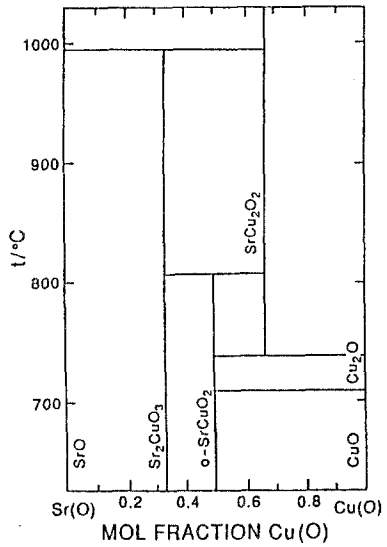

Fig. 8 A *y–t* diagram for the Sr(O)–Cu(O) system at $p_{O_2}=10$ Pa calculated from thermodynamic data; after Ref. [122]

$p_{O_2}=6$ kPa into $SrCuO_2$ and CuO. The $SrCuO_2$ phase gives in turn $SrCu_2O_2$ at 820°C when $p_{O_2}=10$ Pa [123]. Under the same conditions, the Sr_2CuO_3 phase is still stable.

High pressures of oxygen. The *y–p* isothermal phase diagram [130] for 775°C, up to $p_{O_2}=60$ MPa, is shown in Fig. 9. More oxidized phases or structures are stabilized under high pressures of oxygen:

Sr_2CuO_{4-w} {*I4/mmm*; 376.31(1), 1256.01(9)} [131] and related $Sr_{n+1}Cu_nO_{2n+2-w}$ series [132]. The crystal structure [131] of Sr_2CuO_{4-w} is basically of the K_2NiF_4 type (also designated as the T type). It differs from the ambient pressure Sr_2CuO_3 in that the Cu–O coordination squares are appended to approach octahedral coordination, while some oxygen vacancies are created. The symmetry of the oxygen ordering is complex and the superstructure is considered to be incommensurate [133, 134]. An oxygen vacancy content as low as $w=0.1$ is reported [135] after treatment under 16 MPa of oxygen at 400°C, whereas $w\approx0.5$ after a high-pressure synthesis at 6 GPa and 850°C, with $KClO_4$ as a source of oxygen. The significance of this high-pressure phase is seen in the observed high-T_c superconductivity, reaching a maximum T_c of some 90 K at intermediate levels of oxygen content [136].

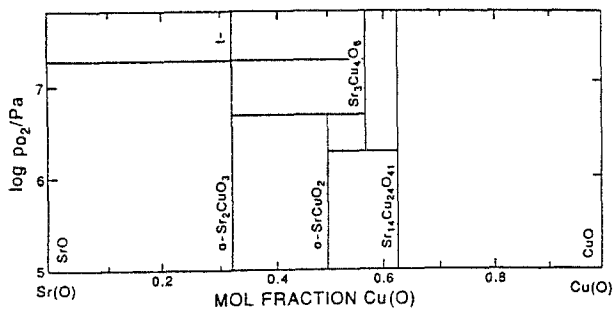

Fig. 9 A *y–p* diagram for the Sr(O)–Cu(O) system at 775°C in oxygen; after Ref. [130]

These high pressure samples are not usually phase pure. One such minor phase has recently been attempted identified as monoclinic $SrCuO_{7/3+w}$, $0<w<1$, {*Pm*; 843, 1110, 364, 83.2}, based on HREM [137]. Another minority phase designated as $Sr_6Cu_8O_w$, {o; 378.9, 802.7,1250} has been reported under $KClO_3$-assisted experiments [138]. However, the same technique led recently to the synthesis of a bulk phase:

$Sr_2Cu_2O_5$ with orthorhombic crystal structure [139] {*Pbam*; 542.4(2), 1083.7(4), 373.1(1)}, having exclusively square-pyramidal copper coordinations, connected at their apices. This non-superconducting [139] phase is of the $Ca_2Mn_2O_5$ type and has also analogues where Sr is completely replaced by La [140] or Nd [141].

High pressures. High-pressure syntheses in belt- or anvil-cell-type apparatus yield several new structures:

t-$SrCuO_2$ {*P4/mmm*; 392.6, 343.2} [142]. The crystal structure [142] of the phase obtained at 6 GPa and 1050°C contains sheets of corner sharing, copper-oxygen coordination squares in an extremely simple, perovskite-like arrangement. A related series, $Sr_{n-1}Cu_{n+1}O_{2n}$, $n=3$, 5..., can be obtained under similar conditions [143].

$Sr_{1-y}CuO_2$, $y\approx1/4$, has an incommensurate structure [130] {oI; 681.82(12), 371.13(7), 1102.03(17); + oF; 681.82(12), 272.90(3), 1102.03(17)}, $25b\approx34b'$, and is related or analogous to the series occurring [119, 120] for AE=Ca.

Oxide carbonates. For compositions most rich in Sr, oxide carbonates may occur:

$Sr_2CuO_2(CO_3)$ has been identified [144] as an intermediate of the synthesis of Sr_2CuO_3 from $BaCO_3$ and CuO. The crystal structure [144] solved from PND data {*P4/mmm*; 390.33(2), 749.25(4)} consists of CuO_2 planes interconnected at octahedral apices by CO_3 groups. In a further investigation of the crystal structure [145], a determination was attempted for the orientation of the carbonate groups in a single-phase material {$I\bar{4}$; 780.5, 1499.3}. The same structure [146] is obtained by replacing, say, 20% of the carbonate groups by borate, {$I\bar{4}$; 778.81(15), 1496.8(3)}. Above some 220°C, a structural transition is observed {$P42_12$; 554.36(1), 753.82(1)} [147]. Another oxide carbonate was obtained almost single phase in an anvil-cell synthesis {$Sr_3Cu_2(CO_3)O_w$; t; 391, 1088} [148], obviously a triple perovskite.

Ba(O)–Cu(O)

The redox equilibria in the Ba(O)–Cu(O) system have been examined [149], by means of thermodynamical modelling on a selected set of reliably defined phases. An experimental

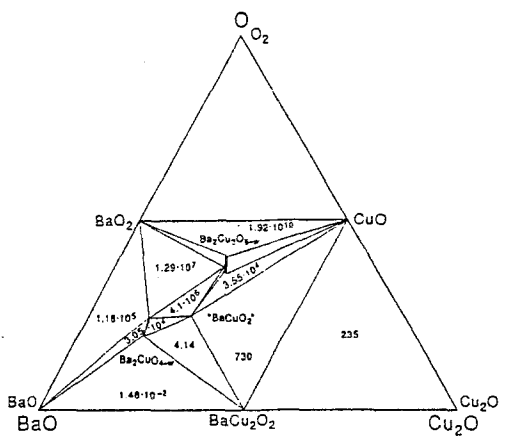

Fig. 10 Isothermal BaO–Cu_2O–O diagram at 727°C calculated from thermodynamic data; after Ref. [149]. p_{O_2} in Pa is given in 3-phase fields

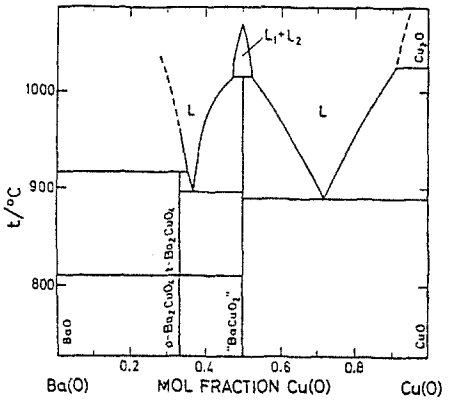

Fig. 11 A y–t diagram for the Ba(O)–Cu(O) system in an Ar/O_2 mixture with p_{O_2}=21 kPa; after Refs [151, 152]

verification of these data and their extension into the Ba-rich region, accompanied by detailed characterizations of the investigated phases (including residual-carbon analyses), appeared recently [150]. Details on the s–l equilibria are also provided in Ref. [150]. As an example for the subsolidus redox relationships, the situation [149] at 727°C is shown in Fig. 10.

Moderately oxidizing conditions. The y–t phase diagram [151, 152] is shown in Fig. 11, as seen by microscopy, DTA and TG, at temperatures relevant for ceramic firing processes, in an atmosphere of p_{O_2}=21 kPa in Ar. At temperatures above some 800°C, two ternary phases are identified, the second one, however, is suspected to be an oxide carbonate.

Ba_2CuO_{4-w}, takes a K_2NiF_4 type, orthorhombically deformed structure [151]. At 810°C and p_{O_2}=21 kPa, an orthorhombic-to-tetragonal transition is observed [152]. According to the p–t–w diagram [150] this transition occurs around $4-w=3.2$ and is accompanied by a small discontinuity (a jump) in the oxygen content of the phase, yielding the high-temperature phase with oxygen content of ≤3.1 per formula. The oxygen content at the onset of the transition (when varied by p_{O_2}) increases slightly with increasing temperature. The phases can be quenched to room temperature, e.g., tetragonal $Ba_2CuO_{3.10}$ {*I4/mmm*; 399.2, 1298.5} [153] from 850°C when $p_{O_2}=10^3$ Pa, or the orthorhombic $Ba_2CuO_{3.30}$ {*Immm*; 1296.6, 410.1, 390.7} [151] from 700°C in oxygen [150]. The relatively high oxidation state of Cu occurs in accordance with the high BaO content in the oxide. The Ba_2CuO_{4-w} phase is not formed on firing of carbonaceous starting materials or in air at temperatures below the melting point in the carbonate system (which is lower [154]) than 890°C [150] for Ba_2CuO_{4-w}), but is readily obtained [152] from the oxides or BaO_2.

$BaCuO_{2+w}$, which undoubtedly is only an approximate formula for this cubic phase with an unusually large unit cell. The oxygen content w can change over a modest range, as corresponds to {v_{Cu}=2.18(2); c; 1830.3(6)} and {v_{Cu}=1.96(4); c; 1828.8(4)} [105]. The crystal structure [155] has several complex and crystallografically somewhat disturbing features and has therefore been a subject of many studies by a variety of structural techniques [116, 156–158]. Two explanations for the encountered structural problems have been suggested: (i) partial occupancies at several Cu- and O-sites, and/or (ii) stabilization by a presence of carbonate ions. As an example for the vacancy problem, two different unit-formulae (Z=96 assummed for both) are obtained for a fully oxidized sample by a single-crystal method [158] and Rietveld refinement from PXD data [159], viz., $Ba_{0.92}Cu_{1.06}O_{2.14}$ and

$Ba_{0.92}Cu_{1.01}O_{2.17}$, respectively. However, PND data [116] give yet another answer, $Ba_{0.92}Cu_{0.94}O_{1.94}$. The idea that this phase actually is an oxide carbonate has been supported by a combined structural [160] evaluation based on PND and PXD data. Rietveld refinements were able to localize carbon where previously a Cu or alternatively an O atom was considered having a "strange" environment, and enabled even the location of the eight O sites appearing due to the statistical disorder of the carbonate-group orientations $\{Ba_{44}Cu_{48}(CO_3)_6O_{81+w}$; $Im\bar{3}m$ 1830.69(2)$\}$. The possibility of $BaCuO_2$ being an oxide carbonate cannot easily be dismissed based on the synthesis conditions because the temperatures were generally under 1000°C and the omnipresence of traces of CO_2 in the chemical environment, starting materials, etc. Further support may be given by the fact that the only structural analogue to $BaCuO_{2+w}$ is a nickel oxide carbonate [161, 162]. There are also observations of some CO_2 evolution during the acid hydrolysis of the sample, and of abnormally high contents of residual CO_2 as compared with other Ba cuprates (like Ba_2CuO_{4-w}) [150].

It has been suggested that additional, Cu-rich phases exist in this system, appearing as satellite phases during the crystallization of the $YBa_2Cu_3O_7$ superconductor. One example is given here for such a structure [163] identified from electron diffraction pattern of the satellite reflections: $BaCu_3O_4$ {*Cmmm*; 1098, 550, 392}. However, a confirmation of this in form of a synthesized bulk material is yet lacking.

Highly oxidizing conditions. Investigations of chemical phase relations in the Ba(O)–Cu(O) system at temperatures below 800°C or at high pressures of oxygen has proved extremely demanding on experimental and analytical techniques. In particular, this is due to the sluggish kinetics during the syntheses at low temperatures, strong affinity of both the starting materials and products towards the carbon dioxide, and the possibility for reaching relatively very high oxidation states of Cu. The phases then can decompose upon liberation of CO_2 and/or O_2 as a function of pressure and temperature, and this complicates their identification. In this situation it was not unreasonable to approach the problem by thermodynamic modelling [149], and the thus obtained phase diagrams are shown in Fig. 12 for y–t coordinates at ambient oxygen pressure and in Fig. 13 for y–p coordinates at 827°C. One highly oxidized phase appears:

$Ba_2Cu_3O_{6-w}$, the elusive low-temperature phase, has only recently been synthesized phase pure [164]. The crystal structure is suggested [164] to be related to those of $NaCuO_2$

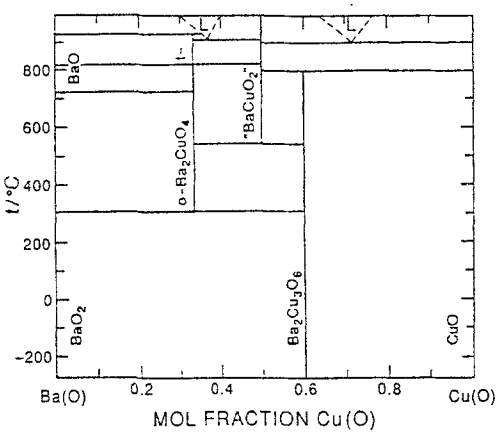

Fig. 12 A "low temperature" y–t diagram for the Ba(O)–Cu(O) system in an Ar/O_2 mixture with p_{O_2}= 21 kPa, calculated from thermodynamic data; after Ref. [149]

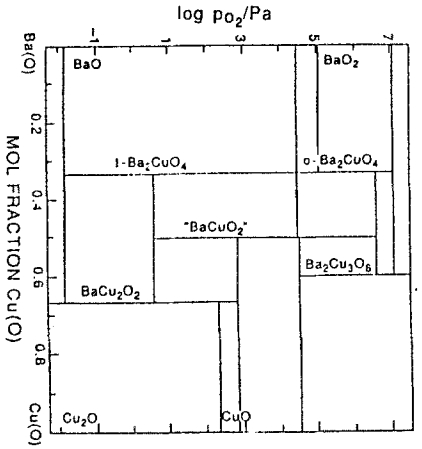

Fig. 13 A y–p diagram for the Ba(O)–Cu(O) system at 827°C calculated from thermodynamic data; after Ref. [149]

and $KCuO_2$ [165], and therefore analogous to the $AE_{1-y}CuO_2$ phases where AE=Ca or Sr. The structure contains edge-sharing chains of square coordinated copper interleaved by Ba layers and mutually ordered into a monoclinic superstructure [166] {*P*2; 848, 733, 1215.4, 110.4}. The superstructure is based on a more elementary structural arrangement [167] referring to the Ba-sublattice [164] {*Cmcm*; 729.8(3), 425.9(2), 1142.1(3)} [168]. In line with the suggested structural prototypes, it is also proposed [164] that there exists a homogeneity region with respect to Ba, $0.33 < y < 0.25$, referring to the formula $Ba_{1-y}CuO_2$. The PXD pattern of $Ba_2Cu_3O_{6-w}$ can be identified as the main component in most of the previously published reports on the high-oxygen, $BaCuO_{2.5}$ phase, either as synthesized at high-pressures [169, 170], or low-temperatures [171–173]. Very often, one of the minor components is then barium carbonate. The saturated oxygen content of this phase [166, 174] at 21 kPa O_2 and 300°C corresponds to $\nu_{Cu}=2.51$. It can be reduced [174] to some $\nu_{Cu}=2.37$ before thermal decomposition above some 700°C [175] into the less oxidized Ba_2CuO_{4-w} and CuO [149], or into, also less oxidized, "$BaCuO_{2+w}$"oxide carbonate and CuO [164, 170, 174, 176]. Barium carbonate would be necessary for the latter reaction, but it can be identified in the PXD diagrams in small amounts in all these cases. The onset of the $Ba_2Cu_3O_{6-w}$ decomposition is reported [176] to be as low as 600°C, and the completion to take a considerable amount of time. The reverse of this reaction, viz., the decomposition of the "$BaCuO_{2+w}$" oxide carbonate into $Ba_2Cu_3O_{6-w}$ (and $BaCO_3$) is observed at low temperatures [177] or at high pressures [178], indicating that the redox component, and not the carbonatization, is the dominant driving force for the reaction. The low thermal stability of the highly oxidized $Ba_2Cu_3O_{6-w}$ severely limits its synthesis conditions to carbonate-free and reactive, usually nitrate-based starting materials [172, 178–180].

High pressures. A high-pressure $BaCuO_{3-w}$ phase is reported [170] in addition to those included in Fig. 13. Its crystal structure [170] {$P222_1$; 982.7(1), 567.83(7), 952.52(4)} seems to resemble that of $BaMnO_3$, but contains an extensive amount of oxygen vacancies.

Reducing conditions. Two new phases appear at low partial pressures of oxygen and high temperatures, $BaCu_2O_2$ and Ba_3CuO_4 (the latter is not included in the phase diagrams in Figs 11, 12 and 13):

$BaCu_2O_2$, with the crystal structure [181] already encountered in the Sr version {$I4_1amd$; 572.2, 1006.4} and monovalent Cu, is the last ternary oxide appearing upon reduction in the Ba(O)–Cu(O) system.

Ba_3CuO_4 {h; 788.3, 1555} [182], perhaps somewhat surprisingly belongs also into this category of reduced phases. The reason is that it decomposes into Ba_2CuO_{4-w} when exposed to an ambient oxygen atmosphere at elevated temperatures. This means that Ba_3CuO_4 has a structurally fixed oxygen content and divalent copper, which, owing to the large content of Ba, can only be maintained at relatively reducing conditions (950°C and $p_{O_2}=0.1$ Pa).

Oxide carbonates. Except for the "$BaCuO_2$" phase which actually may be a carbonate-stabilized phase, a true oxide carbonate occurs in the Ba-rich region:

$Ba_2CuO_2(CO_3)$, is structurally very similar or analogous {t, 400.2(1), 797.4(3)} [183] with the already described Sr variant $Sr_2CuO_2(CO_3)$. It is possible that the oxygen content is variable, in line with the behaviour of the corresponding oxide. The synthesis of a single-phase product is difficult, being hindered by the sluggish kinetics in the closed system syntheses, and this probably prevented specific structural characterizations.

Ca,Sr(O)–Cu(O)

Ambient oxygen pressures. Wide ranges of solid solubility exist between pairs of corresponding cuprates, as can be seen from the phase diagrams for the Ca(O)–Sr(O)–Cu(O) subsolidus system [10, 111, 179, 184]. The situation at 850°C is shown in Fig. 14. In the recent study of Ref. [10], the miscibility gap in the (Ca,Sr)O solid solution is observed, and also the tie lines are redetermined in detail. A complete solid solubility occurs between Sr_2CuO_3 and Ca_2CuO_3 [10, 111, 179, 184, 185]. Roughly half of the strontium may be replaced by Ca in $Sr_{14}Cu_{24}O_{41}$, and in the ambient-pressure phase o-$SrCuO_{2+w}$ at 850°C [184]. Higher solid solubilities are observed at higher temperatures [10, 111, 179]. Structural details for these solid solutions are given in Refs [127, 186]. In addition, a very specific partial Sr,Ca replacement may stabilize the high-pressure structure of the t-$SrCuO_2$ type also under ambient conditions:

$Ca_{1-y}Sr_yCuO_2$ is obtained single phase for $0.13<y<0.17$, as an example, for $y=0.14$ {*P4/mmm*; 386.11(2), 319.95(2)} [187] and for $y=0.16$ {*P4/mmm*; 386.7(2), 321.95(2)} [111]. Detailed variation of the unit-cell parameters as a function of composition is shown in Ref. [188]. The discovery of this phase was given considerable attention, since its crystal structure contains only the infinite sheets of corner-shared squares as the copper oxygen coordinations, and was quickly dubbed "the parent structure of the high-T_c superconductors" (Eventually, the structure has been made superconducting by using high-pressure syntheses

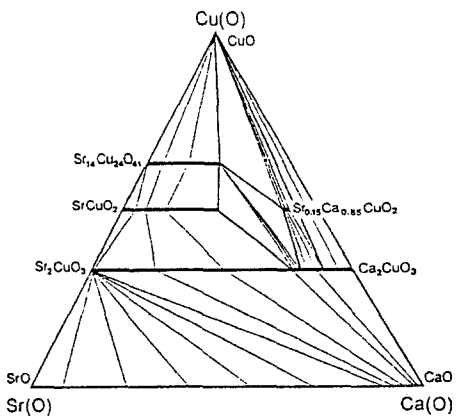

Fig. 14 Subsolidus Sr(O)–Ca(O)–Cu(O) phase diagram at 850°C as observed for syntheses from oxides in air; after Refs [111, 184]

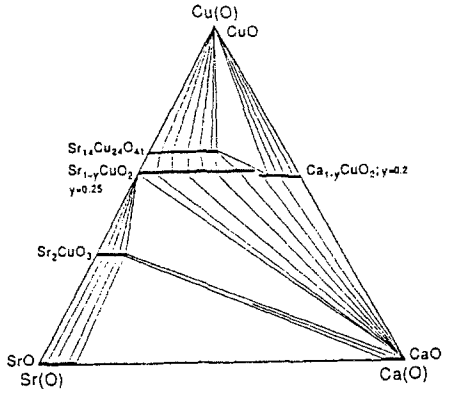

Fig. 15 Subsolidus Sr(O)–Ca(O)–Cu(O) phase diagram at 775°C under high-pressure oxygen, p_{O_2}=35 MPa; after Ref. [191]

for doped versions: A *p*-type superconductor with T_c=110 K is obtained by introducing AE-vacancies [189], and an *n*-type superconductor by Nd-doping [190].).

High oxygen pressures. Both the high pressure and the highly oxidative environment of these experiments affect the stability of the solid-solution phases. The phase diagram [191] at a high pressure of oxygen (p_{O_2}=35 MPa) and a relatively low temperature (775°C) in Fig. 15 is a good example for such oxidizing conditions. The most remarkable change noted here is the restricted solid solubility of Sr_2CuO_{3+w} and Ca_2CuO_3, which otherwise are completely miscible [179] both at ambient conditions and at high pressure (1 GPa, not of oxygen). The obvious reason is that the Sr phase oxidizes into the K_2NiF_4-type structure under the oxygen pressure, whereas the Ca counterpart does not, and retains its structural coordination squares at Cu. The other changes introduced by the high oxygen pressure are that the highly oxidized phases (or structural series) $Ca_{1-y}CuO_2$ and $Sr_{1-y}CuO_2$ emerge, with what appears as complete solid solubility. The $SrCuO_2$-based solid solution is unstable, as well as is the $Ca_{1-y}Sr_yCuO_2$ phase ($0.13<y<0.17$) [191]. On the other hand, the stability of the latter is increased under high-pressure anvil-cell conditions (~6 GPa, not of oxygen) [142, 189].

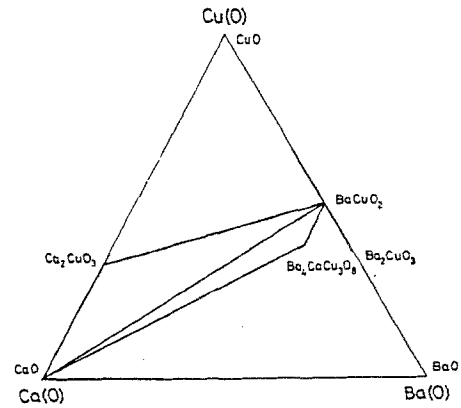

Fig. 16 A portion (indicated by the thick frame) of the subsolidus Ca(O)–Ba(O)–Cu(O) phase diagram as observed for syntheses from $BaCuO_2$ and Ca_2CuO_3 precursors in oxygen at 920–950°C; after Ref. [193]

Ca,Ba(O)–Cu(O)

Oxide systems. The size difference between Ba and Ca is appreciable in the Ba(O)–Ca(O)–Cu(O) subsolidus system (Fig. 16), and only one true quaternary oxide is reported [192, 193]:

$Ba_4CaCu_3O_w$, with a cubic, perovskite-related, $Ba_4YCu_3O_{8.5+w}$-type structure [194], which contains Cu-coordination octahedra and (disordered) squares {$Ba_4CaCu_3O_w$; $Im\bar{3}m$; 813.98(1)}.

Oxide carbonates. Also here the significant size-difference between Ba and Ca provides for a specific ordering in a perovskite-related structure type:

$Ba_4CaCu_2CO_3O_6$ with tetragonal structure [195] contains isolated copper–oxygen coordination squares, bridged at their octahedral apices by carbonate anions, and linear copper–oxygen dumbbels, also occurring in the vicinity of the carbonate groups {*P4/mmm*; 578.79(2), 814.09(3)}. Despite the different coordinations, copper is divalent on the average. A similar or identical phase has been also obtained previously, showing that the details in the oxygen and carbonate content can be variable [196, 197]. The compound is so stable that it can be obtained by direct synthesis in air from carbonaceous components at some 960°C [195].

Several other related, but less-stable phases, or perhaps structural patterns, can be prepared in thin layers by laser ablation, adopting the general formula $(CaCuO_3)_m(Ba_2CuO_2CO_3)_n$ [198].

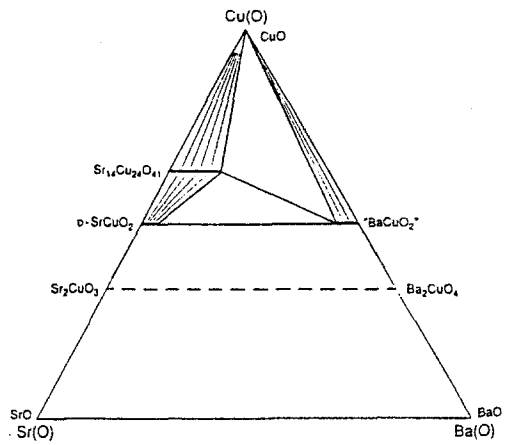

Fig. 17 A portion (indicated by the thick frame) of the subsolidus Sr(O)–Ba(O)–Cu(O) phase diagram as observed in oxygen at 950°C; after Ref. [199]

Sr,Ba(O)–Cu(O)

Oxide systems. Owing to the similarity of these two AEs, no true quaternary oxide occurs, but there are ranges of solid solubility between the corresponding cuprates (Fig. 17) [199]. Of these mixed systems, the mutual solid solubility of Ba_2CuO_{3+w} and Sr_2CuO_3 is investigated in particular [153]. Since the oxygen content of the former phase is variable, whereas rather constant in the latter at ambient conditions, the homogeneity range varies with the partial pressure of oxygen. For samples quenched from 1000°C, there is almost complete solid solubility between Ba_2CuO_{4-w} ($w \approx 1$) and Sr_2CuO_3, with continuous variation in the unit-cell parameters and oxygen content across the composition range.

Oxide carbonates. No new structural arrangements appear as a result of the simultaneous presence of Sr and Ba as compared to the systems with one AE. However, a complete solid solubility is seen in the $(Sr_{1-y}Ba_y)_2CuO_{3-w}(CO_3)$ system [183, 200]. The unit cell of these solid solutions has been described for both the low- and high-temperature types of $Sr_2Cu(CO_3)O_6$. Although a $y=0.5$ sample is of the low-temperature type {*P4/mmm*; 392.81(1), 760.45(2)} according to a PND study [201], single-crystal investigation [202] seems to indicate that a further Sr,Ba mixing stabilizes the ordering of the carbonate groups {$y\approx0.5$; $P42_12$; 556.1, 782.3}. This solid-solution phase is remarkable by its superconductivity ($T_c\approx30$ K), occurring after oxygen doping at 5 MPa [203].

C. *Systems RE(O)–Cu(O)*

A general note. Various structures (phases) are formed depending on the RE element and partial pressure of oxygen. The attainable oxidation state of Cu is somewhat lower than it was the case with the AE elements, in conformity with the difference in the electropositive character between RE and AE. Generally, Cu(II) compounds are formed at ambient oxygen pressures, below 1000–1100°C. Formation of ternary oxides with formally Cu(III) is observed only for the most electropositive REs at high pressures of oxygen. Compounds of Cu(I) are obtained under reducing conditions or at rather high temperatures. The redox equilibria have been studied in detail, both by EMF measurements in a ZrO_2 cell (RE=Y [204], RE=Gd [205, 206] and by coulometric oxygen titration (RE=Y [207]).

Ambient oxygen pressures. Two compositions are observed, $RE_2Cu_2O_5$ and RE_2CuO_4, both appearing in two structure types, their stability [208] being dependent on the RE size:

o-$RE_2Cu_2O_5$, is formed for small RE atoms, such as RE=Dy–Lu, Y, Sc [209]. As an example: {$Y_2Cu_2O_5$; *Pna*2_1; 1080.03(8), 349.53(2), 1245.88(8)} [210]. The crystal structure [210–214] contains slightly deformed Cu–O coordination tetrahedra, and the oxygen content is therefore structurally fixed. The *x–t* phase diagram for the Y(O)–Cu(O) system in air, as obtained [204, 215] by DTA and PXD, is shown in Fig. 18. The $Y_2Cu_2O_5$ phase is entropy stabilized [204, 216] and therefore unstable at low temperatures. A mixture of the binary oxides is more stable below 680°C [175], referring to ambient partial pressures of

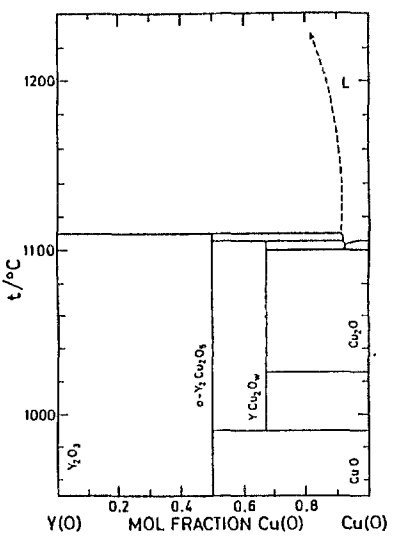

Fig. 18 An *x–t* diagram for the Y(O)–Cu(O) system in air; after Refs [204, 215]

oxygen (730°C, determined [217] from a change in decomposition products of more complex oxides, whereas 700°C is calculated from thermodynamic data [207]).

m-$RE_2Cu_2O_5$, has been observed [218–220] in an extremely narrow region of temperatures just above 1000°C for large trivalent RE=Nd and La. The crystal structure [218–220] {$Nd_2Cu_2O_5$; *C*2/c; 1372.8(2), 365.66(2), 27.549(3), 105.19(1)} [219], contains Cu-coordination octahedra connected by coordination squares, and has divalent copper. This phase is considered [218] to be a member of a structural series $RE_{4+4n}Cu_{8+2n}O_{14+n}$, seen so far only for $n=2$ and $n=3$.

t-RE_2CuO_4, also referred to as the T′ phase, forms for large RE except La (RE=Gd, Sm, Nd and Pr) [209]. As examples: Gd_2CuO_4 {*I4/mmm*; 380, 1180} [221], Nd_2CuO_4 {394.5, 1217.1} [222], and Pr_2CuO_4 {396.01(3), 1223.0(1)} [223]. The crystal structure [221–224] contains sheets of square-planar, corner-sharing cuprate anions, interchanging with layers of isolated oxide anions, both layers interleaved by RE. Therefore t-RE_2CuO_4 is

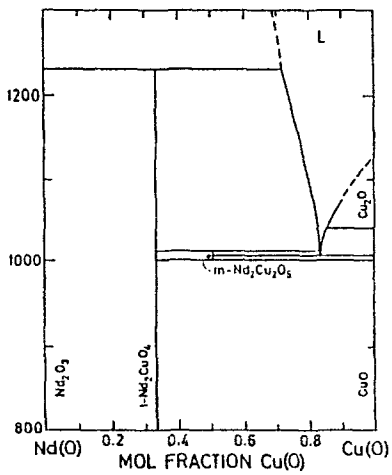

Fig. 19 An *x*–*t* diagram for the Nd(O)–Cu(O) system in air; after Refs [219, 227]

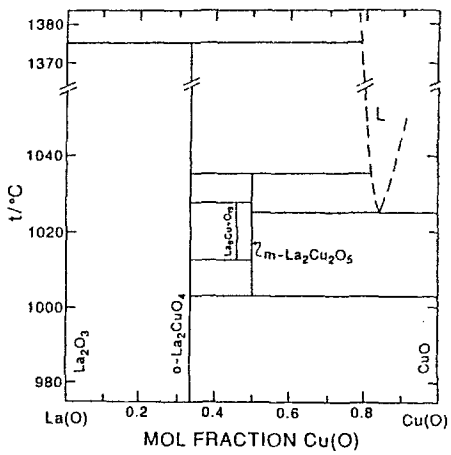

Fig. 20 An *x*–*t* diagram for the La(O)–Cu(O) system in air; after Ref. [220]

really a cuprate oxide, and the formula could as well be written $RE_2(CuO_2)O_2$. Also this structure appears to be entropy stabilized [206]. This series of phases is remarkable in the sense that its members become superconducting upon electron doping, which may be achieved either by partial F for O [225] or Ce for Nd (=RE) [226] substitution, but not by deoxidation, since the oxygen content is structurally fixed. The x–t phase diagram for the Nd(O)–Cu(O) system in air, as obtained [227, 228] by DTA, TG, SEM, EMP and PXD, is shown in Fig. 19. A similar diagram is obtained [229] for RE=Eu.

o-RE_2CuO_4, also referred to as a T phase, forms only for RE=La and has an orthorhombically distorted structure [221, 230] of the K_2NiF_4 type {La_2CuO_4; *Bmab*; 536.3(5), 540.9(5), 1317(1)} [230]. This structure contains layers of octahedral, corner-sharing cuprate anions. The layers are slightly buckled, due to a tilt of the octahedral building units. At ~200°C, the tilt disappears and a transformation into the tetragonal K_2NiF_4-type structure is observed [231]. The T phase, as hole doped by the Ba for La substitution, is the phase which was identified as responsible [232] for the discovery of high-T_c superconductivity [233].

The x–t phase diagram for the La(O)–Cu(O) system in air [220] is shown in Fig. 20. One additional phase with suggested composition $YCu_2O_{2.5}$ is seen [215] between some 1000–1100°C by high-temperature PXD. This phase could not be quenched to room temperature. No structural interpretation is given, but the relatively simple PXD diagram could correspond to a spinel phase. From Fig. 18, however, it seems not likely that it contains Cu(I) as suggested by the formula.

No ternary oxides of tetravalent Ce, Pr and Tb with CuO are hitherto reported [227, 234]. However, there is no reason why these REs should not be accommodated in structures appropriate to RE(III) if reducing conditions are adopted. Pr_2CuO_4 is even high-temperature stable in air [104].

High oxygen pressures. $RE_2Cu_2O_5$ is reported to be stable at p_{O_2}=20 MPa [235]. At even higher pressures, a phase based on Cu(III) is expected to take over, but this prediction has so far only been confirmed [140, 236, 237] for RE=La:

$LaCuO_{3-w}$, with a distorted rhombohedral perovskite structure of the $LaNiO_3$ type {$LaCuO_{3.00}$; r; 550.19(3), 1321.21(5)} [237] is synthesized at pressures of around 6 GPa of oxygen, generated from $KClO_4$ and high temperatures of up to 1500°C. The rhombohedral structure undergoes a transformation into a low-temperature modification (but still probably metastable [238]) of tetragonal [140] symmetry {$LaCuO_{3.00}$; *P4/m*; 381.88(1), 397.27(1)}, which represents a Jahn-Teller elongated, single-perovskite cell. This phase is obtained for $0<w<0.17$ upon annealing the high-pressure rhombohedral $LaCuO_3$ at temperatures of some 500°C, necessary to enable some diffusion, but not to cause any reduction of the oxygen content. When the variation in the oxygen content is attempted by controlling the partial pressure of oxygen at similar low temperatures, the compositions seems to easily vary over an extremely broad region of $0<w<0.5$. This leads to a formation of (at least) two structurally ordered variants:

$La_5Cu_5O_{15-w'}$ with a range of homogenenity of $1.00<w'<1.90$ and a monoclinic structure [238] {*P2/m*; 862.88(1), 383.08(1), 865.15(1), 90.217(1)}.

$La_2Cu_2O_{5+w''}$ with an orthorhombic structure [140, 239] and a homogeneity range [239] of $0.00<w''<0.14$ {*Pbam*; 554.90(1), 1047.74(2), 387.96(1)}. The phase has corner-sharing square-pyramidal coordinations, and has neodymium [141] and strontium [139] analogues.

No data are available for the behaviour of the Nd_2CuO_4-type phases at high oxygen pressures, almost certainly due to the occurrence of superconductivity upon reduction (electron doping), not oxidation. For the same reason, there is an abundancy of data for the high oxy-

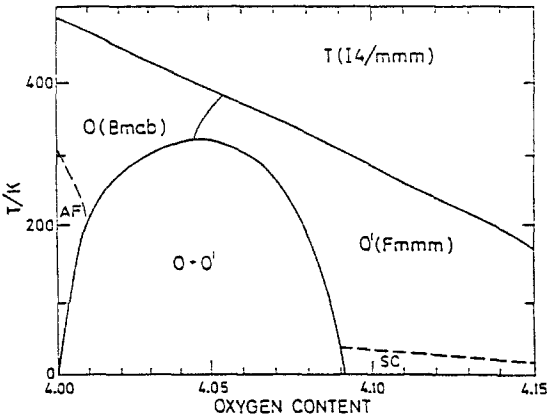

Fig. 21 Low-temperature w–T diagram for La_2CuO_{4+w}; after Ref. [232]

gen pressure behaviour of La_2CuO_4, since weak indications of superconductivity were rather surprisingly recorded for this virtually insulating oxide in oxidative environments. Later it is realized that additional oxygens can be inserted into this K_2NiF_4-type structure and that, below a certain temperature, this results in a separation into two phases: an insulating La_2CuO_4 and a conducting La_2CuO_{4+w}, the latter being responsible for the superconductivity [232, 240–243]. The distinction in oxygen content, which may amount up to 0.09 per formula, depends on temperature [232], but is large enough for the excess oxygen to be structurally [244, 241] located. The relations are illustrated in the phase diagram in Fig. 21.

High pressures. Under the conditions of the anvil-cell apparatus, the existence ranges of the ambient structures are shifted along the RE array. Thus the T′ phase (t-Nd_2CuO_4) transforms [245] under 25 GPa into the T phase (o-La_2CuO_4 type), whereas it is being now formed also for smaller RE=Y, Dy, Ho, Er and Tm [246]. A spinel-type oxide, not seen at ambient conditions, is formed across the RE series:

$RECu_2O_4$, with monoclinically deformed crystal structure [247] containing square-planar Cu {$NdCu_2O_4$; *I*2/*a*, 582.2(2), 969.5(3), 574.8(2), 92.34}.

Low oxygen pressures. The redox equilibria typical for the system containing the smallest RE atoms can be illustratred for the Y–Cu–O system. Investigations of the phase rela-

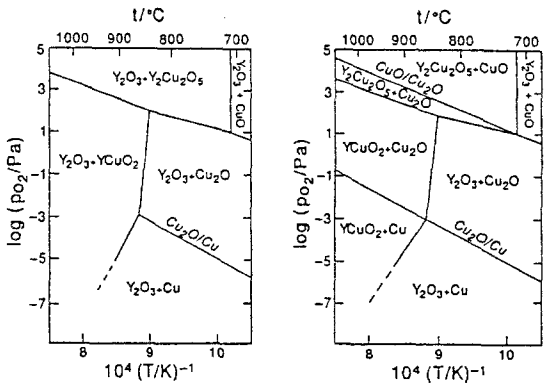

Fig. 22 An isoplethal, Y- and Cu-rich (left and right, respectively) p–t diagram of chemical stability for the Y(O)–Cu(O) system, as calculated from thermodynamic data; after Ref. [207]

tionships proved rather difficult, particularly due to problems with metastability. However, a series of five isothermal Y–Cu–O phase diagrams for five different temperatures can be composed from Refs [204] and [207] with excellent mutual agreement. Since only 1:1 intermediate phases occur, two isoplethal p–t diagrams, one Y-rich and one Cu-rich, are sufficient [207] to cover the entire field, shown in Fig. 22. As compared with the ambient pressures, one new phase appears:

$RECuO_2$, containing monovalent copper in a rhombohedral structure [248, 249] of the delafossite type. This type is adopted by many $MCuO_2$ compounds with monovalent Cu, over a wide range of sizes of the trivalent metal M. From the RE series, the La, Pr, Nd, Eu, Y and Sc variants have been obtained, however, rather different synthesis conditions were

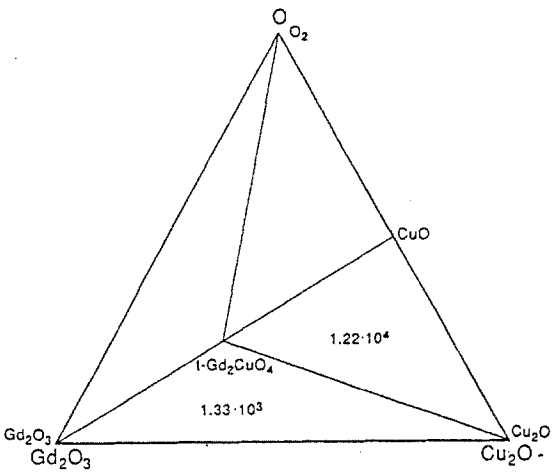

Fig. 23 Isothermal Gd_2O_3–Cu_2O–O diagram at 1000°C as obtained from solid-state galvanic cell measurements; after Ref. [206]; p_{O_2} in Pa is given in 3-phase fields

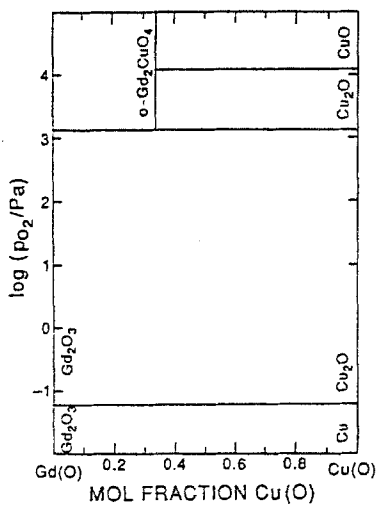

Fig. 24 An x–p diagram (low-pressure) for the Gd(O)–Cu(O) system at 1000°C in oxygen; after Ref. [206]

required in order to obtain the products. {$LaCuO_2$; $R\bar{3}m$; 383.3(2), 1711.0(9)} [250], {$EuCuO_2$; 363.3(1), 1709.1(4)} [250], {$YCuO_2$; 353.3(2), 1713.6(2)} [249], {$ScCuO_2$; 321.55, 1708.9} [251]. The CuO_2 dumbbells connect layers of the RE–O octahedra and can be subjected to a partial oxidation under low-temperature "soft-chemistry" conditions [252]. No high-temperature variation in the oxygen content has been reported.

The redox equilibria for the systems with the largest REs is illustrated for the Gd–Cu–O system in an isothermal phase diagram [206] in Fig. 23 and an x–p diagram in Fig. 24.

At low (partial) pressures of oxygen, only the La_2CuO_4 phase becomes slightly oxygen deficient. Judging from the behaviour of the $(La,Sr)_2CuO_{4+w}$ solid solution, the deficiency goes no further than to an oxygen content of 3.95 per formula, at 900°C and $p_{O_2}=10^{-1}$ Pa [253]. Also the Nd_2CuO_4- and $Y_2Cu_2O_5$-type phases decompose [204, 227] at high temperatures and low oxygen pressures (1120°C and $p_{O_2}=400$ Pa for Nd_2CuO_4).

RE,RE′(O)–Cu(O) systems

The similarity of the REs is reflected in the formation of solid solutions with wide ranges of homogeneity in the RE(O)–RE′(O)–Cu(O) phase diagrams. Individual quaternary oxides are formed exceptionally and are then closely structurally related to the ternary phases. These systems have attracted considerable attention due to the fact that they comprise the t-RE_2CuO_4 (T′-type) structure with square-planar cuprate anions in sheets which becomes superconducting upon electron doping, and the La_2CuO_4 (T-type) structure with octahedral cuprate anions in layers which becomes superconducting upon hole doping.

When mixed crystals are formed involving two REs, each pertinent to one of the two structural types, the decision whether the T or T′ type will be adopted depends on the average size of the atom at the RE site [254, 255]. However, when a smaller RE atom is introduced into the $(La_{1-x}RE'_x)_2CuO_{4+w}$ solid solution, which does not normally support formation of either T or T′ phase, a hybrid structure [256] emerges, designated as the T* type:

$(La_{1-x}RE'_x)_2CuO_4$, is obtained for RE′=Dy and Tb (in a limited extent also for RE′=Gd) within the interval $0.4<x<0.5$ [254]. The crystal structure [256] contains isolated oxide atoms and square-pyramidal copper-oxygen coordinations sharing corners of their basal plane to form sheets {$(La_{0.625}Dy_{0.375})_2CuO_3O$; *P4/nmm*; 386.61(1), 1244.75(2)} [256]. The phase is apparently stabilized by the presence of La in the T-like part of the structure (located between the apices of the cuprate pyramids), whereas the smaller RE′ prevails at the T′-like part (separating the square-planar bases of the pyramids). When synthe-

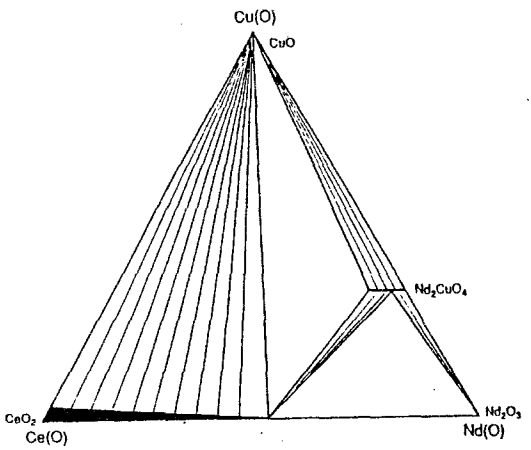

Fig. 25 Subsolidus Ce(O)–Nd(O)–Cu(O) phase diagram at 500°C; after Ref. [227]

ses of the T^* phase are attempted for Y, Ho and smaller REs, three-phase mixtures are obtained, consisting of La_2CuO_4 and $RE_2Cu_2O_5$-type phases and CuO [254]. The T^*-type phase is encountered also for other combinations of larger and smaller REs, however, only upon the condition that the site of the larger RE is shared with another relatively large atom, and this may be, e.g., Sr.

Otherwise, the T′-type structure emerges. Considering the square-pyramidal cuprate layers, it is not surprising that the hybrid T^*-type phases become superconducting on hole doping, either by oxidation under high pressure of oxygen [257] or by a Sr substitution for the larger REs [258]. Electron doping is not successfull in this respect [256, 259].

On the other hand, the T′-type phases with square-planar cuprate anions in sheets become superconducting upon electron doping, and this means that another $(RE_{1-x}RE'_x)_2CuO_{4+w}$ phase, having RE′=Ce as the donor, is of considerable significance [260]. No hole doping leads to superconductivity [261]. Superconductivity is observed when the phase is slightly oxygen-deficient [262], $(Nd_{1-x}Ce_x)_2CuO_{4+w}$ ($w=-0.01$), in a modest interval of the dopant concentrations ($0.075<x<0.085$) [263]. The same effect may also be achieved by other means of electron doping, as an example, by a partial substitution of Cu by In [264].

Only limited phase diagram data are available for these systems. The Ce(O)–Nd(O)–Cu(O) system has been investigated in detail in Ref. [227] and is shown in Fig. 25. A small section describing incongruent melting of $(Nd_{1-x}Ce_x)_2CuO_4$ analogous to that of the unsubstituted phase [227] is given in Refs [265, 266].

IV. Quaternary and related oxides

A. Systems RE(O)–Ca(O)–Cu(O)

The Y(O)–Ca(O)–Cu(O) phase diagram [267], representative of the smaller REs, is shown in Fig. 26. The diagram as seen at 1000°C in air indicates none or very narrow regions of the solid solubility for the Ca- and Y-containing ternary oxides, in line with their rather different structures. However, a quaternary phase appears:

$(RE_{1-x}Ca_x)_{1-y}CuO_2$, where RE=Y, $y=0.2$ and $0.5<x<0.7$, which is nothing else but the low-temperature, high Cu-valence $Ca_{1-y}CuO_2$-type phase stabilized now also at higher temperatures by lowering the valence due to the substitution by Y. The main subcell is completely analogous to the prototype {$x=0.5$; *Fmmm*; 281.7, 618.5, 1059.4} [267], but large changes occur in the relatively strong (incommensurate) superstructure PXD reflections when x is varied.

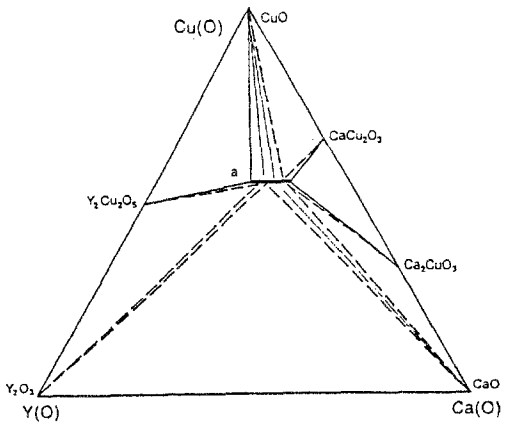

Fig. 26 Subsolidus Y(O)–Ca(O)–Cu(O) phase diagram at 1000°C in air; after Ref. [267]. Phase designation: a – $(Y_{1-x}Ca_x)_4Cu_5O_{10}$ ($0.5<x<0.7$)

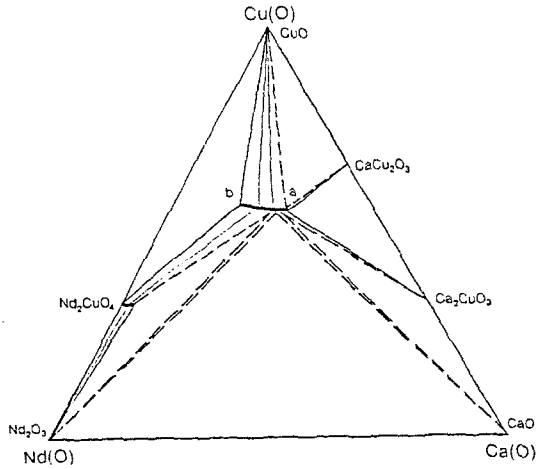

Fig. 27 Subsolidus Nd(O)–Ca(O)–Cu(O) phase diagram at 1000°C in air; after Ref. [267]. Phase designations: a – $(Nd_{1-x}Ca_x)_4Cu_5O_{10}$ $(0.50<x<0.57)$; b – $Nd_2Ca_{2-y}Cu_{5-y}O_{10-2y}$ $(0<y<1)$

The Nd(O)–Ca(O)–Cu(O) phase diagram [267] at 1000°C in air shown in Fig. 27 contains an identical phase, except that it is occurring in the narrower region of $0.50<x<0.57$ of the solid solution $(Nd_{1-x}Ca_x)_{1-y}CuO_2$, still with $y=0.2$. In addition, however, another solid-solution region is adjacent to this for higher Nd contents ($x<0.5$), but not as a simple continuation. A single phase is observed between $Nd_2Ca_2Cu_5O_{10}$ and $Nd_2CaCu_4O_8$, viz., in the direction towards 203. At the Nd-rich limit, the (incommensurate) superstructure peaks merge into a simple PXD pattern corresponding to $a'=4a$.

The La(O)–Ca(O)–Cu(O) phase diagram as seen at the same conditions [220, 268] does not contain the $Ca_{1-y}CuO_2$-type phase. Two genuine quaternary oxides are seen instead (Fig. 28):

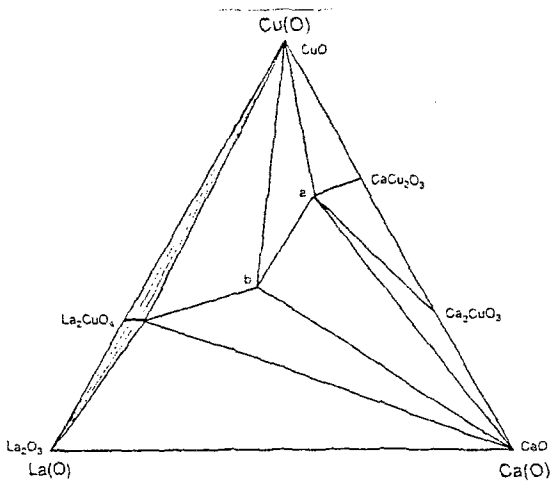

Fig. 28 Subsolidus La(O)–Ca(O)–Cu(O) phase diagram at 1000°C in air; after Refs [220, 268]. Phase designations: a – $LaCa_2Cu_5O_{8.6}$; b – $(La_{0.95}Ca_{0.05})_2Cu_2O_6$

$RE_2CaCu_2O_6$, actually a solid-solution phase $(La_{1-x}Ca_x)_2CaCu_2O_{6+w}$ with $0.0 < x < 0.1$ [269–271]. The range of homogeneity is somewhat tentative for the lower end. For example, the $x=0$ variant is reported [270] only when La_2CuO_4 is used as a starting material. Oxygen contents of no more than some 6.0 per formula are obtained upon treatment in oxygen [271]. The tetragonal crystal structure [270, 272, 273] {$La_2CaCu_2O_{6.04}$; *I4/mmm*; 383.35(1), 1951.7(1)} is derived from the Ruddlesden-Popper-type ($Sr_3Ti_2O_7$) by distributing oxygen vacancies over the corner-sharing Cu-coordination octahedra upon formation of sheets of square pyramids. The La atoms are then located predominantly on the sheet side of the pyramids and Ca atoms predominantly on the apex side. The fact that this structure contains solely the square-pyramidal cuprate sheets has drawn a considerable attention, since this represents another parent structure for the high-T_c superconductors [274]. In $La_2CaCu_2O_6$, the copper-oxygen square-chains are missing, which are considered to act as the "charge reservoirs" in the $YBa_2Cu_3O_7$ superconductor. In line with this, (and in parallel to La_2CuO_{4+w}) only weak indications of superconductivity were observed, even when the oxygen content exceeds the stoichiometric composition. However, bulk superconductivity was achieved by alternative ways of hole-doping, like that caused by a substitution of (20% of) La by Sr [274], or by a heat treatment under high oxygen pressure (40 MPa) [275]. A minute amount of the pressure-intercalated oxygen atoms, 0.014(7) per formula, located [275] between the square-pyramidal cuprate sheets is able to do the job. It is interesting to note that Ba did not have the desired effect as hole dopant [276], and neither could the Sr variant (Ca replaced by Sr) be made superconducting by substitutions. These facts have been discussed in terms of a fine-tuning of the Cu–O bond distances [274].

$RECa_2Cu_5O_{8+w}$, which is seen only for RE=La, is "isostructural" [220, 268] with the $Sr_{14}Cu_{24}O_{41}$ prototype {$LaCa_2Cu_5O_{8.57}$; *Cccm*; 1130.5, 1261.0, 2760.8} [268]. In contrast to the prototype, this phase contains almost exactly divalent copper and is stable up to 1030°C where it melts incongruently [268].

B. Systems RE(O)–Sr(O)–Cu(O)

Ambient oxygen pressures. The phase diagram [277, 278] Y(O)–Sr(O)–Cu(O), as seen at 900°C in ambient oxygen, is shown in Fig. 29. No genuine quaternary intermediate phase

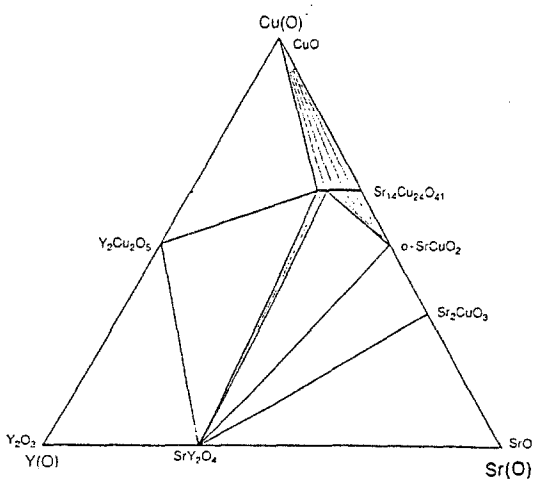

Fig. 29 Subsolidus Y(O)–Sr(O)–Cu(O) phase diagram at 900°C in oxygen at ambient pressure; after Refs [277, 278]

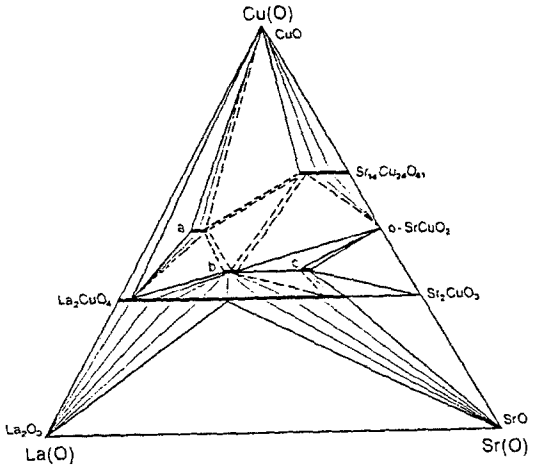

Fig. 30 Subsolidus La(O)–Sr(O)–Cu(O) phase diagram at 950°C in oxygen at ambient pressure; compiled from Refs [199, 269, 277, 279–281]. Phase designations: a – $(Sr_{1-y}La_y)CuO_{3-w}$ $(0.16<y<0.24)$ [281]; b – $(La_{1-x}Sr_x)_2SrCu_2O_{6+w}$ $(0.00<x<0.07)$ [269]; c – $La(Sr_{1-y}La_y)_2Cu_2O_{5+w}$ $(0.025<y<0.075)$ [280]

occurs, and no Y,Sr solid solubility is seen in the fixed-valence compounds $Y_2Cu_2O_5$ and o-$SrCuO_{2+w}$, whereas a significant portion of Sr in $Sr_{14}Cu_{24}O_{41-w}$ can be replaced by yttrium.

The pseudoternary phase diagram for the La(O)–Sr(O)–Cu(O) system is compiled from literature data, [199, 269, 277, 279–281] as expected to look at 950°C in oxygen, and is shown in Fig. 30. Of the strontium cuprates, only $Sr_{14}Cu_{24}O_{41}$ exhibits a significant La for Sr solid solubility (up to 36%) [280]. The K_2NiF_4-related structure of lanthanum cuprate has a broad homogeneity range with respect to Sr, up to $x=0.75$ in $(La_{1-x}Sr_x)_2CuO_4$ [280]. A change into the tetragonal K_2NiF_4-type structure occurs as a consequence of the Sr for La substitution, with a critical concentration of $x=0.04$ as seen [282–284] by PXD at room temperature {$(La_{0.925}Sr_{0.075})_2CuO_4$; *I4/mmm*; 377.17(8), 1322.6(3)} [285]. EXAFS study [286] shows that this composition-induced transition has both displacive and disorder components, maintaining the local tilt of the copper oxygen octahedra. Detailed unit-cell parameter data as a function of x and the analyzed oxygen content are given in Ref. [282]. The practically stoichiometric oxygen content, as obtained in oxygen at 600°C, remains constant upon substitution, increasing up to some $x=0.14$ at ambient pressure. Beyond that, the Sr acceptor is compensated by creation of the oxygen vacancies. $(La_{1-x}Sr_x)_2CuO_4$ melts incongruently, which means that single crystals cannot be grown directly from melts, and a CuO solvent technique must be used instead [287].

Except for the solid solutions based on the ternary oxides, several new quaternary phases are encountered:

$RE_6Sr_2Cu_8O_{20}$ is actually a solid solution expressed, e.g., for RE=La by the $(La_{1-x}Sr_x)_8Cu_8O_{2-w}$ formula with $0.16<x<0.24$ [281]. A slightly different value of $x=0.20$ is found for the lower limit in Ref. [280]. The phase is formed in an oxygen atmosphere at 950°C, and represents an oxygen-deficient perovskite with structural [281] ordering over 8 single-perovskite units ($a=a_p2\sqrt{2}$) {$(La_{0.8}Sr_{0.2})_8Cu_8O_{19.8}$; *P4/mbm*; 1084.0(4), 386.1(2)}, forming corner-sharing Cu-coordination octahedra, pyramids and squares [281, 288, 289]. The oxygen content is not easily varied, although some formation of Cu vacancies in the copper–oxygen octahedra is indicated [288]. Different orderings

may occur instead: $(La_{1-x}Sr_x)_5Cu_5O_{13}$ with $x=0.167$ formed upon further oxidation [290] or $(La_{1-x}Sr_x)_8Cu_8O_{20-w}$ with $0.135 < x < 0.15$ [291], formed under low-temperature conditions. Despite the rather fixed oxygen content, a mixed Cu valence occurs in these compounds and is manifested in a metallic nature of the phases. Yet, no superconductivity is observed [289].

$RE_2Sr_6Cu_8O_{16}$, or perhaps a solid solution (RE=La); $(La_{1-x}Sr_x)_8Cu_8O_{16}$ with $x\approx0.75$ [292], is not observed at the conditions relevant to Fig. 30, but is obtained [293] under slightly reducing conditions. This phase has a crystal structure [292] similar to the previous one, but the La/Sr ratio is inverted and the oxygen content somewhat different {$(La_{0.25}Sr_{0.75})_8Cu_8O_{16.07}$; *P4/mbm*; 1104.64(2), 363.90(1)}. Assuming that the oxygen content in this and other similar phases in question is structurally fixed, stable structures would be formed only under narrowly specified conditions, where both the La/Sr ratio and a structurally definable oxygen content are precisely adjusted to the attainable Cu valence defined by the average electronegativity of the La/Sr atom. This indeed seems to be the case, as yet another ordered and somewhat more oxidized variant appears, having 18 oxygens per formula {$(La_{0.25}Sr_{0.75})_8Cu_8O_{18.14}$; *P4/mbm*; 1084.20(1), 376.27(1)} [292].

$RE_2SrCu_2O_6$, is actually a solid solution expressed, e.g., for RE=La by the formula: $(La_{1-x}Sr_x)_2SrCu_2O_{6+w}$ with $0.00 < x < 0.07$ [269]. A slightly different value of $x=0.025$ is given for the lower limit in Ref. [280]. The phase has an "air-quenched" oxygen content as corresponds to $w\approx0.0$, which can be increased to some $w=0.25$ upon heating in pure oxygen at ambient pressure and temperatures between 200 and 400°C [272]. The latter treatment converts the original semiconductor into a metal [294]. The tetragonal crystal structure [272, 273] is derived from that of the Ruddlesden-Popper type in the same manner as seen for the Ca variant, vide supra. Contrary to the Ca variant, however, the more electropositive and larger Sr atoms allow for accommodation of more oxygens, and the homogeneity range for oxygen extends from, e.g., $La_2SrCu_2O_{6.08}$ {*I4/mmm*; 386.7(2), 1991(1)} [271] to $(La_{0.925}Sr_{0.075})_2SrCu_2O_{6.25}$ {385.30(1), 2008.33(3)} [272]. Formation of analogous structures is observed also for RE=Pr, Nd, Sm, Eu and Gd [295, 296]. However, except for RE=Pr, a specific ordering of oxygen vacancies with a tripling of *b* is observed by PXD [296, 297], HREM [298] and PND [299] (the latter on a Co-version). The presence of, inter alia, the infinite square-pyramidal cuprate sheets in this structure suggested that this phase should become superconducting upon hole doping. Quite surprisingly, despite the "correct" overall Cu-valence, superconductivity was not observed in the Sr-version (see Sec. IV A).

$RESr_2Cu_2O_6$ with crystal structure [300] related to the Ruddlesden-Popper-type phases by tripling the unit-cell parameter *b* upon ordering of both cations and oxygen vacancies. As an example for RE=Nd, $NdSr_2Cu_2O_{5.66}$ {*Immm*; 375.47(1), 1148.82(4), 2009.76(7)}. The ordering involves chopping the Ruddlesden-Popper double octahedra layers into segments or "ribbons" of square-pyramidal coordinations connected by distorted squares, i.e., trippled (along *b*), much like in the $YBa_2Cu_3O_7$ superconductor, but much more distorted. This is apparently the reason why this structure shows only minor variation in the oxygen content, between 5.66 and 5.76 per formula [300, 301]. Despite the mixed-valence state of copper, superconductivity is not observed [301]. This phase actually represents an end member of a solid solution where the RE atom can replace a portion of Sr. For RE=La, non-zero lower limit of this solid solution is seen ($0.025 < x < 0.075$) in $La(Sr_{1-y}La_y)_2Cu_2O_{5+w}$ [280].

High oxygen pressures. Phases in the Y(O)–Sr(O)–Cu(O) system have been investigated under conditions of very high oxygen pressures created at high temperatures from $KClO_3$ in gold capsules [138]. Several PXD-indexable phases emerge at oxygen pressure of $p_{O_2}=$ 7 GPa and 1380°C in this system:

$YSr_2Cu_3O_w$, as an example, is obviously a structural analogue [138, 302] of the known superconductor {*P4/mmm*; 379.5, 1141} [302]. At somewhat lower oxygen pressures, an orthorhombic version appears [138]. The compound could not, however, be obtained completely phase pure. Due to the nature of the synthesis procedure, the stabilization of the phase by Cl or K and/or by CO_2 from the chemical environment cannot be excluded.

In the La(O)–Sr(O)–Cu(O) system, a treatment by high-pressure oxygen at high temperatures is reported [292] to increase the oxygen content of several of the quaternary phases. Another effect is to extend the range of solid solutions formed by acceptor substitutions, which would otherwise tend to create oxygen vacancies and destabilize the structure. As an example for the latter, the $La_{1-x}Sr_xCuO_3$ perovskite has been obtained recently for up to $x=0.25$ in a two-step solid-state synthesis, where $KClO_3$ was added in the second step to obtain full oxygen occupancy under treatment in the belt-type apparatus at 7 GPa and 1000°C. The composition corresponds to a valence of copper well above +III [303].

High pressures. High-pressure syntheses have been essential for obtaining superconductivity in the t-$SrCuO_2$ perovskite which contains the infinite sheets of copper oxygen squares. Electron doping by a Nd substitution $(Sr_{1-y}Nd_y)CuO_2$ with $0.14<y<0.16$ was the other necessary key to superconducting properties [190]. A solid solution series with $0.00<y<0.12$ was identified to form at 3 GPa. Variants with RE=La to Er have been obtained in anvil-type cells under pressures up to 7 GPa at temperatures around 1000°C [304, 305].

RE,RE′(O)–Sr(O)–Cu(O) systems

Solid solutions of Sr in the T^* phases are widely studied as means of hole doping and for fine tunning and stabilizing the T^* phases (the $(La_{1-x}RE_x)_2CuO_{4+w}$ type, see Sec. III C). The Sr-substituted T^* phases cover a wide variety of RE combinations, RE=Sm, Eu, Gd, Tb, Dy, and Y as compared to only Tb and Dy without Sr substitution [306]. Other REs than La are also stabilized by the Sr substitution at the RE site, and $(Nd,Sr,Ce)_2CuO_4$ was actually the first T^* phase observed and found superconducting [307]. There is no oxygen excess detected in the Sr-substituted samples (3.99 per formula) [306], and the attainable oxygen deficiency is also very low, corresponding to some 0.03 per formula unit between 1000°C and ambient temperature [306]. An ordered distribution of the metal atoms between the non-equivalent sites is observed [308, 309], with the larger REs and Sr preferring the site between the pyramid apices (resembling hence the T phase) and the smaller REs preferring the site between the pyramid squares (resembling hence the T phase).

Owing to similarity of the REs, new phases appear rarely as a consequence of addition of RE′ into the system. A notable exception is when tetravalent Ce is introduced. Phases with structures combining the layered cuprate features with the fluorite arrangement pertinent to CeO_2 are then formed for combinations of RE and RE′=Ce, which conform with the cuprate network:

$RESr_2Cu_3O_7(CeO_2)_2$, containing double fluorite units (see Sec. II B) which are interleaved with the cuprate triperovskite layers (see Sec. IV C 1) [310]. As an example: $(Ho_{0.33}Ce_{0.67})_3Sr_2Cu_3O_{11}$ {*P4/mmm*; 382.4(1), 1722(1)}.

C. Systems RE(O)–Ba(O)–Cu(O)

Owing to the extent of the data for these systems, subsolidus phase relationships and identification of the encountered structures are treated in this section. Details on the redox and x–t equilibria will follow separately, devoted to the $YBa_2Cu_3O_7$-based systems in Sec. V B. For the subsolidus phase descriptions, REs are divided into two groups, according to ionic size.

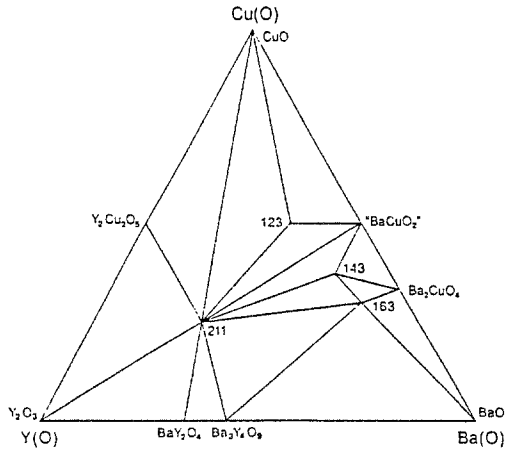

Fig. 31 Subsolidus Y(O)–Ba(O)–Cu(O) phase diagram at 900°C in oxygen at ambient pressure; compiled from Refs [105, 311, 312], with special attention on avoidance of oxide carbonates

1. Small REs

Moderately oxidizing conditions. As a starting point for the description of the phases encountered for RE=Dy, Ho, Er, Tm, Yb, and Y, the situation for RE=Y at $p_{O_2}=100$ kPa and 900°C is presented in Fig. 31. The diagram is based on data [105, 311, 312] selected with particular attention on phase-identification problems occurring when oxide carbonates may appear in the picture. A consensus appears in the copper- and yttrium-rich portion among the numerous diagrams published for Y [77, 313–322] and other REs from this group: RE=Dy, [322, 323], RE=Ho, RE=Er [209], RE=Tm [324] and RE=Yb [325]. Large discrepancies occur, however, in the Ba-rich region. The phase diagram for the RE=Lu system is different also in the Cu-rich region [325]. Four quaternary oxides are included in Fig. 31:

o-RE_2BaCuO_5, adopted for all trivalent REs smaller than Sm (inclusive) [326], represents a typical stoichiometric compound with very low electrical conductivity. The oxide of bright green colour has isolated square-pyramidal cuprate anions in the crystal structure [311, 327, 328] {Y_2BaCuO_5; *Pbnm*; 713.35(6), 1217.63(6), 565.90(4)} [311]. For a Cu(II) compound, Y_2BaCuO_5 is extremely stable. It melts incongruently at 1270°C [329], and the proclaimed [330] phase transition at 1265°C is nothing but a decomposition into solid Y_2O_3 and melt. Considering the structurally fixed Cu valence of this compound, practically no homogeneity limits for aliovalent substitutions should occur. The suggested [331] substitution of Cu for Y in Y_2BaCuO_5 is unlikely, and, since the expected three-phase mixture appears at higher temperatures, it could rather indicate a formation of an intermediate oxide carbonate from the carbonate starting materials used.

$YBa_4Cu_3O_{8.5+w}$ is formed by Sm and all smaller REs [332]. This mixed-valence compound has crystal structure [333] already encountered in Sec. III B for the Ca-version (replacing Y) {$YBa_4Cu_3O_{9.2}$; $Pm\bar{3}$; 810.2} [105]. The oxygen content is variable depending on temperature and partial pressure of oxygen. After oxidation in ambient oxygen at 320°C, $w=0.7$ is reached [105], whereas quenching from 1000°C results in $w=0$ [333]. The $YBa_4Cu_3O_{8.5+w}$ phase is formed readily from nitrate precursors, while an unsuccessful synthesis is reported [333] from carbonates. However, above 960°C in pure O_2, the carbonate route is possible, but the system is close to melting [94]. These facts give confidence that this phase is not an oxide carbonate.

$REBa_6Cu_3O_{10+w}$, seen formed for Sm and smaller REs [332], has not yet been appropriately characterized. This compound appears close to the composition where an oxide carbonate solid-solution region occurs (see Sec. IV E). The conditions for syntheses are generally very demanding in this Ba-rich area owing to the high basicity of BaO, and strict precautions must be adopted to maintain CO_2-free conditions [334]. The crystal structure is proposed [334] to be of an orthorhombically distorted Ruddlesden-Popper type, i.e., corresponding to the formula $Ba_3(Cu_{0.75}Y_{0.25})_2O_{7-w}$. The shared crystallographic site between Cu and Y represents a somewhat disturbing feature of this model, since this is normally not attained above a 2% level even for the smallest RE=Sc in $YBa_2Cu_3O_7$ [335] and not found for the related RE cuprates of the single K_2NiF_4 type. In a positive sense, however, this could be explained away as a structural ordering. This phase is reported in Ref. [332] to have a considerable variation in oxygen content; e.g., being obtained from $YBa_6Cu_3O_{10.2}$ {*I4/mmm*; 398.1(8), 406.5(8), 2211(1)} to $YBa_6Cu_3O_{11.0}$ {400.4(4), 411.1(4), 2158.5(8)}.

$REBa_2Cu_3O_{6+w}$ is formed for all REs except Lu and the typically tetravalent Ce and Tb [325, 335, 336]. Also the end members of this series require specific precautions for the synthesis: For RE=Yb, the temperature must be lowered in order to prevent decomposition [94]. The variants with RE=Nd, Pr and La can only be obtained upon ceramic syntheses at low partial pressures of oxygen and at temperatures between 850 and 875°C [337]. The fully oxygen saturated version can then be obtained by the standard oxygen treatment at lower temperatures. Normal firing procedure would otherwise lead to a replacement of a portion of Ba by these large RE atoms [335].

As a representative example, the crystal structure of $YBa_2Cu_3O_{6+w}$ contains cuprate triperovskite layers formed by linear ($w=0$) or square-planar ($w=1$) coordinations connecting two layers of corner-sharing square pyramids, much like in a sandwich. Upon variation in the oxygen content, the crystal symmetry switches from tetragonal [338–341] for the reduced version {$YBa_2Cu_3O_{6.00(5)}$; *P4/mmm*; 385.83(1), 1182.53(8)} [105] to orthorhombic [341–343] for the oxidized version {$YBa_2Cu_3O_{6.95(2)}$; *Pmmm*, 381.87(3), 388.59(3), 1167.95(11)} [105]. For details on the structural parameters as functions of oxygen content w, see PND studies in Refs [340–342] (Ref. [341] performed on single crystals.) Structural details as functions of temperature are studied in Refs [338, 344], as functions of pressure in Ref. [345] (hydrostatic) and Ref. [346] (calculated, both hydrostatic and uniaxial). Detailed unit-cell parameter data as a function of composition are also provided, e.g., in Refs [347, 348]; as a function of temperature (thermal expansion) in Refs [347, 349]. Small deviations from the ideal symmetry are discussed in Refs [344, 350]. For systematic determinations of the structure data for all $REBa_2Cu_3O_{6+w}$ phases over the entire series, see the PND studies in Ref. [351] (oxygen saturated, however, the RE for Ba substitution for RE=Nd, Pr and La vide supra is neglected).

The maximum oxygen content of $YBa_2Cu_3O_{6+w}$ is $w = 0.96(2)$ and is reached in ambient oxygen at a relatively low temperature of some 310°C [217]. For details on models for the oxygen equilibria and diffusion, see Sec. V C. Since the deoxidation of this phase can be induced thermally, an orthorhombic to tetragonal transition is observed upon heating of the fully oxidized version [311, 338], depending also on the O_2 pressure [347, 352]. This transformation into the tetragonal structure is, however, a combined result of the thermally induced deoxidation and a thermally induced disorder concerning the fraction w of the oxygen atoms [353]. The oxygen content when the transition occurs ($w_{o,t}$) is therefore not constant and increases with the temperature of the transition. For the interval of $823 < T_{o,t} < 973$ K, a linear approximation is valid [352]:

$$w_{o,t} = 0.152 + 0.483 \cdot 10^{-3} T_{o,t} \quad (5)$$

when $T_{o,t}$ is being increased by higher oxygen pressure (in Pa, for $714 < T_{o,t} < 1000$ K, calculated from data in Ref. [349]):

$$\log_{10} p_{O_2} = 14.87(70) - 9734(609)/T_{o,t} \quad (6)$$

This is one of the reasons why orthorhombic or tetragonal samples can be obtained for the same w in the interval of some $0.25 < w < 0.4$, depending on synthesis conditions [340, 342, 354]. Below some 300°C, an additional slow ordering of the oxygen atoms and vacancies occurs for $w \approx 0.5$, as documented using TEM techniques [355–359] and X-ray [360] or neutron diffraction [361, 362] on single crystals. Rapidly quenched oxygen-deficient samples undergo subtle changes even at room temperature [363]. Formation of an ordered orthorhombic phase, denoted OII, has first been proposed from physical properties and theoretical calculations [364–366]. The superstructural model for the OII phase with $w = 0.5$ involves alternation of the square-planar "chains" and rows of the linear coordinations at Cu [360]. The corresponding phase diagram is usually created by computational modelling [367, 368], and the combined phase properties are illustrated in Fig. 32, based on Refs [342, 347, 367, 369, 370].

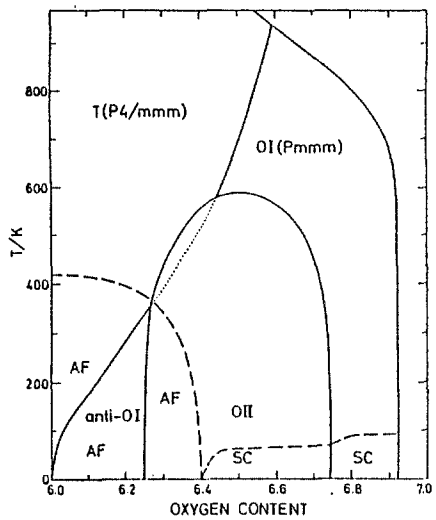

Fig. 32 Low-temperature w–T diagram for $YBa_2Cu_3O_{6+w}$, constructed from data for OII/OI [367], AF [369], SC [354] and o/t [347] transitions

Highly oxidizing conditions. As seen in previous sections, highly oxidized cuprates of AE or RE are formed in oxygen at moderate temperatures or under high pressures, and similar situation may be expected in the pseudoternary field in question. The phase diagram as seen in pure oxygen around 800°C, compiled from experimental (synthesis) data based on reactive [105] and/or carbon free [175, 312, 371] precursors, is shown in Fig. 33. One additional quaternary oxide is seen:

$REBa_2Cu_4O_8$, has crystal structure [372, 373] quite analogous to the previous phase, except that it contains double Cu–O squares, which are appended into chains through a zigzag edge-sharing. These chains appear instead of the simple corner-sharing chains in the related $YBa_2Cu_3O_7$-type structure {$YBa_2Cu_4O_{7.995}$; *Ammm*; 384.3(1), 387.0(1), 2725.0(5)} [105]. The edge-sharing of the coordination squares makes the oxygen content structurally

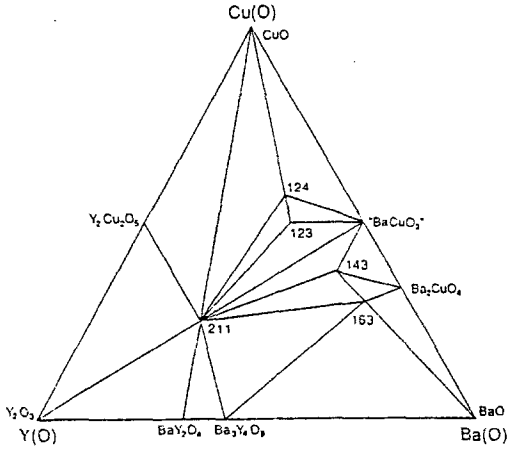

Fig. 33 Subsolidus Y(O)–Ba(O)–Cu(O) phase diagram at 800°C in oxygen at ambient pressure; after Refs [105, 175, 312, 371]

fixed and this highly oxidized phase is hence less thermally stable [374]. Although it was obtained originally at high pressures [375], $YBa_2Cu_4O_8$ can be prepared at some 820°C from atomic-mixed carbonate starting-materials in purified oxygen [376, 377], and also nitrate [378] and (123 + CuO) [379] routes are described. In an oxygen atmosphere at ambient pressure, $YBa_2Cu_4O_8$ decomposes above 840°C into CuO and $YBa_2Cu_3O_{6.44}$ [380]. Note the low oxygen content for the latter phase, which is of significance for the pressure-stability relationships. The structural building principle of this phase can be generalized into a struc-

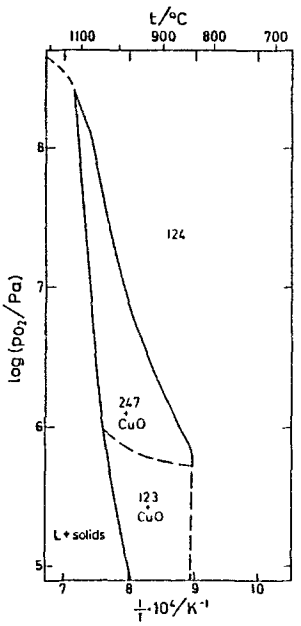

Fig. 34 A p–t diagram for the 124 ($YBa_2Cu_4O_8$) composition; after Refs [386, 388]

tural series having increasing content of Cu and also a rapidly decreasing stability [381]. As an example, thermodynamic prediction of existence conditions for $YBa_2Cu_5O_9$ gives a stability limit of 470°C in ambient oxygen [382]. Also a structural combination between the 124 and 123 phases is possible:

$RE_2Ba_4CuO_{14+w}$, with crystal structure [383] being a combination of the $YBa_2Cu_3O_7$ and $YBa_2Cu_4O_8$ arrangements {$Y_2Ba_4Cu_7O_{15}$; *Ammm*; 385, 387, 5030}. In accordance with this, there occurs a homogeneity range of some $0.0 < w < 1.0$ with respect to the oxygen content [384–386]. This phase can be formed by deoxidation of $YBa_2Cu_4O_8$ at elevated oxygen pressures in a narrow temperature range above 900°C [386], and also appears briefly around 885°C in ambient oxygen [387]. An equilibrium p–t diagram is experimentally determined [386, 388] for the nominal 124 composition and oxygen pressures up to 300 MPa, showing regions of stability for the solid phases involved, 124, 247 and 123 (Fig. 34). Similar stability fields have also been obtained by calculation from thermodynamic data derived from calorimetry, EMF measurements and equilibration procedures [380, 389].

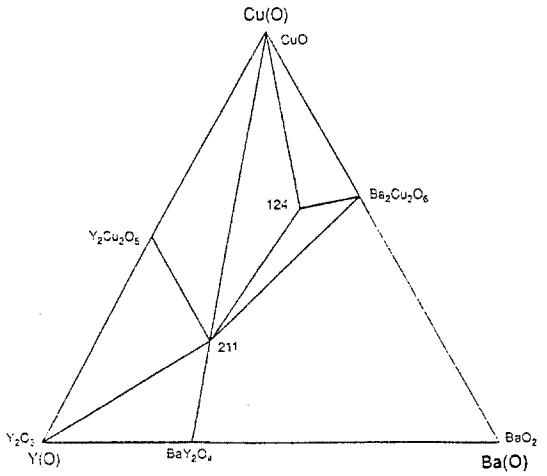

Fig. 35 Subsolidus Y(O)–Ba(O)–Cu(O) phase diagram at 1000°C in oxygen under p_{O_2}=9 MPa; after Ref. [178]. Ba-rich region is omitted

The RE(O)–Ba(O)–Cu(O) system changes profoundly when exposed to high oxygen pressures (Fig. 35) [178]. Under an oxygen pressure of 9 MPa at 1000°C, $YBa_2Cu_3O_{6+w}$ becomes unstable against decomposition into the more oxidized and now stable phase $Ba_2Cu_3O_{6+w}$ (plus 124 and 211). The $YBa_2Cu_4O_8$ phase, which has structurally fixed high oxygen content, is promoted in stability by high oxygen pressure.

Even more than the diagrams for ambient-conditions, the published results for high oxygen pressures [178, 235] show considerable disagreement about the Ba-rich corner, which is therefore excluded in Fig. 35. Several phases have been suggested seen, but the claims do not withstand the scrutiny of excluding the possibility that they are in fact oxide carbonates, formed in the closed systems from traces of carbonate in the starting materials and/or CO_2 in the (compressed) atmosphere. As another example, a failed attempt to prepare $YBa_4Cu_3O_{8.5+w}$ at high O_2 pressures, contrasted by the finding that it persists (100 h) at the same conditions, when first synthesized at ambient pressure [178], illustrates another problem of the studies at high oxygen pressures. The experimental points in the recorded phase

diagrams are often obtained starting from binary oxides instead of using amorphous precursors, and actually performing the syntheses under the high oxygen pressure conditions instead of cross-checking both the formation and stability of the products.

Similar problems are encountered when the isothermal phase systems are investigated in ambient atmospheres at temperatures lower than the thermodynamic firing temperatures from carbonaceous precursors. Below some 700 to 800°C the difficulties are so severe that the phase diagrams are rather constructed by calculation from measured thermodynamic data. High-accuracy, high-temperature solution calorimetry [154, 390, 391] is commonly used. Such data are also simulated for existing or even hypothetical compositions [392–396]. Unfortunately, unavailable structural and compositional definitions for some of the variable-valence phases, rather than the error margins, seem to be at the root of the problem. This concerns in particular $Ba_2Cu_3O_{6-w}$, as discussed, e.g., in Refs [1, 397]. Nevertheless, the calculations (referring to oxygen at ambient pressure) are quite consistent in showing that the highly oxidized phases indeed become more stable upon lowering the temperature (corresponding to the increased oxidation effect), and that they occur at the expense of the phases which have lower Cu-valence under the given conditions. According to Refs [390, 175], $YBa_2Cu_3O_{6+w}$ and Y_2BaCuO_5 become unstable under some 650 to 750°C *vs.* formation of $Ba_2Cu_3O_{6-w}$ and Y_2O_3 and Ba_2YO_4. Ultimately, the most oxidized phase, $Ba_2Cu_3O_{6-w}$, becomes stable next to binary oxides and BaO_2, as calculated for 25°C. However, none of these reactions can actually be observed due to kinetic hindering. As an example for the calculated isothermal phase diagrams, Fig. 36 shows the situation at 700°C.

Reducing conditions. Upon decreasing partial pressures of oxygen, or increasing temperature, the analogous principle to the above governs the phase stability in the subsolidus region. Phases with low valence of copper like Cu_2O, $BaCu_2O_2$ and $YCuO_2$ become stable, until the most reduced phase emerges, elemental Cu, coexisting with Y_2O_3, BaO and the binary Y,Ba oxides [1, 105]. The isothermal subsolidus reduction has been attempted for the Y- and Cu-rich portion of the Y(O)–Ba(O)–Cu(O) system and the phase stabilities, mapped upon *p,t*-equilibrations combined with EMF measurements [398], are shown in Fig. 37. For details on the course of the reduction of the 123 phase, see Sec. V B.

High pressures. Phase equilibria in the Y(O)–Ba(O)–Cu(O) system at 950°C under 1 MPa pressure were investigated [399] using a piston-cylinder-type apparatus and SEM analyses. The Y- and Cu-rich portions of the thus established phase diagram are identical

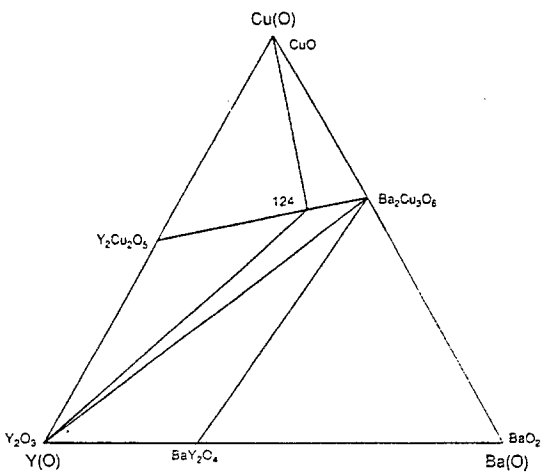

Fig. 36 Subsolidus Y(O)–Ba(O)–Cu(O) phase diagram at 700°C in oxygen at ambient pressure calculated from thermodynamic data; after Ref. [175]. Ba-rich region is omitted

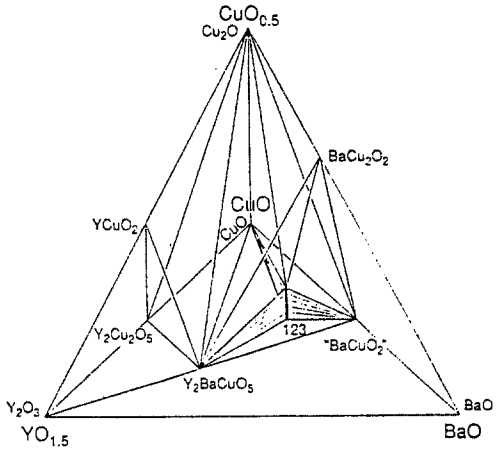

Fig. 37 Isothermal $YO_{1.5}$–BaO–CuO–$CuO_{0.5}$ diagram at 950°C; after Ref. [398]. $YO_{1.5}$, BaO, and CuO form the base of the tetrahedron. The presence of L close to "$BaCuO_2$" and the small oxygen-solubility range of the latter phase are disregarded. Ba-rich region is omitted

with the situation seen at 900°C in ambient oxygen (Fig. 31), whereas the rest of the diagram suffers with formation of oxide carbonates. The 124 phase is not found in Ref. [399], and it would be interesting to see whether this can be rationalized by the fact that the molar volume of 124 is larger than the sum of molar volumes of CuO and $YBa_2Cu_3O_{6+w}$ for any w.

2. Large REs

In order to outline the development of the phase and structure stabilities along the line of the increasing size of the trivalent RE ions, the phase diagrams and the descriptions of the newly appearing phases in this entire section will follow the said order.

RE=Gd and Eu. For all larger RE(III)s than Gd, the o-$Y_2Cu_2O_5$-type cuprate is no longer stable. However, for RE=Gd and Eu, the pseudoternary RE(O)–Ba(O)–Cu(O) field (at say, 950°C in ambient oxygen) remains similar to that for smaller REs in that there still occurs a tie line between 211 and CuO [209]. An example for such a diagram, compiled for RE=Eu from phase diagrams in Refs [400, 401] and other data in Refs [80, 332, 334] for 950°C and oxygen atmosphere, is shown in Fig. 38.

One very important distinction occurs for the large REs in the $YBa_2Cu_3O_{6+w}$-type structure, in that certain occupancy distribution of RE is allowed over the RE and Ba sites: $RE(Ba_{1-y}RE_y)_2Cu_3O_{6+w+y}$, is hence a solid-solution range which is appended or close to the 123 composition [402]. It is derived by a simple replacement of some Ba in the 123 structure by the RE atom. The extent for the solid solubility of RE at the Ba site increases towards the group of the four largest trivalent RE atoms, $y \leq 0.10$, 0.25, 0.30, 0.33, 0.35 and 0.26 for RE=Gd, Eu, Sm, Nd, Pr and La, respectively, referring to 950°C and air atmosphere [209, 401, 403, 404]. These data are not easy to establish precisely, since, upon the possible formation of a related oxide carbonate phase (Sec. IV E), the solid-solubility limits are substantially increased [78]. Also the lower limit of solid solubility varies as a function of the increasing RE size. Beginning with Nd, the RE site (located between the cuprate layers) will not accommodate the atom concerned unless some RE is simultaneously present at the Ba site inside the cuprate network. This is manifested by the appearance of a non-zero lower limit of homogeneity (y) [335, 402]. When the $REBa_2Cu_3O_{6+w}$ nominal compositions (having therefore $y=0$) are attempted synthesized for RE=Nd, Pr and La in pure oxygen and fired at 910°C

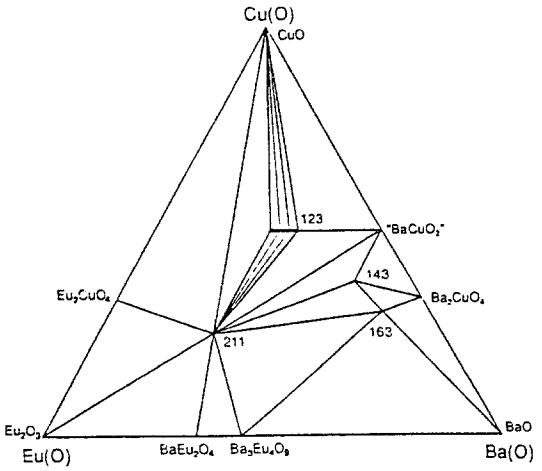

Fig. 38 Subsolidus Eu(O)–Ba(O)–Cu(O) phase diagram at some 950°C in oxygen at ambient pressure. Compiled from Refs [80, 332, 334, 400, 401] with special attention on avoidance of oxide carbonates

until no further change in the products occurs, $RE(Ba_{1-y}RE_y)_2Cu_3O_{6.96+y}$ is formed instead, with $y=0.030(5)$, 0.05(1), and 0.09(2) for RE=Nd, Pr and La, respectively [335]. In contrast to these oxygen-saturated samples, the reduced version of 123 is able to fully accommodate Ba and large RE separately at their sites [337]. Generally, the replacements of the trivalent RE for divalent Ba result in an almost proportional increase in the attainable oxygen content (ambient oxygen pressure), which may then exceed seven per formula unit [335]. The formal Cu valence decreases only slightly, being defined by the degree of the electropositive character of the "cations" as counterparts to the poly-cuprate "anions". The symmetry of the crystal structure as a function of the substitution y and the oxygen content w is governed by the order/disorder situation in the square-planar coordinations around Cu(1). Both the accommodation of the relatively small RE atoms at the Ba site and either increase or decrease of the oxygen content from 7 per formula act in the direction of disorder at Cu(1), i.e., a tetragonal symmetry for the phase. The combined effects of the variations in y and w on the unit-cell parameters (e.g., for Sm [404]) result hence in an orthorhombic envelope, centered at $y=0$ and $w=1$, similar to that determined in Ref. [405] for the La for Ba substitution in 123. Several specific examples illustrating these relationships may be mentioned. At the lower limit of solid solubility, the crystal structure of the oxygen saturated $RE(Ba_{1-y}RE_y)_2Cu_3O_{6+w+y}$ phases is orthorhombic {$Nd(Ba_{0.97}Nd_{0.03})_2Cu_3O_{6.99(1)}$; *Pmmm*; 386.14(5), 391.60(8), 1175.1(2)}, except for the La version, where this limit is so high that the phase already is tetragonal [335]. An increase in y switches also the oxygen saturated variants with Eu, Sm, Nd, and Pr to tetragonal symmetry [104, 402, 404, 406]. As an example: $Nd(Ba_{0.8}Nd_{0.2})_2Cu_3O_{7.19(1)}$ {*P4/mmm*; 387.4(3), 1165.9(4)} [406]. The *p–t–y–w* equilibria governing the formation of the $RE(Ba_{1-y}RE_y)_2Cu_3O_{6+w+y}$ solid solutions were studied for RE=La [407] and Nd [408] and evaluated in terms of appropriate thermodynamic models.

At lower temperatures or higher oxygen pressures, the 247 and 124 phases will appear in the RE=Gd, Eu, Sm, Nd and Pr systems [409–412], e.g., $EuBa_2Cu_4O_8$ {*Ammm*; 387.6(6), 389.4(6), 2721(4)} [413]. The stability regions for the 124 and 247 phases become narrower with increasing size of RE [414]. The Pr variant can only be obtained under rather specific high-pressure conditions, but retains all the structural [412] features of the

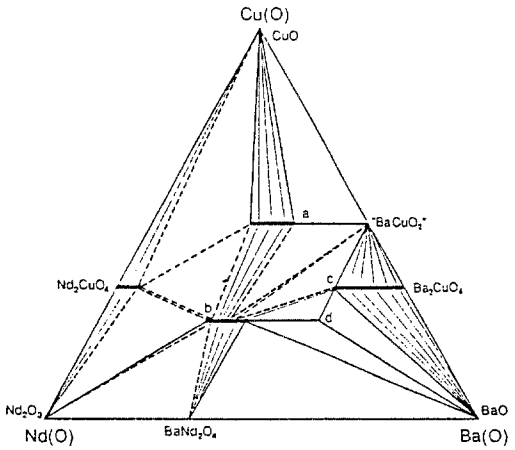

Fig. 39 Subsolidus Nd(O)–Ba(O)–Cu(O) phase diagram at some 950°C in oxygen at ambient pressure. Compiled from Refs [94, 104, 105, 228, 332, 415, 416] with special attention on avoidance of oxide carbonates. Phase designations: a – $Nd(Ba_{1-y}Nd_y)_2Cu_3O_{6+w+y}$ ($0.03<y<0.33$) [104, 335, 470]; b – $(Nd_{1-x}Ba_x)_2BaCuO_5$ ($0.00<x<0.15$) [94, 420]; c – $(Ba_{1-y}Nd_y)_2CuO_{3+w+y}$ ($0.06<y<0.25$) [332]; d – $Nd_2Ba_4Cu_2O_9$ [422]

prototype, including the oxygen content {$PrBa_2Cu_4O_8$; *Ammm*; 388.59(1), 390.31(1), 2732.06(7)}.

RE=Sm. Upon the increasing size of REs, Sm is the last to form the 143 and probably also the 163 phase [332]. However, obtaining any conclusive data for these Ba-rich phase requires strong precautions against the oxide carbonate formation and that involves also exclusion of $BaCO_3$ as the starting material for the solid-state synthesis.

RE=Nd. A tentative phase diagram for the Nd(O)–Ba(O)–Cu(O) system is selected here from phase diagrams in Refs [104, 228, 415, 416], and other data in Refs [94, 105, 332], and is shown in Fig. 39. One principial difference occurs, compared with the Eu (and smaller REs) case, in that the o-RE_2BaCuO_5 structure no longer is stable, and another phase with similar composition is formed instead:

t-$(RE_{1-x}Ba_x)_2BaCuO_5$, a brown oxide (cf. the green Y_2BaCuO_5) with a homogeneity range [94] of $0.00<x<0.15$ and crystal structure [417–419] having isolated square-planar cuprate anions. As an example: the phase for RE=Nd at the homogeneity limits; Nd_2BaCuO_5 {*P4/mbm*; 669.80(2), 582.10(2)}, and $(Nd_{0.85}Ba_{0.15})_2BaCuO_5$ {670.36(5), 582.19(4)} [94]. This phase is formed for Nd and the larger REs [105]. For RE= La, one observes an analogous (converse) size effect to the Ba–RE occupation discussed above, in that the phase exists with a full occupation at the Ba site only when Ba is partially present at the La site. The range of homogeneity does not include $x=0$, and extends from $x=0.04$ {$(La_{0.96}Ba_{0.04})_2BaCuO_5$; *P4/mbm*; 685.64(5), 587.37(6)} [94] to $x=0.4$ [420]. The instability of the "stoichiometric" composition has apparently confused the structural description in Ref. [417] and led to the rather complicated formula $La_{4-2x}Ba_{2+2x}Cu_{2-x}O_{1-2x}$ for this phase. Also the 311 formula, proposed [104] for this 211 phase, must be originating from a misjudgement of these solid-solution features.

A significant solid solubility for the large REs at the Ba site is seen also in the Ba_2CuO_{4-w}-type structure. Up to $y=0.25$ of the Ba atoms can be replaced by Nd in $(Ba_{1-y}Nd_y)_2CuO_{4-w}$ [415]. When quenched from 950°C, the series with increasing y exhibits a crystal symmetry

switch at around $y=0.05$, from the original high-temperature tetragonal symmetry (pertinent to the parent phase) to the orthorhombic symmetry, which is normally adopted by the more oxidized low-temperature version of Ba_2CuO_{4-w} [415]. The reason for this behaviour is that the oxygen atoms necessary for this transition are supplied by the RE substitution for Ba. A similar situation is seen also for RE=La [421], except for higher solid-solubility limit (up to $x=0.33$) and a possible gap emerging between $x=0.025$ and 0.125 (950°C), which separates the just mentioned tetragonal and orthorhombic solid solutions.

One additional phase is found [415] in the Ba-rich region of the Nd(O)–Ba(O)–Cu(O) system, under synthesis conditions strictly excluding any CO_2 or carbonates from the reaction environment:

$Nd_2Ba_4Cu_2O_9$, with tetragonal crystal structure [422] {$P\bar{4}n2$; 1207.2, 387.4}, containing corner sharing cuprate square-pyramids connected into chains. In the RE=La system, this phase apparently disappears under occurrence of one broad homogeneity region of the $(RE_{1-x}Ba_x)_2BaCuO_5$ type.

RE=Pr. The Pr(O)–Ba(O)–Cu(O) system [104, 423] has features very similar to the RE=Nd analogue, and Pr behaves approximately as a trivalent RE in the phase system under ambient [335] and low [423] oxygen pressures. Of the quaternary phases, only the 211 phase is not formed, and the $BaPrO_3$ perovskite dominates the region instead, still stable at $p_{O_2}=10$ Pa [423].

RE=La. The La(O)–Ba(O)–Cu(O) phase diagram at 950°C in oxygen is shown in Fig. 40, compiled from phase diagrams in Refs [279, 420, 424] and other data from Refs [94, 332, 335, 421, 425]. In addition to the already discussed features, two additional phases emerge for the largest and most electropositive RE=La:

$BaLa_4Cu_5O_{13+w}$, is an ordered, oxygen-deficient perovskite with $a=a_p\sqrt{5}$, containing a network of octahedral and square-pyramidal cuprate coordinations [425]. The oxide is a metallic conductor but no superconductivity is reported. The oxygen saturated phase of tetragonal symmetry [425] has a rather high copper valence {$BaLa_4Cu_5O_{13.16}$; $P4/m$; 864.75(1), 385.94(1)} and the oxygen content decreases only slightly ($-0.2<w<0.16$) with tempera-

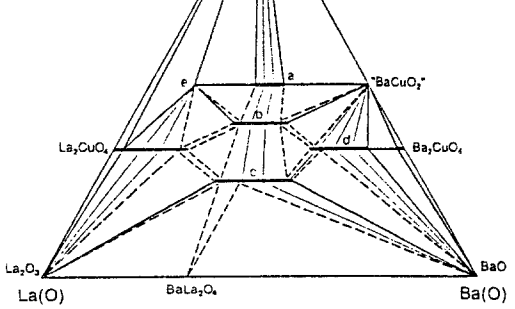

Fig. 40 Subsolidus La(O)–Ba(O)–Cu(O) phase diagram at some 950°C in oxygen at ambient pressure. Compiled from Refs [94, 279, 332, 335, 420, 421, 424, 425] with special attention on avoidance of oxide carbonates. Phase designations: a – $La(Ba_{1-y}La_y)_2Cu_3O_{6+w+y}$ ($0.09<y<0.26$) [94, 335]; b – $(La_{1-x}Ba_x)_2BaCu_2O_{6+w}$ ($0.10<x<0.40$) [279]; c – $(La_{1-x}Ba_x)_2BaCuO_5$ ($0.04<x<0.40$) [94, 420]; d – $(Ba_{1-y}La_y)_2CuO_{3+w+y}$ ($0.12<y<0.33$) [332]; e – $BaLa_4Cu_5O_{13}$ [426]

ture increasing up to 1015°C at ambient oxygen pressure [426]. At low oxygen partial pressures and high temperatures, the oxygen content can be varied between $-0.5 < w < 0.16$ without a bulk decomposition into Cu and La, Ba oxides [426]. However, when the oxygen content is varied in contact with a hydrogen-containing atmosphere at temperatures lower than 400°C, the oxygen content can be further reduced (to $w = -2.0$) upon formation of structural variants with, inter alia, linear Cu(I) coordinations in the still intact matrix of metal atoms [426, 427], e.g., $BaLa_4Cu_5O_{12}$ {*P2/m*; 890.1(2), 377.1(2), 869.1(2), 88.60(2)}. All these reduced compounds can be reoxidized into the oxygen saturated structure [426]. Thermodynamics of the oxygen-exchange reaction is investigated in Ref. [428].

$(La_{1-x}Ba_x)_2BaCu_2O_{6+w}$, with $0.1 < x < 0.4$ [279], is of the Ruddlesden-Popper-type structure, analogous to the Sr variants described in Sec. IV B.

3. Two REs

The presence of two REs does not usually bring enough difference in size and bond peculiarity to promote a new structure type. Instead, wide solid-solution ranges emerge within the structure types of the quaternary oxides.

The 123-type solid solutions. At conditions defined by firing at 910°C in a pure oxygen atmosphere and subsequent oxygen saturation at 340°C, full mutual miscibility occurs at the RE site of $REBa_2Cu_3O_7$ for RE = Y in combination with RE′ = Yb–Dy, Gd, Eu and Sm [335, 429–433]. Less compatibility is found for the potentially tetravalent Ce and Tb, whose solid solubility at the Y site does not exceed a few per cent for Ce and less than 25% for Tb [94, 335]. Substitution of Y by the smallest lanthanide Lu is limited [434] and occurs up to some 30% [335]. For the large Nd, Pr and La atoms, an equilibrium distribution between the Y and Ba sites exists. This implies that Nd and larger REs will not enter solely the Y site unless some RE also finds its way to the Ba site [402]. When a partial or complete replacement of only Y is attempted by Nd and larger REs, the "$BaCuO_{2+w}$" phase is formed to tie up the amount of Ba which has been replaced by RE [335]. On the other hand, only La is large enough to participate at the Ba site alone, up to $y = 0.36(2)$

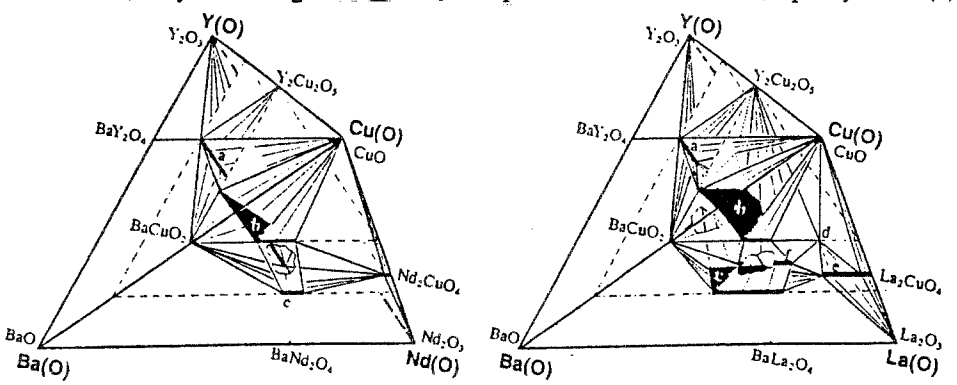

Fig. 41 Subsolidus (pseudoquaternary) tetrahedral phase diagrams of the Y(O)–Nd(O)–Ba(O)–Cu(O) and Y(O)–La(O)–Ba(O)–Cu(O) systems at 900°C in oxygen, covering the neighbourhood of the $YBa_2Cu_3O_{6+w}$-type phase and the Cu-rich corner; after Refs [105, 435]. Phase designations: a – $(Y_{1-x}RE_x)_2BaCuO_5$ (RE = Nd: $0.00 < x < 0.85$; RE = La: $0.00 < x < 0.30$) [105, 435]; b – $(Y_{1-x}RE_x)(Ba_{1-y}RE_y)_2Cu_3O_{6+w+y}$ (RE = Nd [104, 335, 470]: $y = 0.0$ for $x = 0$ and $0.03 < y < 0.33$ for $x = 1$; RE = La [94, 335, 435]: $0.0 < y < 0.36$ for $x = 0$ and $0.09 < y < 0.26$ for $x = 1$); c – $[(RE_{1-x}Ba_x)_{1-x'}Y_{x'}]_2BaCuO_5$ (RE = Nd: $0.00 < x < 0.15$ for $x' = 0$ and $0.0 < x' < 0.05$ for $x = 0$; RE = La: $0.04 < x < 0.40$ for $x' = 0$ and $0.0 < x' < 0.15$ for $x = 0$) [94, 105, 420]; d – $BaLa_4Cu_5O_{13}$; e – $(RE_{1-x}Ba_x)_2CuO_4$ (RE = Nd: $0.0 < x < 0.05$?; RE = La: $0.0 < x < 0.15$?); f – $(La_{1-x}Ba_x)BaCu_2O_{6+w}$ ($0.10 < x < 0.40$) [279]

[335, 435]. When the just mentioned critical concentration is exceeded, a substitution of Y by La also occurs, and $Y_2Cu_2O_5$ appears as a second phase. This situation and the relative difference between the size effect of Nd and La is illustrated in the selected parts of the tetrahedral diagrams [105, 435] for the Y(O)–Nd(O)–Ba(O)–Cu(O) and Y(O)–La(O)–Ba(O)–Cu(O) systems on Fig. 41. As seen in the previous sections with similar mixed-valence solid solutions, the average oxidation state of Cu is conserved upon substitution of the trivalent RE for Ba. For the 123-type phase this means that its saturated oxygen content is increased by the value of y per formula [435]. When the oxygen content exceeds seven, the additional oxygens are accommodated at the vacant sites adjacent to the copper-oxygen squares. This also turns the originally orthorhombic structure into tetragonal when y exceeds a certain value, as a combined effect of the oxygen insertion and a structural deformation due to the partial replacement of the large Ba by the smaller RE [402, 435–438]. For example, oxygen saturated $Y(Ba_{1-y}La_y)_2Cu_3O_{6.95(2)+y}$ is tetragonal at ambient temperatures for $y>0.140(5)$ {$Y(Ba_{0.8}La_{0.2})_2Cu_3O_{7.15}$; *P4/mmm*; 385.46(2), 1156.6(1)} [435]. When the oxygen content is varied, T_c of the $Y(Ba_{1-y}La_y)_2Cu_3O_{6+y+w}$ solid solution is neither coupled to the orthorhombic feature nor to whether or not the oxygen content exceeds 7 per formula. A correlation occurs between T_c and the calculated Cu bond valence in the square-pyramidal sheets. The valence is influenced by the substitution-induced deformations of the bond lengths and by introduction of additional Cu–O bonds in the square-planar chains. Therefore, despite the constant overall Cu valence in $Y(Ba_{1-y}La_y)_2Cu_3O_{6.95(2)+y}$, T_c decreases with y. In addition, it also decreases with any reduction in the oxygen content (viz., compared with the oxygen saturated samples [405]).

The 211-type solid solutions. Extended regions of solid solubility are found [105] also between the Y_2BaCuO_5 and Nd_2BaCuO_5 phases; 85% Nd on the Y side and 5% Y on the Nd side (the corresponding figures for La as the solute being 30 and 10%, respectively). The Nd_2BaCuO_5-type structure may moreover accommodate some Ba at the RE sites, viz., up to 15% in the RE=Nd case and 4–40% for RE=La [105, 420].

The $BaCuO_2$-type solid solutions. A possibility for a minute substitution of Ba by the larger REs (Nd–La) in the "$BaCuO_{2+w}$" phase follows from observations of unit-cell volume changes for this phase in poly-phase equlibrium samples [94].

The 124-type solid solutions. As seen in Sec. IV C2, the $REBa_2Cu_4O_8$ phase favours smaller RE atoms than $YBa_2Cu_3O_7$ [414]. This means that the larger REs tend to favour the combination of 123 and CuO *vs*. 124. However, also in the 124 phase, La can partially substitute for Ba [439] and $Y(Ba_{1-y}La_y)_2Cu_4O_8$ is formed for $0.0<y<0.1$ [439, 440]. Above this limit, the reported observation of CuO could indicate that La simultaneously enters the Y site. The La substitution does not bring about any change in the oxygen content and a rapid decrease in T_c is observed [439] with increasing y. This is in line with the rigid, double-square chains of the cuprate anions.

Intermediate oxides. Genuine quintenary oxides appear rarely in the RE(O)–RE'(O)–Ba(O)–Cu(O) systems, owing to the similarity of the REs. One possibility is when the tetravalent Ce is introduced. Phases are then formed which can structurally be described as combinations of simpler structure types, supplemented with degrees of solid-state miscibility:

$(RE_{1-x}Ce_x)_2(Ba_{1-y}RE_y)_2Cu_3O_{8-w}(O)_2$, which contains slabs of corner-sharing cuprate units (with some vacancies) reminiscent of those in $YBa_2Cu_3O_7$, except that the squares in the chains are partially filled up and disordered to form octahedra [441, 442]. These $[Cu_3O_{8-w}]_n$ slabs contain a Ba,RE mixed-occupied site and are separated by fluorite-arranged layers of RE,Ce and isolated oxygen atoms, very much reminiscent of CeO_2. As an example: $(Eu_{0.67}Ce_{0.33})_2(Ba_{0.67}RE_{0.33})_2Cu_3O_{8-w}(O)_2$ {*I4/mmm*; 385.04(1), 2846.0(1)} [441]. The oxygen content corresponds to $w\approx1$ even after a high-pressure oxygen

saturation, and the formal copper valence is relatively low, but still in excess of +II [443]. The variations in the oxygen non-stoichiometry in the interval of $1.0 < w < 1.2$ have been studied in detail by coulometric titration (on a Nd variant) [444]. This structure is formed only for a narrow size-span of RE=Nd, Sm and Eu and the phases in question are superconducting with $T_c \approx 43$ K [441]. A large number of substituted variants has appeared [445–447].

Another example of new structures as a consequence of the introduction of the second RE element comes about when there is a large size difference between the (otherwise trivalent) RE elements. Thus, La and Lu, the largest and smallest lanthanoid, give rise to a new structural arrangement:

$La_2LuBa_3Cu_6O_{14+w}$, with $w \approx 0.3$ and crystal structure [448] derived from that of the $YBa_2Cu_3O_7$ type by cation ordering. The oxygen saturated phase (at ambient oxygen pressure) is tetragonal [448] {*P4/mmm*; 546.6, 1161.5} but becomes orthorhombic upon oxidation at $p_{O_2} = 5$ MPa and also superconducting with $T_c = 40$ K [448].

Also other quintenary oxides are formed with RE=La; based on other than 123 structures in the La(O)–Ba(O)–Cu(O) system:

$La_6RE'BaCu_8O_{20}$, where RE'=Y or Dy, is related to $La_4BaCu_5O_{13}$. The monoclinic crystal structure [449] contains an ordered network of cuprate octahedra, square-pyramids and squares, and is considered as a first member of a structural series. The symmetry of the structure is described in terms of subcell-supercell relations based on an orthorhombic subcell {381.4(1), 386.9(1), 385.8(1)}.

There is certainly more distinct phases to be expected upon increasing the number of components. Simultaneously, however, will their stability be only marginally distinct from the neighbouring phases and their characterization will therefore more and more rely on high-resolution methods.

D. Systems RE(O)–AE,AE'(O)–Cu(O)

RE(O)–Ca,Sr(O)–Cu(O)

Only certain significant compositions are studied in this rather specialized system. Perhaps the most interesting example has been the $La_2CaCu_2O_{6-w}$ phase, which becomes superconducting ($T_c \approx 60$ K) upon partial substitution of La by Sr [450]. The substitution increases both the Cu valence (hole-doping) and the content of oxygen vacancies $\{(La_{0.8}Sr_{0.2})_2CaCu_2O_{5.94(2)}$; *I4/mmm*; 382.08(1), 1959.93(7)$\}$ which are located at the apical sites of the square-pyramidal coordinations in the crystal structure described in Sec. IV A. A variant with Nd instead of La is also described [451].

RE(O)–Ca,Ba(O)–Cu(O)

In accordance with ionic size relations, no Ca–Ba mixing is observed. However, Ca shows solid solubility with the smaller REs, and new structures are formed in combination with the larger REs.

For obvious reasons the most studied system is that with RE=Y, where wide Ca/Y solid-solution regions occur. In the $YBa_2Cu_3O_7$ structure, Ca can replace up to 1/4 of Y. Substitutions up to $x = 0.5$ were reported when the pressure was enhanced as little as to $p_{O_2} = 400$ kPa [452]. The observation of a $BaCuO_2$-type impurity in Ref. [452] indicates a possible simultaneous Ca for Ba substitution. Facilitation of this behaviour by a formation of an oxide carbonate in the closed system is possible [78]. This would also explain the observed transition into tetragonal symmetry and shortened *c* axis.

The oxidized structure as obtained at ambient pressures after oxidation at 300°C (cf. the metastability in Sec. IV C 1) compensates for the aliovalent substitution by formation of

oxygen vacancies, according to the formula $(Y_{1-x}Ca_x)Ba_2Cu_3O_{6.95-x/2}$, and T_c is not increased [94, 453, 454]. However, when the structure is appreciably deoxygenated ($YBa_2Cu_3O_{6.1}$, non-superconducting and also tetragonal) the energy of formation for oxygen vacancies becomes higher, and the Ca substitution causes a localized hole doping at the pyramidal sheets of the cuprate anion. Hence, superconductivity reappears with low T_c [455, 456]. The structure remains tetragonal, but changes in bond distances confirm the hole doping [457].

Such a hole doping and an increase in T_c are observed [458, 459] also for the 124 phase which has a structurally fixed oxygen content. Because formation of the oxygen vacancies is not possible, all the extra charge brought about by the aliovalent substitution is accummulated within the cuprate network, thus increasing the formal Cu valence (and in turn T_c [459]). This acts *vs.* a high solid solubility of Ca at the Y site [458]. Also the stability region of the Ca-substituted 124 phase is shifted towards higher oxygen pressures and Ca-substitution vanishes entirely for the 247-type structure [458], perhaps similarly as it was decreased by the presence of the large early REs at the Y site [414]. When the substitution of Ba by Ca in 124 is attempted, appearance of some Y_2BaCuO_5, CuO and $BaCuO_{2+w}$ indicates that also (or rather) the Y site has been attacked. However, some presence of Ca at the Ba site in such samples is evidenced by NQR [460, 461]. The situation with Ca doping in 124 apparently involves an equlibrium distribution of Ca between the RE and Ba sites.

In crystal structures which allow for the necessary extent in the oxygen vacancy variation induced by the aliovalent substitution, a complete replacement of, e.g., Y by Ca is possible. One such example is $YBa_4Cu_3O_9$ [193]. A wide solid solubility is accordingly expected between the Ca and Y variants. On the other hand, only negligible Ca–Y homogeneity region applies to the stoichiometric Y_2BaCuO_5 phase.

An important example for a replacement of RE by Ca is the "$Ca(BaLa)Cu_3O_{6+w}$" superconductor [462–464] with T_c of some 80 K, which actually is a solid-solution series:

$RE_{1-x}Ca_x(Ba_{1-y}La_y)_2Cu_3O_{6+w}$, with non-zero lower limits of solubility for RE=La $0.22<x<0.5$ and $0.09<y<0.25$ [403], in the crystal structure [465] of the 123 type. The upper limits of solid solubility have integer fraction values, yet no conclusive suggestions for a structural ordering can be drawn based on TEM investigations [466, 467]. Contrary to the structural prototype $LaBa_2Cu_3O_7$ which is orthorhombic [337], the symmetry of the unit cell is tetragonal throughout the solid-solution region, e.g., $La_{0.5}Ca_{0.5}(Ba_{0.75}La_{0.25})_2Cu_3O_{7.01}$ {*P4/mmm*; 387.42(1), 1171.38(4)} [465]. The disordering on the oxygen sites leading to the tetragonal symmetry is explained [465] as compressing of the cuprate slab, in a similar manner as for the La for Ba substitution [405, 435] in the prototype structure. The variation in the oxygen content, as seen [465] in the solid-solution region after the standard treatment in oxygen under ambient pressure at 400°C, indicates two different compensation mechanisms for these two aliovalent substitutions. The substitution by Ca is compensated by formation of holes in the cuprate network, whereas the substitution by La is compensated by creation of oxygen vacancies. T_c follows the copper valence [465] in the solid-solution region. When an individual composition is deoxidized, T_c shows a similar "double plateau" behaviour as the 123 phase in Fig. 32 [468]. Since the substitution by Ca is always at least partially compensated by the presence of La at the Ba site, the oxygen content does not exceed the value of approximately 7 per formula. This probably provides the rationale for the extent of this solid-solution series, in addition to the mixed Ba–La occupancy features discussed in Sec. IV C 2 for the Ca-free version. It is interesting to note that the original "CaBaLa" formula does not correspond to single phase and accordingly lies outside the solid-solution region [469]. The extent of the solid solution is illustrated in Fig. 42, drawn into a pseudoternary phase diagram CaCu(O)–BaCu(O)–LaCu(O) and compared with the situation seen [335] when Ca in the phase diagram is exchanged with Y, having similar size, yet different valence. The reason behind this arrangement is to include the $YBa_2Cu_3O_7$ phase into the picture and illustrate the complex interplay between size and valence in formation of the triple

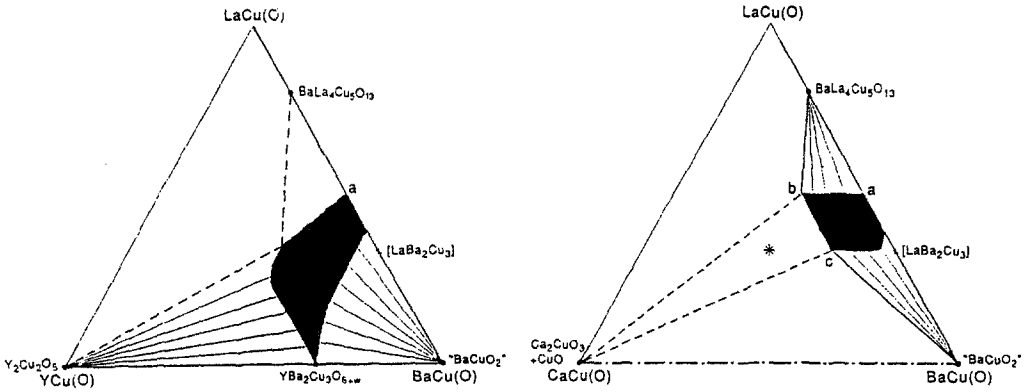

Fig. 42 Regions of stability for the 123 type structures, drawn into the ECu(O)–BaCu(O)–LaCu(O) phase diagrams for E=Y [94, 335] (oxygen, 910°C) and E=Ca [403] (air, 950°C). The difference in conditions is believed to be unimportant for the overal picture. The "CaBaLa" composition is marked with a star. Other significant compositions: a – $La(Ba_{0.75}La_{0.25})_2Cu_3$; b – $La(Ba_{0.50}Ca_{0.25}La_{0.25})_2Cu_3$; c – $La(Ba_{0.75}Ca_{0.25})_2Cu_3$

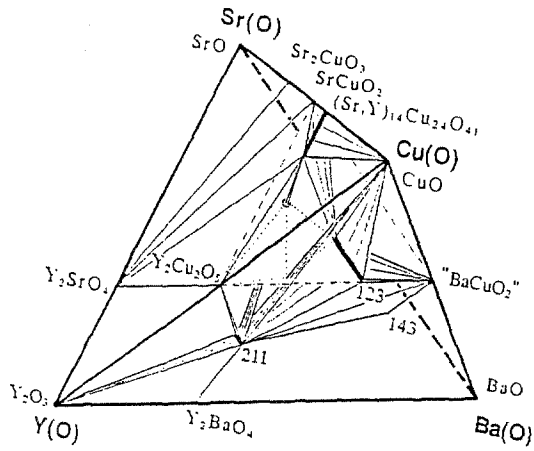

Fig. 43 Subsolidus (pseudoquaternary) tetrahedral phase diagram of the Y(O)–Sr(O)–Ba(O)–Cu(O) system at 900°C in oxygen, covering the neighbourhood of the $YBa_2Cu_3O_{6+w}$-type phase and the Cu-rich corner; after Refs [199, 471]

perovskite structure. A similar result has been obtained when RE=Nd, with the main difference being in the solubility limits ($0.15 < x < 0.4$; $0.04 < y < 0.33$) [470].

RE(O)–Sr,Ba(O)–Cu(O)

The pseudoquaternary phase system Y(O)–Sr(O)–Ba(O)–Cu(O) has been investigated to some extent in conjunction with effects of Sr substitution in the $REBa_2Cu_3O_{6+w}$ phase, particularly for RE=Y [199, 471] and RE=La [472]. In the RE=Y system, regions of solid miscibility are observed for Sr and Ba (Fig. 43). In the "green" cuprate $Y_2(Ba_{1-y}Sr_y)CuO_5$, $y \approx 0.10$ is seen as the miscibility limit after equilibration in pure oxygen at 910°C followed by oxidation at 340°C, whereas $y \approx 0.4$ in $Y(Ba_{1-y}Sr_y)_2Cu_3O_{6.95}$ under the same conditions

[471]. When a higher degree of substitution is attempted for the latter phase, $Y_2(Ba_{0.9}Sr_{0.1})CuO_5$ and $(Sr_{2/3}Ba_{1/3})_{14}Cu_{24}O_{41}$ emerge. A practically zero substitution limit is found for substitution of Y by Sr. The $Y(Ba_{1-y}Sr_y)_2Cu_4O_8$ phase allows only for rather low substitution levels of Sr, even when the Ba site is concerned. The substitution limit in this 124 phase is $y=0.10$, referring to 800°C in ambient oxygen [309]. When RE=La, solid solutions based on both Ba, Sr or La are possible. As an example:

$La(Ba_{1-y-y'}Sr_yLa_{y'})_2Cu_3O_{6+w}$, where the substitution by Sr is limited to the Ba site. Both the lower limits of solubility are non-zero, $0.16<y<0.25$ and $0.09<y'<0.25$, but the extent of the solid solution is quite significant, as it means that up to 1/2 of the barium can be replaced [472]. The solid-solubility region drawn into the phase diagram is practically identical with that for the Ca version in Fig. 42, in spite of Ca entering the RE site in the 123 structure, not the Ba site as it is the case for Sr. A similar result has been obtained for RE=Nd, the limits of solubility being $0.06<y<0.20$ and $0.04<y'<0.33$ [470].

$(La_{1-x}Ba_x)_2SrCu_2O_{6+w}$, is a solid solution where Ba replaces partially ($0.000<x<0.125$) at the RE site, while the Sr site remains intact. The crystal structure [473] features, including the variability in the oxygen content, remain essentially as those of the prototype (Sec. IV B). As an example: $x=0.05$, $w=0.30$ {*I4/mmm*; 385.43(1), 2021.55(3)}. However, the substitution by Ba is compensated by creation of oxygen vacancies, and the saturated oxygen content decreases with increasing x: $x=0.125$, $w=0.11$ {385.14(1), 2021.63(7)} [473]. Despite the high and mixed Cu valence, no superconductivity is observed.

E. Oxide carbonates

Existence of oxide carbonates is well documented for the group of large REs [58]. Their crystal structure can be derived from that of the pure oxides by replacing an appropriate portion of oxygen atoms by carbonate groups, accompanied by structural distortions. In a similar way, $CaCO_3$ is related to CaO. Also the Ba-rich ternary oxides of Ba and REs form easily oxide carbonates [77]. Apart from the structural relationship, a clear link is seen between the stability of oxide carbonates and the basicity of the oxides. Since the copper carbonate itself is instable, it took some time to acknowledge that also AE,RE cuprates may accommodate certain portion of carbonate groups in their crystal structures. At first, significant contents of CO_2 were reported analyzed in the Ba-rich samples of the quaternary oxides from the Y(O)–Ba(O)–Cu(O) system [474]. Soon it was found that CO_2 indeed is being built into these phases and the oxide carbonate name came in use [313]. A similar history can be traced for the 123 phase which was also found to accommodate some carbonate ions [105, 475, 476]. Longer it took before it was realized and confirmed that the carbonate groups do not occupy the oxygen atom positions, but Cu sites (first shown for the $Sr_2CuO_2CO_3$ case [145]. This meant that the cuprate coordination polyhedron is replaced by the carbonate triangle in the centre of the single-perovskite "cube". Generally, the tendency to form oxide carbonates increases with the overall basicity of the multicomponent oxide. This is illustrated in Fig. 44, showing the $Y(O/CO_3)$–$Ba(O/CO_3)$–$Cu(O/CO_3)$ system at 800 and 900°C, as obtained from a large number of samples [78, 105, 474]. The oxide carbonate phases in question are stable in a narrow shell defined by the degree of basicity for the constituents (notably the BaO content), and delimited by the concentration of CO_2 in the surrounding atmosphere and the temperature. At lower BaO contents and CO_2 concentrations, as well as at higher temperatures, pure oxide phases become stable. For larger BaO contents, higher CO_2 concentrations or lower temperatures, $BaCO_3$ is stabilized next to the oxides of the other metals. Except for the pseudoternary Y,Ba- and Ba,Cu-oxide carbonates, described in Secs III A and III B, two quaternary oxide carbonates are seen in Fig. 44:

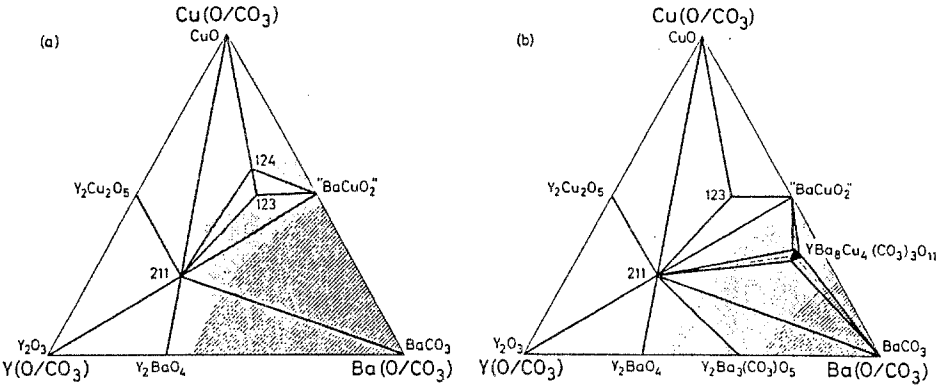

Fig. 44 Phase compatibilities in the $Y(O/CO_3)$–$Ba(O/CO_3)$–$Cu(O/CO_3)$ system, from Ref. [78], as seen by PXD after repeated firings of citrate precursors at (a) 800 and (b) 900°C in oxygen of ambient pressure containing ~40 ppm CO_2. Phenomenological frontiers of the oxide carbonate stability are shown by dotted shading, of carbonate stability by line shading

$Ba_8[Cu_{4+z}Y_{1+x}(CO_3)_{3-x-z}]O_{10+w}$, with $0.0<x<0.3$ and $0.0<z<0.4$, is the actual composition [78, 94, 105, 474] of the elusive "other perovskite phase" in this system. The composition is remarkable in that carbonate groups can replace both Cu and Y. As a result of this, a distinct region of homogeneity occurs [474] for this phase in the pseudoternary phase diagram $Y(O/CO_3)$–$Ba(O/CO_3)$–$Cu(O/CO_3)$ in Fig. 44, extending towards both Y and Cu from the "184" formula $Ba_8[Cu_4Y(CO_3)_3]O_{10+w}$. Also the oxygen content is variable [78]. For the 184 formula, $0.05(2)<w<1.08(2)$. The span is similar also for compositions with non-zero x and/or z, merely shifted due to the valence balance. The crystal structure of this oxide carbonate has been recently determined [477] for one specific composition (a 142 oxide carbonate [478]), which lies reasonably close to the Y-rich end of the solid-solution region {$x=1$, $z=0$, w=unspecified; *P4/m*; 8.1973(4), 8.0360(5)}. The structure is similar to that suggested [479] previously for the (as refined) composition close to the Cu-rich end of the solid-solution region, indexed with a half-volume unit cell {$x=1$, $z=0.54$, $w=4.08$; *P4/mmm*; 578, 800}. The $Ba_8[Cu_{4+z}RE_{1+x}(CO_3)_{3-x-z}]O_{10+w}$ oxide carbonate solid solution is formed for all REs smaller than Sm (including Sc, excepting Tb) [480]. Synthesis of well crystallized samples of this oxide carbonate is not straightforward. When the amount of carbonate ions is controlled via the starting mixture, the system must be kept closed and reacted at relatively low temperatures, and this causes problems with the homogeneity of the product. When the amount of carbonate ions is controlled via a controlled equlibrium content of CO_2 in the flowing atmosphere at a given temperature, problems with establishing the equilibrium and the narrow region of stability with respect to temperature may cause decompositions. The structural features are not easy to decipher in the only slightly deformed, nearly cubic *2a* perovskite cell with random orientation of the carbonate groups. These problems are also projected into the poor compositional resolution of the phase. This oxide carbonate was considered to be a 132 oxide [314, 316–319], a 153 oxide [322] or 163 oxide [311, 321] (the latter composition lies on the border of the homogeneity range of the oxide carbonate). It is not clear whether the compositions 152 and 385 in Ref. [77] represent single phases, oxides or oxide carbonates.

$YBa_2Cu_{3-u}(CO_3)_uO_{6+w-3u/2}$, with $u\approx0.2$ and $w\approx0.8$ for oxygen saturated sample, as determined by chemical analyses [481]. This phase has a crystal structure [481] very similar to that of the 123 (superconductor) oxide, and is derived by replacing the portion u of the

Cu(1) atoms in the cuprate squares by the carbonate triangles. Rietveld refinement of PND data for the above sample gives a composition of $YBa_2Cu_{2.85}(CO_3)_{0.15}O_{6.73}$ {*P4/mmm*; 387.17, 1160.7)} [481]. The telltale sign for identifying the oxide carbonate against the pure 123 oxide (both being oxygen saturated) is the occurrence of tetragonal symmetry for the oxide carbonate, accompanied by a decrease in the unit-cell parameter *c*. The pure oxide, on the other hand, becomes tetragonal only upon a substantial chemical reduction, accompanied by an increase in the *c*-parameter from some 1170 pm to around 1190 pm. An interesting compositional feature of this oxide carbonate is that it promotes accommodation of rather small "sized" cations at the Ba site. Atoms as small as Hg, Ca or Y can now partially replace Ba in the structure; as an example: $Y(Ba_{0.8}Y_{0.2})_2Cu_{2.8}(CO_3)_{0.2}O_{6.77}$ {*P4/mmm*; 387.7(2), 1157.3(13)} [78, 94]. Similar Y for Ba substitutions have variously been reported in the literature [482, 483] before the existence of the cuprate carbonates was realized. Note the further contraction of *c* occurring due to the exchange of the large Ba with the smaller Y. It is not surprising that also the vice-versa accommodation of the carbonate ions in the 123-type structure is being promoted when Ba is replaced by the smaller Sr or Ca atoms (a partial replacement for the latter). Several such variants have been structurally characterized in detail [198, 484–488] showing that the carbonate group can act as a bridge between the two Cu(2) sites. This orientation may become preferred owing to the small size of the atom at the "Ba-site". For an overview of the crystal chemistry of such oxide carbonates, see Ref. [488]. Finally, also other oxoanions can function in place of carbonate groups in similar 123-type compounds, e.g., nitrate [489], borate [490], phosphate [491] and sulphate [492]. The $YBa_2Cu_{3-u}(CO_3)_uO_{6+w-3u/2}$ oxide carbonate occurs as an intermediate phase during synthesis of the 123 oxide from carbonaceous precursors [78, 79, 105, 377, 493]. As a function of temperature during such syntheses (O_2 atmosphere), oxide carbonate would be formed around some 780°C, together with the appropriate amount of CuO. Upon an increase in temperature, CuO would partially and temporarily react upon formation of the 124 phase, before the system is converted to the 123 phase [94, 481]. Even if a high enough temperature is chosen, part of the oxide carbonate can remain trapped inside the sample in cases when the release of CO_2 into the surrounding atmosphere is not fully facilitated, for example when the sample is densely sintered [377]. The accommodation of the carbonate groups very efficiently quenches the superconductivity of the 123 phase [78, 494], and therefore the carbon pathway and the residual carbon contents upon the ceramic syntheses have been a subject of considerable interest [79, 494, 495]. On the other hand, the synthesis of the pure oxide carbonate $YBa_2Cu_{3-u}(CO_3)_uO_{6+w-3u/2}$ is rather difficult to conduct under equilibrium conditions. When an open system is adopted, the equilibrium partial pressure of CO_2 is too low to be easily controlled in the narrow window of the low temperatures between the kinetic limitation of the synthesis proper and the formation of the 124 phase or melting. In a closed system, problems with the homogeneity arise. This has delayed the correct structural and compositional characterizations. The features typical of the oxide carbonate unit cell were first seen in some samples of the 123 phase synthesized in a special manner (closed system [311], plasma spraying [496], CO_2 atmosphere [497]), but only later attributed to an oxide carbonate formation [105, 475, 476]. Particularly syntheses in closed pressurized systems are prone to formation of oxide carbonates. Any CO_2 inadvertently brought into the reaction chamber, either as a surface, atmosphere or carbonate-phase impurity, will not leave the system during the experiment, and the elevated pressures will increase the thermal stability of the oxide carbonates. For example, the typical structural indicatives for the 123 oxide carbonate can be seen in the high-pressure studies in Refs [235, 498].

When the BaO content is lowered below that of the 123 composition, the formation of the possible oxide carbonate is even more difficult. The possible existence of such a phase, derived from the 247 composition, is indicated in a recent high-pressure study [499]. At am-

bient oxygen pressures, experiments with a parallel synthesis of the 123 and 124 oxide carbonates at 800°C yielded the desired phase only for the 123 composition, whereas a pure oxide was formed for the 124 composition [105]. In contrast, both 123 and 124 were found stable at the same temperature for at least 1000 h in pure (CO_2 free) oxygen of atmospheric pressure [105].

V. YBCO and variants

A. Chemical properties

The individual elements which form the components of $YBa_2Cu_3O_7$ each bring its own specific chemical properties to this phase. Most dominant is Ba which introduces an enhanced Lewis basicity to the oxygen atoms. As a result, $YBa_2Cu_3O_7$ is reactive towards Lewis acids (e.g., Al_2O_3, SO_2, SiO_2, CO_2, H^+– even from H_2O). Copper brings about its variable valence and easy reducibility, and has also an influence on the behaviour in aqueous systems (formation of complexes).

Properties relevant to Cu. The perovskite-type structure allows for extensive oxygen vacancies, and gives space for wide variations in the Cu valence upon exchange of oxygen with the surrounding atmosphere. This feature will be dealt with in detail in Sec. V C. The reduced, oxygen vacant phase $YBa_2Cu_3O_6$ may be oxidized also by some non-oxygen agents like NF_3 (fluorination) and halogens. These processes will be described as chemical substitutions in Sec. V D. The oxidative power of $YBa_2Cu_3O_{6+w}$ strongly increases when w approaches 1.0. In contact with acidic aqueous systems, the solid oxidizes H_2O into O_2, and Cl^- and Br^- into Cl_2 and Br_2, upon formation of Cu(II). Iodide ions are oxidized into I_2 upon formation of Cu(I). The latter reactions form the basis for several methods of wet chemical analyses of the oxygen content in the $YBa_2Cu_3O_{6+w}$ phase. In the solid state, the noble character of elemental copper causes $YBa_2Cu_3O_{6+w}$ to be (ultimately) reduced into metallic Cu already under moderately reducing conditions. The solid-state chemical equlibria associated with such a reduction of $YBa_2Cu_3O_6$ involve several intermediate compounds and will be described in Sec. V B.

The specifics of the copper chemistry in aqueous systems can be manifested in an interesting reaction when the mixed-valence phase dissolves in aqueous ammonia [311]:

$$2YBa_2Cu_3O_{6.5} \xrightarrow{11H_2O,\ 24NH_3} 2YO(OH) + 4Ba^{2+} + 6[Cu(NH_3)_4]^{2+} + 20OH^- \quad (7)$$

Such a reaction does not occur for the stoichiometric cuprate Y_2BaCuO_5.

Properties relevant to Ba. Reactivity towards Lewis acids, including protons from "hydrogen acids" is strongly enhanced by the high content of barium. Possible reactions with the surrounding chemical environment are of the greatest concern. Solid-state reactions of $YBa_2Cu_3O_{6+w}$ with acidic transition-metal oxides [500] and analogous materials [501, 502] are found to proceed readily upon formation of Ba containing oxides. The complex equilibria occurring in contact with molten halides were investigated [503] and NaCl/KCl melts found to be the least reactive towards $YBa_2Cu_3O_{6+w}$. Also the reaction with liquid H_2O is of particular importance. The reaction gives yttrium and copper oxides, barium hydroxide and barium copper hydroxide as main products. The real pathway is considerably more complex due to the omnipresence of CO_2 [504]. Similar products are also obtained after exposition to the atmosphere [505]. For the possibility of incorporation of OH^- ions into $YBa_2Cu_3O_{6+w}$ in aqueous systems, see Sec. V D. As an example of a gas–solid, Lewis-type reaction, an interaction with NO_2 at 200°C can be cited [506], interesting in that both the acidic and oxidative properties of NO_2 are in effect when reduced 123 is involved. A mix-

ture of oxidation and degradation products is formed, consisting mainly of the oxidized 123 and barium nitrite.

The reaction with gaseous CO_2 is probably the most important of the degradation reactions of $YBa_2Cu_3O_{6+w}$, since CO_2 is present in the air and in traces in most of the chemical environments. This reaction is also the reverse of the commonly used carbonate synthesis route for $YBa_2Cu_3O_{6+w}$. Depending on the temperature, several reaction products are observed [217, 507] when $YBa_2Cu_3O_{6+w}$ is exposed to dry mixture of CO_2 and O_2. For $400 < t < 730$°C:

$$2YBa_2Cu_3O_{6+w} \xrightarrow{4CO_2} Y_2O_3 + 4BaCO_3 + 6CuO + (w - 0.5)O_2, \quad (8)$$

for $730 < t < 950$°C:

$$2YBa_2Cu_3O_{6+w} \xrightarrow{4CO_2} Y_2Cu_2O_5 + 4BaCO_3 + 4CuO + (w - 0.5)O_2, \quad (9)$$

and for $t > 950$°C:

$$2YBa_2Cu_3O_{6+w} \xrightarrow{3CO_2} Y_2BaCuO_5 + 3BaCO_3 + 5CuO + (w - 0.5)O_2, \quad (10)$$

where w and the question whether CuO or Cu_2O is formed depend on p_{O_2} and temperature. The observed [217] partial pressures of CO_2 at equilibrium with $YBa_2Cu_3O_{6+w}$ are shown in a van't Hoff plot in Fig. 45, together with calculated [508, 509] dissociation pressures of $CaCO_3$, $SrCO_3$ and $BaCO_3$. Using the original data from Ref. [217], the onsets of carbonatization or decarbonatization reaction of $YBa_2Cu_3O_{6+w}$ in oxygen-rich atmospheres according to Eq. (9) can be expressed as follows (in Pa, K):

$$\log_{10} p_{CO_2} = 11.217(313) - 9270(340)/T \quad (11)$$

The kinetics of these carbonatization processes as a function of temperature and particle size has been investigated and an empirical rate equation with a 1.5 order dependence has

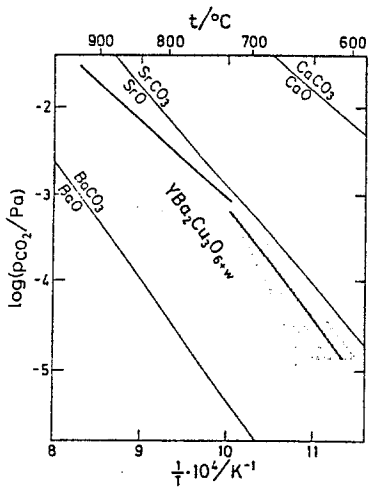

Fig. 45 $YBa_2Cu_3O_{6+w}$ stability with respect to carbonatization in O_2/CO_2 atmospheres at ambient pressure; after Ref. [217]. Equilibrium according to Eq. (8) is indicated by shaded area, equilibrium according to Eq. (9) by solid line. Data for AEs are given for comparison

been derived [510]. The reaction with CO_2 has a very significant effect on the processing and superconducting properties of $YBa_2Cu_3O_{6+w}$ [475, 511, 512]. Severe degradation in the critical current occurs before even a slight weight increase can be observed [513].

B. Reduction and melting

For the easily reducible $YBa_2Cu_3O_{6+w}$, both moderately increased temperatures and moderately reduced partial pressures of oxygen are significant factors which lead to chemical reduction upon formation of other phases.

The temperature-induced reduction and decomposition is characterized by the incongruent melting (upon formation of Y_2BaCuO_2 and a liquid) [514] at the temperature T_m. T_m of $YBa_2Cu_3O_{6+w}$ decreases with w and in turn also with decreasing partial pressure of O_2 in the surrounding atmosphere. DTA-based data for T_m, obtained [515] in atmospheres with oxygen partial pressure varied in the interval of $10^2 < p_{O_2} < 10^5$ Pa, can be approximated linearly as follows (in Pa, K):

$$\log_{10} p_{O_2} = 37.6(9) - 42256(1137)/T_m \qquad (12)$$

and lie between some 900 and 1024°C (the latter in pure O_2). However, indications of the liquidus are often observed at lower temperatures than stated above. Examinations [516] of cyclically annealed phase-pure $YBa_2Cu_3O_{6+w}$ indicated that, already below the melting point, Cu may have a tendency to migrate to the surface of the bulk particles. According to Ref. [516] this excess of Cu on the grain boundaries causes a formation of a peritectic liquid which in turn results in a partial phase separation upon cooling. Vaporization studies [517, 518] have shown measurable partial pressures of both Cu and Ba species over $YBa_2Cu_3O_{6+w}$ at temperatures around melting. At 890°C, vapor pressure values (in Pa) of $1.2 \cdot 10^{-4}$ for Cu, $2.2 \cdot 10^{-5}$ for CuO and $2.5 \cdot 10^{-5}$ for BaO under 21 kPa of oxygen are obtained in Ref. [518]. No Y-containing vapor is detected at this temperature.

The low-pressure induced reduction and decomposition of $YBa_2Cu_3O_{6+w}$ in the solid state occurs when $w \approx 0$ [105, 519–522], defined by the partial pressure of oxygen at the decomposition temperature T_{dec}. For the interval $1023 < T_{dec} < 1148$ K, the following expression is valid (in Pa, K; calculated from data in Ref. [523]):

$$\log_{10} p_{O_2} = 12.28(30) - 11975(328)/T_{dec} \qquad (13)$$

For the continuation to higher temperatures, see Ref. [524]. Very similar values are obtained in Ref. [522] for the interval $993 < T < 1222$ K.

1. Redox equilibria

For the specific situation in the vicinity of the 123 stoichiometry, the pattern of subsequent redox reactions occurring upon the gradual removal of oxygen from various nominal compositions has been investigated by solid-state coulometric titration [523, 525, 526] and TG in controlled atmospheres [522] followed by PDX. Details for the isothermal pseudoternary Cu-rich subsystem according to Refs [523, 526] are shown in Fig. 46, referring to the p_{O_2}-plateaus "seen" by coulometric titration at 850°C (chosen in order to maintain acceptable kinetics of the solid-state reactions). Nevertheless, even then, a liquidus briefly appears as a function of the decreasing partial pressure of oxygen. Table 1 lists nine observed invariant reactions occurring between the ten individual situations drawn in Fig. 46 and the respective partial pressures of oxygen ("plateaus") for each reaction. Unfortunately, the Ba-rich perovskite phase participating in these equilibria has only been identified as "132" in

Ref. [526]. This composition does not refer to an existing phase in this system and therefore it is replaced for our purpose by an "X". Since $YBa_4Cu_3O_{9+w}$ is not stable [105] already at the partial pressure of the first plateau (p_{O_2}=560 Pa), it is quite probable that this X phase actually is the Cu-rich composition of the $Ba_8[Cu_{4+z}RE_{1+x}(CO_3)_{3-x-z}]O_{10+w}$ oxide carbonate (see Sec. IV E). Similarly, the "$BaCuO_2$" phase also possibly represents an oxide carbonate (see Sec. III B). With these facts in mind, the data in Table 1 and Fig. 46 illustrate how a "real" Cu-rich system behaves upon removal of oxygen.

The nature of the solid-state decomposition products of the $YBa_2Cu_3O_6$ phase remains still ambiguous [522]. Three sets of decomposition products are generally reported: (1) Y_2BaCuO_5, "$BaCuO_2$" and Cu_2O have been considered in Refs [519, 521], however, based on later unconfirmed citations. (2) Y_2BaCuO_5, "$BaCuO_2$" and $BaCu_2O_2$ are observed in

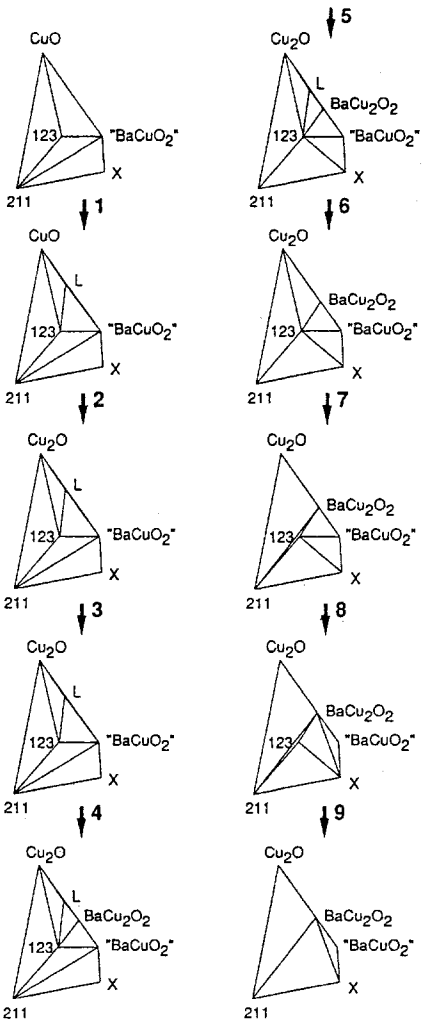

Fig. 46 Cu-rich sections of the pseudoternary Y(O)–Ba(O)–Cu(O) phase diagram upon reduction at 850°C by means of coulometric titration, after Refs [523, 526]. Numbers at the arrows refer to Table 1

Table 1 Phases involved and oxygen partial pressures (in Pa) for invariant reactions (not balanced) near 123 at 850°C [526]

R[a]	p_{O_2}	Reaction components[b]
1	560	$YBa_2Cu_3O_{6+w}+BaCuO_2+CuO \leftrightarrow L+O_2$
2	410	$CuO \leftrightarrow Cu_2O+O_2$
3	300	$BaCuO_2+L \leftrightarrow BaCu_2O_2+O_2$
4	300	$BaCuO_2+L \leftrightarrow YBa_2Cu_3O_{6+w}+BaCu_2O_2+O_2$
5	270	$Y_2BaCuO_5+BaCuO_2 \leftrightarrow YBa_2Cu_3O_{6+w}+X+O_2$
6	150	$L \leftrightarrow BaCu_2O_2+Cu_2O+YBa_2Cu_3O_{6+w}+O_2$
7	100	$YBa_2Cu_3O_{6+w}+Cu_2O \leftrightarrow Y_2BaCuO_5+BaCu_2O_2+O_2$
8	70	$YBa_2Cu_3O_{6+w}+BaCuO_2 \leftrightarrow X+BaCu_2O_2+O_2$
9	40	$YBa_2Cu_3O_{6+w} \leftrightarrow X+Y_2BaCuO_5+BaCu_2O_2+O_2$

[a]Number refers to the pressure plateau in Fig. 46.

[b]X denotes the reported Ba-rich perovskite. However, most probably the 184 oxide carbonate.

Ref. [398] and this situation is shown in Fig. 37. (3) Y_2BaCuO_5, $BaCu_2O_2$ and the X phase are identified in Refs [514, 523] and this situation appears in Table 1 and Fig. 46. The reason for these disagreements can be twofold: (i) An undefined degree of stabilization by oxide carbonates even while the values of p_{O_2} are well under control. (ii) The poor resolution in terms of p_{O_2} and temperature for the reaction proper of the decomposition of 123, the reactions of the decomposition of "$BaCuO_2$" into $BaCu_2O_2$, and the formation of the phase X. Several indistinct TG plateaus are observed in Ref. [522] in a close follow up upon increased temperature, at low partial pressures of oxygen, after the stability limit of the 123 phase has been crossed. This is suggested to indicate that the three sets of reaction products indeed occur in the said order upon the solid-state reduction of the nominal 123 composition. At the very first TG plateau, before these profound reduction processes occur, a demixing of a small amount of Y_2BaCuO_5 from the 123 phase is seen in Ref. [522]. This further increases the ambiguity as to the actual solid-state decomposition point of the 123 phase.

When the chemical reduction of the RE(O)–Ba(O)–Cu(O) system is adopted by means of increasing temperature, the oxide carbonate problem is somewhat alleviated. However, the solidus–liquidus equilibria are soon entering the picture. A large number of isobaric and isothermal sections is necessary for a description of the *s–l* relationships and these diagrams are treated separately in the following section.

2. *s–l* diagrams

The solidus–liquidus equilibria in the Y(O)–Ba(O)–Cu(O) system are complex and their investigations have therefore usually been limited to various pseudobinary sections, a few such cuts [313, 527–530] being edited together in Fig. 47. When interpreting these data, it should be born in mind that the crucial problem concerning any phase diagram, i.e., whether a real equilibrium state is achieved or not, is considerably enhanced for *s–l* boundaries. In fact, each examination (microscopy, diffraction, thermal analyses, quenching, physical phase separation, etc.) provides a slightly different viewpoint. Refs [528, 530] give instructive examples for quenching *vs.* DTA. Different primary crystallization fields were found in a section of the pseudoternary system very close to Cu(O), resulting from the lack of equilibrium conditions during a DTA experiment. Hence, crystallizations of either $Y_2Cu_2O_5$ (DTA) or Cu_2O (quenching) are observed for one and the same composition in a certain composition interval.

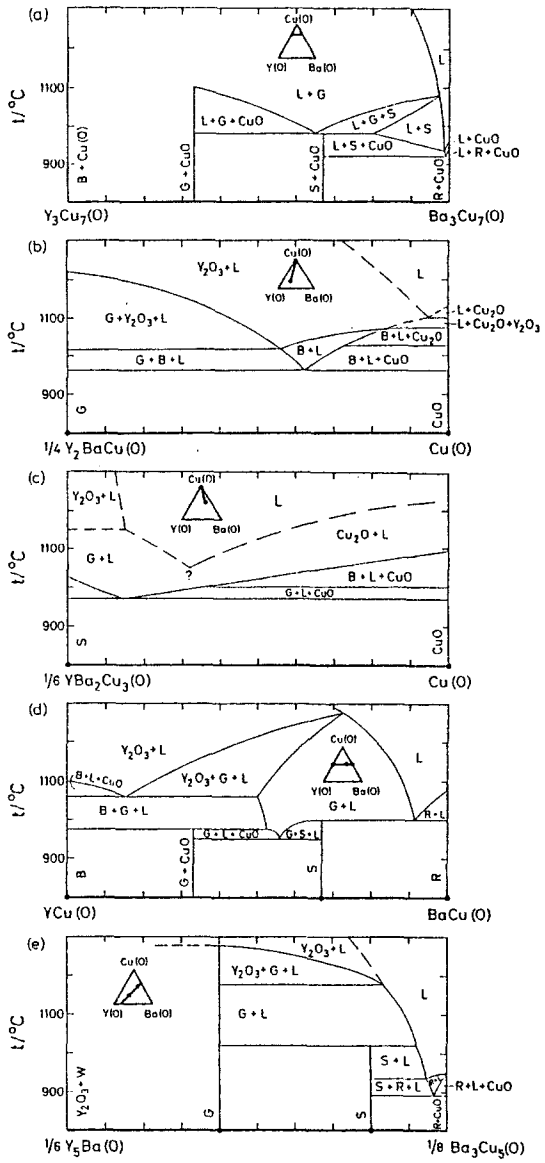

Fig. 47 Pseudobinary x–t diagrams for certain cuts (shown in the thick-line insets) of the Y(O)–Ba(O)–Cu(O) system: (a) from Ref. [527], (b) from Ref. [528], (d) from Ref. [313] and (e) from Ref. [529] in air, (c) from Ref. [530] in oxygen. Ternary and quaternary phases are marked as follows: B – $Y_2Cu_2O_5$, G – Y_2BaCuO_5, R – $BaCuO_{2+w}$, S – $YBa_2Cu_3O_{6+w}$ and W – BaY_2O_4

A combination of all available information into a spatial, x–y–t pseudoternary diagram was also attempted [531], but here attention will only be focused on the liquidus surface for the Cu-rich portion of the system (Fig. 48). Eleven invariant reactions were observed [329] in this system, and are listed in Table 2.

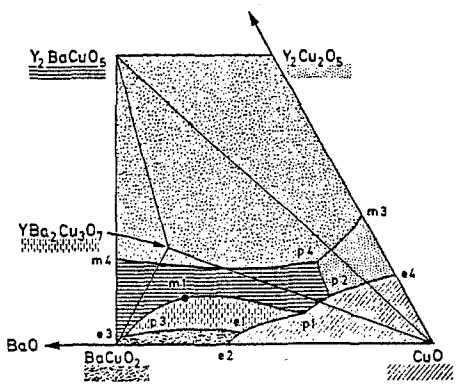

Fig. 48 Liquidus surface of Cu-rich portion of the Y(O)–Ba(O)–Cu(O) phase diagram in air; after Refs [329, 523, 531]. Primary crystallization fields for individual phases are distinguished by shading, labelling of the points corresponds to Table 2

Table 2 Phases involved and temperatures (°C) for invariant reactions (not balanced) at the liquidus surface in air, according to Ref. [329]

t	IP[a]	Reaction components
890	e1	$YBa_2Cu_3O_{6+w}+BaCuO_2+CuO \leftrightarrow L(e1)$
920	e2	$BaCuO_2+CuO \leftrightarrow L(e2)$
940	p1	$YBa_2Cu_3O_{6+w}+CuO \leftrightarrow Y_2BaCuO_5+BaCuO_2+L(p1)$
975	p2	$Y_2BaCuO_5+CuO \leftrightarrow Y_2Cu_2O_5+L(p2)$
1000	e3	$Y_2BaCuO_5+BaCuO_2 \leftrightarrow L(e3)$
1000	p3	$YBa_2Cu_3O_{6+w}+BaCuO_2 \leftrightarrow Y_2BaCuO_5+L(p3)$
1015	m1	$YBa_2Cu_3O_{6+w} \leftrightarrow Y_2BaCuO_5+L(m1)$
1015	m2	$BaCuO_2 \leftrightarrow L$
1026		$CuO \leftrightarrow Cu_2O$
1110	e4	$Y_2Cu_2O_5+Cu_2O \leftrightarrow L(e4)$
1122	m3	$Y_2Cu_2O_5 \leftrightarrow Y_2O_3+L(m3)$
1270	m4	$Y_2BaCuO_5 \leftrightarrow Y_2O_3+L(m4)$

[a]Invariant point; labelling corresponds to Fig. 48; e – eutectic, p – pseudoperitectic, m – melting.

These reactions explain why the degree of sintering of the 123 samples varies (depending on whether or not a small excess of CuO is present), since a liquid phase is involved above 940°C, and acts as a transport medium. An analogous explanation applies to the strong densification often observed upon the first firing since the intimate mixtures of the particles of the individual components may produce sufficient amounts of the lowest melting eutectic (890°C) to promote sintering.

The equilibria occurring upon melting in the region close to the pseudoternary eutectic have been investigated in order to obtain data for the single-crystal growth of the 123 superconductor which is obtained from only a rather narrow crystallization field. The pseudoternary eutectic point is located [532] at the composition $Y_{0.005(1)}Ba_{0.232(5)}Cu_{0.764(10)}$, by a

soaking technique with MgO wick, confirming previous results [533] by a similar method. According to Ref. [532], the eutectic occurs at 923(10)°C, referring to a dry, CO_2-free air, and contains nearly all the copper as Cu(I). This temperature is somewhat higher than that reported for the point e1 in Table 2 and this is explained in Ref. [532] as an effect of reduction and/or impurities. The temperatures for the points p1 and p2 given by Ref. [532] (947 and 967°C, respectively) agree well with Table 2. These experimental data, as well as the extent of the melt region as a function of temperature, are in a good agreement with the situation calculated [534] from estimated thermodynamic values.

C. Oxygen-exchange

1. Equilibrium

The variable valence of Cu in $YBa_2Cu_3O_7$ leads to a variable oxygen content in the solid state:

$$YBa_2Cu_3O_{(6+w)+\Delta w} \leftrightarrow YBa_2Cu_3O_{6+w} + \frac{\Delta w}{2} O_2 \tag{14}$$

The equilibrium is defined by p_{O_2}, T, and, in contrast to the reactions occurring between fixed compositions, also by the compositional variable w. Accordingly, when w is maintained constant, a normal, linear van't Hoff plot is valid. Such a plot is shown in Fig. 49, obtained [217] by actually varying p_{O_2} at different temperatures, under the thermogravimetric control of $w=0.5$. The least-squares approximation of the data in Fig. 49 gives for $YBa_2Cu_3O_{6.50}$ (in Pa, K):

$$\log_{10} p_{O_2} = 12.75(20) - 8148(177)/T \tag{15}$$

However, when p_{O_2} is maintained constant, no linear van't Hoff plot is extracted for the compositional variable. This illustrates that w is a composite value which, as such, does not represent an actual participant in the equilibrium in Eq. (14). These real components have been attempted approached by two types of models: (i) a defect-chemistry model, based on solid-state equilibria among variously charged and clustered defects, and (ii) a lattice-gas model, based on structural features of the oxygen "sublattice" and statistical thermodynamics.

Experimental data. Great many studies report some data on the oxygen-exchange equilibria in Eq. (14). However, only a few covers a reasonably wide range of the p–t–w vari-

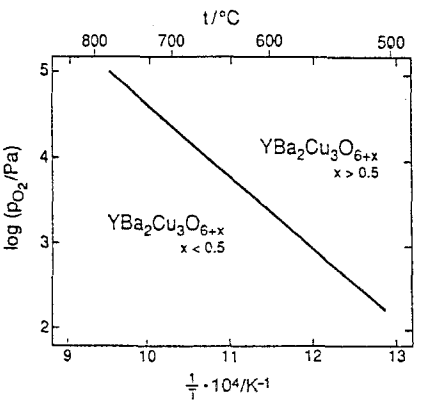

Fig. 49 $YBa_2Cu_3O_{6.50}$ stability with respect to oxygen uptake and release, according to Ref. [217]

ables. Such data are obtained by a variety of techniques: TG accompanied by quenching of selected samples and by chemical and PXD analyses (RE=Y [535–539] and Er [540]), coulometric titration (RE=Y [521] and RE=Pr [541]), direct pressure measurements (RE=Y [352] and RE=Er [542]), and, at high pressures, by equilibration and cooling techniques (RE=Y [543, 544]). As stated in several of the cited studies, a reliable determination of the oxygen content is crucial for the accuracy of the *p–t–w* data, especially when it concerns the reference composition for TG or coulometry. In particular, hydrogen-reduction analyses can be burdened by systematic errors due to the presence of a residual carbonate in samples, resulting into somewhat higher-than-real oxygen contents. Even when these problems are eliminated, the resulting *p–t–w* data have a non-ideal character, caused by the large span of the phase-homogeneity region *w* and the order/disorder phenomena related to the accommodation of oxygen in the crystal structure. As a combined consequence of these factors, a precise description of the non-stoichiometry in $YBa_2Cu_3O_{6+w}$ has not yet been satisfactorily worked out.

The defect chemistry approach. Defect chemistry models assume that there occur equilibria in the solid state between variously charged point defects that participate in the oxygen-exchange reaction. During this reaction, the formation of these aliovalent, differently charged atoms or their clusters is the essence of the redox-process in the solid state. However, when the span of the redox process covers an entire unit of valence, as for $YBa_2Cu_3O_{6+w}$, it becomes less clear which oxidation state is the aliovalent one. In addition one can expect a non-ideal behaviour of the defects when their concentration becomes high. The usual approach is to identify the stoichiometric state and use this as the basis for the definition of the defects. The stoichiometric state appears at an integer composition where a *n*-to-*p* semiconducting transition occurs corresponding to the intrinsic situation with the Fermi energy in the middle of the gap [545]. This situation also corresponds to a minimum in the oxygen ion diffusivity [546]. Based on both these criteria, the stoichiometric situation occurs at the composition $YBa_2Cu_3O_6$, i.e., having Cu(I) with its typical linear coordination at the Cu(1) site and Cu(II) at the two square-pyramidal Cu(2) sites [547, 539]. Unfortunately, the phase stability boundary coincides with this composition, and this somewhat complicates measurements at low defect-concentrations in $YBa_2Cu_3O_{6+w}$, where otherwise a more ideal behaviour would be expected. Only some of the experimental techniques used, like TG and coulometric titration, provide direct information on the partial pressures of oxygen and the changes in *w* for derivation of the defect models for the oxygen exchange reaction. Other methods, like measurements of the electrical conductivity, Hall and Seebeck coefficients, witness more about the nature and mobility of the charge carrying defects.

The data from TG [352, 537, 539] and coulometric titration [521] for $YBa_2Cu_3O_{6+w}$, which have been obtained over a wide span of *w*, provide a very consistent picture for $\log p_{O_2}$ *vs.* *w*. Even more significantly, when the non-stoichiometry is expressed as $\log[w/(1-w)]$, these isotherms become linear, having slopes of approximately 3. A slope of 3.00 is evaluated from data in Ref. [521] also for the vicinity of the stoichiometric situation. In the defect-equilibrum approach, the mass-action term of the $w/(1-w)$ type appears in a model with localized holes or electrons where the total number of the participating structural sites is constant [545]. This means that for every defect site created by the incorporation of oxygen (including holes; appearing on the right hand side of the formal defect-reaction equation), there is one stoichiometric structural site available (including vacancies; appearing on the left hand side of the equation). The slope then refers to the number of defects formed in the originally stoichiometric solid by an accommodation of 2 oxygen atoms (from the O_2 molecule) subjected to the electroneutrality condition. The problem is, however, that the simple ionic defect reaction of this type:

$$\frac{1}{2}O_2 + V_i + 2Cu_{Cu}^{\times} \leftrightarrow O_i'' + 2Cu_{Cu}^{\cdot} \tag{16}$$

gives a slope of 6 instead of 3. Such a serious disagreement is usually attempted solved by abandoning the assumption of the ionicity from the defect model and/or considering defect clusters instead. In the extreme case, such an approach [545, 548]

$$\frac{1}{2}O_2 + V_i \leftrightarrow O_i^{\times} \tag{17}$$

gives a slope of 2. Taking into consideration also the structure-chemical information that the additional oxygens are being accommodated in the linear Cu(I) coordinations (dumbbells) upon formation of the typical chains of Cu(II) squares, one can easily balance that per every oxygen atom accommodated, one Cu(I) is converted into one Cu(II). That leaves one hole to be located at the other Cu sites,

$$\frac{1}{2}O_2 + Cu_{Cu}^{\times}V_i + Cu_{Cu}^{\times} \leftrightarrow Cu_{Cu}^{\cdot}O_i'' + Cu_{Cu}^{\cdot} \tag{18}$$

and the slope is 4. A slope of 3 would be obtained upon the simple summation of Eqs (17) and (18), but also upon the assumption that the accommodation of oxygen happens in pairs:

$$O_2 + Cu_{Cu}^{\times}V_iCu_{Cu}^{\times}V_i + 2Cu_{Cu}^{\times} \leftrightarrow Cu_{Cu}^{\cdot}O_i''Cu_{Cu}^{\cdot}O_i'' + 2Cu_{Cu}^{\cdot} \tag{19}$$

Both possibilities have their merits, as recent Hall coefficient data seem to show that only 1/2 to 1 hole is generated per every oxygen atom accommodated [549]. Formally, one may then express $\log p_{O_2}$ from the equilibrium constant K_{19} for Eq. (19), by taking the concentrations $2[Cu_{Cu}^{\cdot}O_i''Cu_{Cu}^{\cdot}O_i'']=[Cu_{Cu}^{\cdot}]$ from electroneutrality, and that $[Cu_{Cu}^{\cdot}O_i''Cu_{Cu}^{\cdot}O_i'']=w/2$:

$$\log p_{O_2} = -\log K_{19} + 3\log \frac{w}{1-w} \tag{20}$$

This equation then fits the experimental data fairly well across the entire span in w. Naturally, none of the fine variations occurring [352, 542] around the structural o,t-transition can be modelled by these simple defect-chemistry approximations. It should perhaps just be briefly noted that the indirect methods for investigation of the oxygen-exchange equilibria, like thermopower and electrical conductivity measurements [550], have isotherms with slopes around 3 and 2, respectively, when plotted as a function of $\log p_{O_2}$.

The existence of the stoichiometric $n=p$ situation at the state where the Cu(1) site atoms are monovalent has apparently been confused against the fact that the hole superconductivity is correlated with valence states of copper higher than +II. It is the structural peculiarity of this phase which localizes the oxygen exchange to the Cu(1) region, whereas superconductivity is associated with the states at Cu(2). This could have misled several attempts [366, 551–554] into expressing the defect equilibria based on the stoichiometric state with Cu(II). Nevertheless, since the span in w is approximately 1, the term $w/(1-w)$ is then merely inverted and reasonably linear isotherms are still obtained [551]. This apparent flexibility has also contributed to a considerable confusion in the understanding of the defect equilibria processes occurring upon the oxygen-exchange reaction of $YBa_2Cu_3O_{6+w}$.

The lattice-gas approach. Lattice-gas models consider only oxygen atoms under assumption that the oxygen absorption and desorption takes place exclusively at the (*a,b*-)

plane of Cu(1). Whereas fairly precise predictions are obtained [353, 367] for the oxygen-related OD phenomena like the p–t dependence of the orthorhombic to tetragonal transition, discrepancies are seen [555] in thermodynamics of the oxygen accommodation in $YBa_2Cu_3O_{6+w}$, particularly for high w. Experimental data seem to show that the partial molar enthalpy of oxygen is not strictly constant as a function of w, having a broad non-linear region around compositions corresponding to the o,t structural transition and linear dependences otherwise [352, 542]. As a consequence of that, statistical models (where w enters only in the term for the ideal partial molar configurational entropy of mixing) do not describe well the transition region for cases where high precision p–t–w data are available [352, 542]. In such models, e.g., Refs [352, 542], the oxygen-exchange reaction is assumed as follows,

$$\frac{1}{2}O_{2(g)} \leftrightarrow O_{(s,YBa_2Cu_3O_{6+w})} \tag{21}$$

with equilibirium constant expressed via chemical potentials as the partial molar free energy for incorporation of 1 mol of oxygen atoms in the solid, Δg_O. Referring, say, to the standard state of unity pressure and the actual temperature:

$$\Delta g_O = \Delta h_O - T\Delta s_O = \frac{1}{2}RT \ln p_{O_2} \tag{22}$$

Both enthalpy and entropy are further expressed in Refs [352, 542] as a sum of the standard values (w-independent) and the excess values (to account for an apparent non-ideal behaviour)

$$\Delta h_O = \Delta h_O^\circ + h_O^E \tag{23}$$

with the concentration dependence appearing as a configurational entropy:

$$\Delta s_O = \Delta s_O^\circ + s_O^E + R \ln\frac{2-w}{w} \tag{24}$$

which assumes that structurally there are two oxygen sites, O(1) and O(5) to choose between. However, when one expresses the partial pressure of oxygen from Eqs (22–24) as a function of the concentration term, the standard and excess values can be regrouped to give an equilibrium constant referring obviously to the oxygen-exchange reaction in Eq. (21):

$$\ln p_{O_2} = -2\ln K_{21} + 2\ln\frac{w}{2-w} \tag{25}$$

where $-\ln K_{21}=(\Delta h_O^\circ+\Delta h_O^E)/RT-(\Delta s_O^\circ+\Delta s_O^E)/R$. Equation (25) is conspicuously similar to Eq. (20) derived from the defect-model considerations. Two differences appear, viz., in that the slope of the isotherms is 2, originating from Eq. (21), and in that two sites are considered in the configurational entropy term. Given the fairly reasonable fits based on Eq. (20), it is perhaps not surprising that the detailed and accurate experimental data in Refs [352, 542] show profound deviations from ideality when tested by the thermodynamic model behind Eq. (25) in the references cited. The large excess values obtained then merely reflect the misfit of the model adopted, both in the slope and in the composition term. Typically for the latter, it is even suggested in Ref. [541] that, with increasing w, the number of available sites in this configurational entropy term decreases to 1.

Since these simple lattice-gas and defect-chemistry models for the oxygen exchange lead to a very similar or perhaps common formal description, it is quite obvious that there actually is only one universal model to be developed. The peculiar structural characteristics of these triple perovskites, including the two types of copper coordinations, three valence states of Cu, and the high covalence of the cuprate network, are likely to be the essential components for such a description.

2. Kinetics

A measurable oxygen uptake by $YBa_2Cu_3O_{6+w}$ samples is observed [217] already at temperatures around 300°C, and this implies that the chemical diffusivity of oxygen at higher temperatures may be very high. The possible reason for this becomes apparent when realizing that the oxygen transport takes place as a bipolar diffusion, via a coupled movement of the oxygen ions and the corresponding holes. The conductivity with respect to both of these species is expected to be high. The ionic conductivity is high due to the open and vacant character of the oxygen "sublattice", the electronic conductivity is high due to the extensive mixed-valence character of $YBa_2Cu_3O_{6+w}$.

A great variety of experimental techniques have been used to investigate the kinetics of the oxygen exchange for $YBa_2Cu_3O_{6+w}$. The methods which more or less directly measure the oxygen transport and evaluate it as chemical diffusivity adopt either a transient or permeation mode. The transient mode consists of monitoring the response of the sample to a sudden state change. This can be either a change in the partial pressure of oxygen (p-jump, coulometric titration) or temperature (T-jump, temperature-programmed desorption), while the response is monitored as a change in the weight (TG) [539, 556–558], in the electrical conductivity [559–561], in the gas volume [562], in the gas pressure [563], or in the thermal conductivity of a carrier gas [564]. The permeation methods achieve a steady state of oxygen permeation through the sample under a small gradient of p_{O_2}, and the flowing oxygen is monitored either electrochemically, or by gas chromatography or mass spectrometry. The oxygen-transport properties can also be computationally simulated [565].

Self-diffusivity of oxygen in $YBa_2Cu_3O_{6+w}$ is evaluated by several techniques. Tracer-diffusion methods use ^{18}O as the tracer and SIMS as the depth-profiling detection technique. Data both on powders [566, 567] and single crystals [568] have been obtained in such a manner. Indirect methods involve measurements of internal friction [569] and various spectroscopic studies. Also determinations from the individual oxygen-ion conductivities have been attempted, based on dc- or ac-conductivity measurements with electronically blocking, yttria-stabilized, zirconia electrodes [548, 570, 571]. However, the most recent studies combine this method with ac-impedance spectroscopy, recognizing the profound importance of the contact/interface phenomena on such measurements [572, 573].

The chemical diffusion coefficients obtained by various authors scatter rather widely and their temperature dependences are only approximately linear in the Arrhenius plots. A good illustration of this situation is compiled in Ref. [572]. When choosing only the data obtained on sintered compact samples in Refs [539, 574, 575] one can say that the average D increases from some 10^{-8} cm^2 s^{-1} at 320°C to almost 10^{-4} cm^2 s^{-1} at 900°C. The data which are obtained by TG, and therefore have the advantage of the oxygen content being monitored simultaneously, show [539] clearly that the chemical diffusion coefficient decreases with decreasing w in $YBa_2Cu_3O_{6+w}$. Also a coulometric study of oxygen permeation [576] confirms such dependence. As pointed out in Ref. [576], one of the reasons for the discrepancies in the question of the dependence on w could be that the Arrhenius plots are not consistently plotted for a constant value of w, and the oxygen content, for that matter, is not monitored.

When the chemical diffusion coefficients are evaluated from measurements [556, 557, 560] performed on monodispersed particulate samples (non-sintered powders), data two or three orders of magnitude smaller than values measured for sintered samples are obtained. This discrepancy is most probably caused by the effect of the additional diffusion distance through the gas phase and grain boundaries inside the conglomerate of grains, whereas only the netto grain size is being considered for the evaluations.

The self-diffusion coefficients evaluated from tracer experiments [566, 567] or internal friction measurements [569] vary between some 10^{-12} cm^2 s^{-1} at 320°C and 10^{-8} cm^2 s^{-1} at 900°C. The difference between the chemical- and self-diffusion coefficients is therefore about four orders of magnitude. This larger-than-usual difference is being explained away as a consequence of cracks and pores in the samples used for measurements of the chemical diffusivity which comes out then somewhat too high [566]. The self-diffusivity is also practically independent of the partial pressure of oxygen and thus of w. Perhaps in line with this, also the purely ionic conductivity is found almost independent of w in Ref. [572]. These facts can be reconciled with the other data by using the concept of the bipolar oxygen diffusion in $YBa_2Cu_3O_{6+w}$. In this picture, the electronic (hole) conductivity would be higher than the ionic conductivity, and also strongly dependent on w, increasing thus the overall rate of diffusion and giving it the non-stoichiometry dependence.

In the conclusion of this paragraph, it is important to note that the oxygen diffusivity in $YBa_2Cu_3O_{6+w}$ is strongly anisotropic, in line with the crystal structure. Diffusion occurs almost exclusively in the *a, b* plane of the copper oxygen chains. The diffusivity in the direction of the *c*-axis is six orders of magnitude lower than the overall diffusion in polycrystals [568]. The diffusivity in the direction of the *b*-axis is 100 times higher than in the direction of the *a*-axis, and this suggests that the oxygen transport takes place along the oxygen rows (copper-oxygen chains) via the completely vacant sites between them.

D. Substitutions

1. Hydrogen, proton and hydroxyl

For variety of reasons, the only path to the hydrogen-substituted variants of $YBa_2Cu_3O_{6+w}$ is the interaction of the master phase with gaseous H_2 or H_2O. The reactions involved have two main components, one redox and the other acidobasic, both causing easily a destruction of the phase, the former due to the reduction into the (ultimately) metallic Cu, the latter due to the hydrolysis. Both decompositions can be avoided by adopting low temperatures for the interactions, and, at higher temperatures, by maintaining the appropriate low partial pressures of the gaseous species.

Under such mild conditions, the reacting centres are the Lewis-base oxygens in $YBa_2Cu_3O_{6+w}$ which have strong affinity towards the Lewis-acid protons and form hydroxide defects. These hydroxide defects are the regular hydroxide groups occurring, e.g., in the structures of various metal hydroxides, where they behave effectively as a spherical anion with a radius of some 153 pm [577]. This radius is only slightly larger than the generally accepted radius for O^{2-} (140 pm), since the covalent O–H bond is short. However, the migrating hydrogen species in the solid state are not the hydroxide groups as such, but the protons alone [578–580], and therefore the defects are often denoted in the literature simply as $H_i^{\cdot}$.

Adopting the same standard stoichiometric state as for the oxygen equilibria in Sec. V C, and for simplicity formally assuming that the changes occur in the Cu(1) region, the formations of the hydroxide defects from H_2 and H_2O are expressed in terms of defect reactions in the following. The incorporation of n moles of H_2 into 1 mol of $YBa_2Cu_3O_{6+w}$ will create $2n$ mol of the hydroxide defects and reduce the overall formal Cu valence by $2n/3$, while the

overall number of the occupied "oxygen" sites per formula remains constant at $6+w$. The span of the Cu valence states compatible with the given structure type is then likely to be the limiting factor for the extent of this reaction.

$$H_2 + 2O_i'' + 2Cu_{Cu}^{\cdot} \leftrightarrow 2(OH)_i' + 2Cu_{Cu}^{\times} \quad (26)$$

The incorporation of n moles of H_2O into 1 mol of $YBa_2Cu_3O_{6+w}$ will create $2n$ mol of hydroxide defects and maintain the Cu valence constant, while the overall occupancy of the "oxygen" sites increases by n per formula. The occupancy span for the "oxygen" sites is then likely to be the limiting factor for the extent of this reaction.

$$H_2O + V_i + O_i'' \leftrightarrow 2(OH)_i' \quad (27)$$

It is more or less a matter of formality that these equations can be rewritten to involve the $O_O^{\times}$ oxygens instead of the O_i'' (the latter being the w per formula oxygens), holes $h^{\cdot}$ instead of $Cu_{Cu}^{\cdot}$, or, for that matter, also $H_i^{\cdot}$ and O_i'' instead of $(OH)_i'$.

In a sensitive redox system like this, the acidobasic reaction in Eq. (27) is expected to be significantly accompanied by the redox reaction in Eq. (26) when the system contains H_2 in its atmosphere and by the redox reaction in Eq. (16) for systems with O_2 atmospheres. Moreover, these equations can be combined with the equations for dissociation of water into the elements and for the intrinsic condition to achieve different combinations of the involved defects for expressing equilibrium constants.

It is experimentally established that some incorporation of hydrogen into $YBa_2Cu_3O_{6+w}$ takes place, both by reaction with dihydrogen [581–583] and with water [584, 585]. In fact, NMR analyses indicate that the standard ceramic syntheses of $YBa_2Cu_3O_{6+w}$ may result in as much as 0.2 hydrogen atoms per formula, originating presumably from water vapour [586].

The low-temperature hydrogenation of $YBa_2Cu_3O_{6+w}$ seems to be the most reproducible method for synthesis of the protonated phases. Their characterization, however, has proved extremely difficult, particularly due to the analytical problems with hydrogen being the lightest atom (TG, PXD) and an incoherently scattering element (PND), as well as due to the inhomogeneities and the enhanced reactivity of the products. A somewhat clearer picture can be extracted from a combination of several recent studies adopting special methods like the ^{15}N nuclear reaction method [587], HREM [588] and PND at variable temperatures [589], as well as special substrates like the thin film arrangement in Ref. [587]. The data show consistently that the incorporation of hydrogen proceeds in two steps. The first step occurs at low temperatures, below some 200°C (under 1 atm of H_2, the temperature being even lower under higher pressures [589] and vice versa [588]). Small amounts of hydrogen, up to some 0.3 per formula are absorbed (say, according to Eq. (26)) while some water is released (say, according to Eq. (27)). This results in rather insignificant changes in the lattice parameters and T_c of the matrix phase. According to other reports, [590, 591] a hydrogen content up to some 1 per formula can be achieved, accompanied by a structural change into tetragonal symmetry and a decrease in the c parameter. In the second step, occurring above 200°C, and up to, say, 300°C, this phase gradually disappears and another, yet closely related triple-perovskite phase is being formed, containing at saturation approximately 2 hydrogen atoms per formula. The oxidation state of Cu is then the same as in $YBa_2Cu_3O_6$ having monovalent copper in the Cu(1) site. Typical for this newly recognized perovskite structure is that it has the c-axis extended by almost 200 pm as compared with the original material, according to Ref. [587], and this can be corroborated by the data in Ref. [588] (although probably erroneously referred to the 124 or 147 phases) and in

Ref. [589] (although giving an obviously misprinted value). During the formation of this phase, the release of water seen [589] by TG is comparable with that during the first step, whereas the continuing reduction of copper, particularly at Cu(1), is manifested by the superstructure features seen by HREM [588], by iodometry [591] and apparently also by the appearance [592, 593] of the antiferromagnetic ordering typical for the $w \rightarrow 0$ versions of the original phase. The additional hydrogen-containing defects are tentatively located [587] in the Cu(1) coordination sphere and this provides a good possible explanation for the *c*-axis extension: Whereas the Cu(1) atom is reduced to Cu(I) and should presumably adopt the linear (dumbbell) coordination in the *c* direction, there are now hydroxide groups OH^- located around Cu(1) in high concentrations. For bond-valence reasons and also due to the size of the hydroxide groups, the *c*-axis bond distance at Cu(1) must then extend substantially. It should be mentioned that also the $YBa_2Cu_4O_8$ phase absorbs around 2H per formula unit and that this does not cause any such significant *c*-axis extension [587]. It seems that a moderate hydrogenation is reversible in pure oxygen at 200 to 400°C [588, 594].

The detailed compositional and structural characterization of both $YBa_2Cu_3O_{6+w}$ with the hydrogen defects and of the fully hydrogenated phase is still missing. However, several computational studies [595, 596] are available, dealing with the location of protons and hydroxide groups in the perovskite-type structures. These atomistic simulations confirm the O–H bond distance (94 pm in Ref. [596]), the location of the protons close to the direction of the adjacent oxide ion, and the occurrence of a low-energy barrier for the proton transport.

2. Halogens

The partial substitution of oxygens in $YBa_2Cu_3O_{6+w}$ by the lighter halogen atoms is structurally similar to the substitution by the hydroxide groups, both when ionic charge and radius are considered. Also here the feasible synthesis route is the direct halogenation of $YBa_2Cu_3O_{6+w}$ at slightly elevated temperatures, preferably [597] by NF_3 in case of fluorine. Attempts to introduce halogens as Ba halogenides into the ceramic syntesis yield no reaction [598, 599]. However, an important difference between halogenation and hydrogenation is that halogenation oxidizes copper (formation of Cu–X bonds), whereas hydrogenation reduces it (formation of O–H bonds). The incorporation of *n* moles of X_2 (X = halogen) into 1 mol of $YBa_2Cu_3O_{6+w}$ will increase the overall formal Cu valence by $2n/3$ and will also increase the overall occupancy of the possible "oxygen" sites by $2n$ per formula. Both the valence and occupancy spans can restrict the extent of this reaction, which, in some similarity with Eq. (26), can be expressed as follows:

$$X_2 + 2V_i^{\cdot} + 2Cu_{Cu}^{\times} \leftrightarrow 2X_i' + 2Cu_{Cu}^{\cdot} \tag{28}$$

It is experimentally well established that fluorine [597, 600, 601], chlorine and even bromine [602] enter the vacant oxygen sites in the Cu(1) coordination sphere, in concentrations decreasing in the said order. Quantum-chemical calculation [602] of the alternative structures for the thus formed halogenide cuprate anions show that upon the reaction with the molecular halogens only the vacant oxygen sites are reasonable candidates for accommodation of the halogen atoms. Moreover, only the most electronegative of them, fluorine, should be able to enter also the normally empty sites between the copper oxygen square-chains, transforming them into octahedra. Chlorine and bromine, on the other hand, would only enter the vacancies inside the chains. This is in accordance with structural data from PND [597, 602].

Since the substitution of halogens (as well as hydroxyls) for oxygen is aliovalent, it can be used for fine tuning of the valence state and structural environment of copper. Both elec-

tron and hole doping (for superconductivity) can be achieved, by either substituting for oxygens and vacancies, respectively. As the oxide halogenides are relatively stable, successful attempts have been made to synthesize halogenated versions of also other cuprates than 123, like $Sr_2CuO_2F_{2+\delta}$ with the o-La_2CuO_4-type structure (T phase) [603], $Ca_2CuO_2F_{2+\delta}$ with the t-Nd_2CuO_4-type structure (T′-phase) [604], $(Ca,Sm)_2CuO_3Cl$ with the tetragonal T*-phase structure [605] and $(AE)_2CaCu_2O_4Cl_2$ with the $RE_2CaCu_2O_6$-type (Ruddlesden-Popper-type) structure [606, 607]. However, any information towards a systematic phase-diagram mapping is very scarce.

3. Metals except AEs and REs

The diversion brought into the RE(O)–AE(O)–Cu(O) systems through the introduction of a fourth kind of metal is much more drastic than when similar AEs or REs are involved. However, the problem is that not even the RE(O)–AE(O)–M(O) systems are known well. Only for specific cases concerning superconducting phases, there is relatively abundant information available about the solid solubility with respect to various metals M, but only rarely the phases occurring in equilibrium at the solubility limits are identified.

Solid solubility at the RE site. Only few other elements than REs and AEs are able to significantly enter these sites. Of the alkaline metals, sodium may apparently be present at the Y site up to a few atom percent, provided a matching amount is allotted to the Ba site [105]. Syntheses of homogeneous, single-phase oxides which contain the alkali metals are difficult due to the high volatility of the alkali metal peroxides and superoxides. Usually, a deficiency in alkali metal is found in the subsequent analyses of the products, despite the precautions taken. A more straightforward situation occurs with the metals of the actinide series, which are chemically similar to the REs. Curium forms a non-superconducting $CmBa_2Cu_3O_7$ phase [608]. Also an equiatomic Th,Ca mixture enters partially at the Y site of $YBa_2Cu_3O_{6+w}$, $x \leq 0.1$ [609]. Of the other metals, cadmium is reported [610] to substitute at the Y site in $YBa_2Cu_3O_{6+w}$ up to some $x=0.5$, with a rather surprisingly negligible effect on T_c, despite the observed structural conversion from orthorhombic to tetragonal at $x=0.4$. However, the presence of $BaCuO_2$ impurities suggests that Cd may also be entering at the Ba site, although this possibility was not considered in Ref. [610].

Solid solubility at the Ba site. Also this type of substitution occurs rarely for other elements than Sr (see Sec. IV D) and large REs (see Sec. IV C 2). Alkali metals again are practically the only candidates, and minute amounts of K, Rb and Cs are reported either at the Ba site [611] or at both the Y and Ba sites in $YBa_2Cu_3O_{6+w}$ [105, 612]. Somewhat surprisingly, no incorporation of Pb at the Ba site is found, and a different (although 123-related) structure is in fact formed when PbO is introduced into the Y(O)–Ba(O)–Cu(O) system [613, 614].

Solid solubilities at the Cu sites. The chemical and ionic-size similarity governs also here. For the $YBa_2(Cu_{1-z}Mz)_3O_{6+w}$-type substitution, an overview of candidates for substituents is presented in Table 3, together with the phases involved in the equilibrium at the solid-solution limits. Despite the comprehensive literature on these substitution phases, such key data are not frequently reported, simply because the extra labour has not been undertaken to perform the tedious experimental work on poly-phase materials to ensure equilibrium. This statement is particularly valid for the investigations on substituents with very low limits of solid solubility [615], where also the detection threshold for the adopted analytical method should be taken into consideration. With the high sensitivity PXD instrumentation used in Ref. [615], the detection limit is some 0.5 and 1 wt% for the nearest neighbour phases Y_2BaCuO_5 and $BaCuO_{2+w}$, respectively. Therefore, substitution limits with $z < 0.01$ cannot be ascertained.

Table 3 Equilibrium phase compositions at the limit of solid solubility for M in $YBa_2(Cu_{1-z}M_z)_3O_{6+w}$ for samples fired at 910°C in pure oxygen and oxidized at 340°C, according to Ref. [615]

M	Y_2BaCuO_5	$BaCuO_{2+w}$	Other observed phases[a]	z_{lim}
Li	+	+	$BaCO_3$	0.04(1)
Mg	+	+	MgO	0.04(1)
Sc	+	–	$BaSc_2O_4$	0.01(1)
Ti	+	–	Ba titanates, TiO_2	0.00(2)
V	+	–	$Ba_3V_2O_8$	0.00(4)
Cr	+	–	$BaCrO_4$	0.02(1)
Mn	+	–	$Ba_3Mn_2O_8$	0.00(3)
Fe	–	+[b]	$YBa(Cu_{1-z}Fe_z)_2O_5$[c]	0.22(1)
Co	–	–	$YBa(Cu_{1-z}Co_z)_2O_5$[d]	
			$Ba(Co_{1-z}Cu_z)O_w$[e]	0.30(5)
Ni	+	+	NiO	0.08(1)
Zn	+	+	ZnO	0.09(1)

[a] A small amount of an additional phase is expected to occur in case of Li, Sc, V. and Mn

[b] {$Ba(Cu_{0.70(5)}Fe_{0.30(5)})O_{2+w}$; $Im\bar{3}m$; 1842.4(4)}

[c] {$z=0.4$; $P4mm$; 387.0(1), 767.1(1)}

[d] {$z\approx0.5$; $P4mm$; 387.2(1), 756.2(2)}

[e] {$z\approx0.0$, $w=2.80(3)$; h; 571.65(2), 444.00(2)}.

The solubility limits in Table 3 agree reasonably well with other literature data, viz., with those not very frequent cases where such data are explicitly stated. As an example for the further data: Fe ($z=0.18$) [616]; Co ($z=0.25$) [617]; Ni ($z=0.04$) [618]; ($z=0.09$) [619]; ($0.10<z<0.17$) [620]; Zn ($z=0.10$) [621]; ($z=0.12$) [622]; Al ($z=0.04$) [621, 623, 624]; Ga ($z=0.05$) [625]; Au ($z=0.10$) [626–628] and Pd ($z=0.17$) [629]. For the group of the most compatible substituents, Fe, Co, Ni, Zn and Mg, the three- or four-phase neigbourhoods occurring at the solid-solubility limits are illustrated in the tetrahedral diagrams in Fig. 50.

For oxygen saturated $YBa_2(Cu_{1-z}M_z)_3O_{6+w}$, the oxidation state of Cu according to iodometry remains approximately constant as in the pure matrix phase. When the typical valence of a given substituent exceeds the valence of Cu, e.g., Fe(III), Co(III), Ni(>II), Al(III), Ga(III), the oxygen content hence may exceed seven per formula [615, 630]. These oxygen-saturated samples then often exhibit a crossover from orthorhombic to tetragonal symmetry, seen by PXD, which occurs at surprisingly low substitution levels, usually below $z=0.05$ [615, 621, 625]. This behaviour coincides with the fact that Fe, Co, Al, and Ga introduce a tendency for non-planar coordination at the square-planar Cu(1) site and concentrate themselves at the twin-domain boundaries [631–633]. With increasing z, the amount of such boundaries must increase at the expense of the bulk material and the domain size is reduced to the nanometer scale, below the PXD detection threshold, but observable by HREM [634, 635]. However, the orthorhombic structure persists at quite high substitution levels of iron (and cobalt) if a reducing atmosphere is applied during the firing, and the samples are reoxidized at low temperatures [636, 637]. The probable reason is that, under reducing conditions, these higher-valent substituents tend to be located primarily at the square-pyramidal Cu(2) sites where, due to the site symmetry, they are not coupled via twinning. The critical concentration for the orthorhombic to tetragonal transition for the low-temperature reoxi-

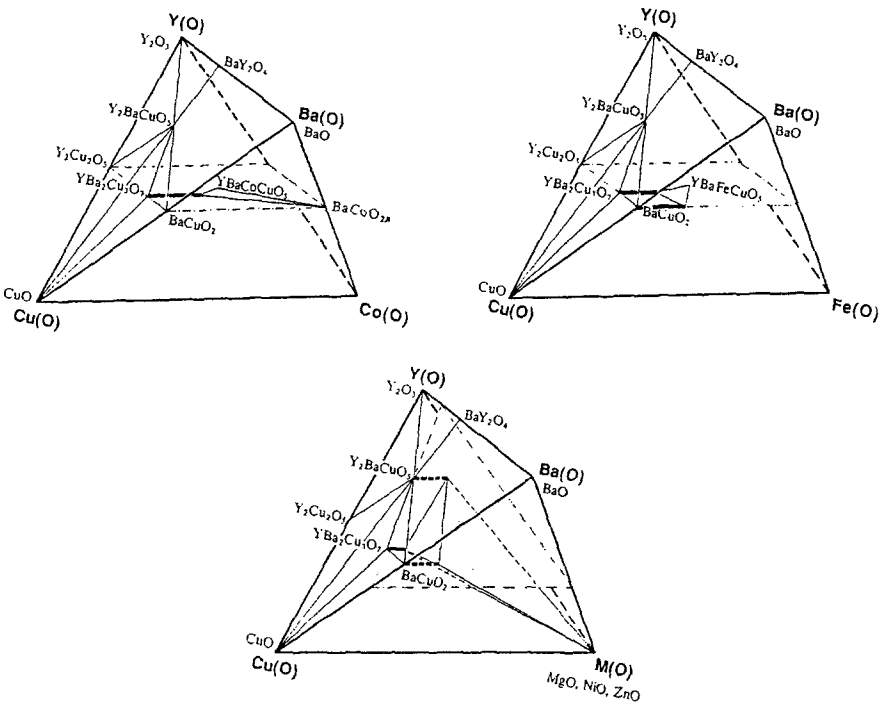

Fig. 50 Four-phase tetrahedral envelopes adjacent to the M-saturated $YBa_2(Cu_{1-z}M_z)_3O_{6+w}$ solid solutions for M=Fe, Co and Ni/Zn/Mg, in subsolidus (pseudoquaternary) tetrahedral phase diagrams, as seen by room temperature PXD after firing at 900°C in oxygen

dized samples is increased to $z_{0,t}\approx 0.15$. This is about the same as found for the La for Ba substitution, where it is attributed to the linkage of the copper–oxygen chains by the entering additional oxygens [435].

It should be mentioned that also other phases in the Y(O)–Ba(O)–Cu(O) system are liable to similar substitutions. For example, $YBa_2(Cu_{1-z}Fe_z)_4O_8$ is prepared up to $z=0.1$ and found tetragonal and non-superconducting above $z=0.04$ in direct contrast to the relatively benign effect of Fe towards superconductivity in the 123 phase [638].

E. Isostructural triple perovskites

Y(O)–Ba(O)–M(O). A complete replacement of Cu in the $YBa_2Cu_3O_7$-type structure by the first-row transition metals and Au has been tested [94] under conditions (temperature, partial pressure of oxygen) appropriate to the presumed stabilization of di- or tri-valent ions of these metals (whichever applicable) in the oxide. With the notable exception of Fe, all systems yielded a disordered perovskite or mixtures of phases which are thus more stable than the triple-perovskite arrangement. As an example, Sc forms a disordered perovskite, Ti (at very low p_{O_2}'s) forms a (light-blue coloured) mixture of the $(Y_{0.2}Ba_{0.8})TiO_3$ perovskite and the $Y_2Ti_2O_7$ pyrochlore, etc., up to Au, which gives an ordered Ba_2AuYO_6 perovskite and leaves the rest of the Au metal unreacted [94].

$YBa_2Fe_3O_{8+w}$: the exception is a triple perovskite, obtained phase pure [639, 640] from citrate precursors by repeated prolonged annealing at around 1000°C. At lower tempera-

tures, like those used for the syntheses of the $YBa_2Cu_3O_7$ cuprate counterpart, the ordering into the triple perovskite becomes very slow. In an oxygen atmosphere, the phase is stable only up to some 1250°C, and melts incongruently between 1250 and 1300°C. $Ba(Fe_{1-z}Y_z)O_3$ ($z \approx 0.1$, cubic), $YFeO_3$ and $BaFe_2O_4$, are seen after quenching [94]. The oxygen content of 8 per formula represents a hypothetical oxygen-rich extension of the cuprate, where the square-chains are fully developed to octahedra, and the structure [639] has tetragonal symmetry {$w=0.01$; *P4/mmm*; 391.81(5), 1182.4(2)} [641]. Upon reduction, these octahedra begin to approach the square-planar situation for $M=Cu$, but long before it happens, the homogeneity range ends at $w=-0.25$ and Fe(II) phases are formed [641–643]. Shortly before that (at some $w=-0.20$) the symmetry nevertheless turns orthorhombic, mirroring in this respect the behaviour of the tetragonal $YBa_2Cu_3O_6$ upon oxidation {$w=-0.24$; *Pmmm*; 390.98(4), 392.76(4), 1177.85(18)} [642]. In line with the cuprate, indications are obtained by fine-focus Raman analyses of occurrences of domains with different oxygen content [644]. The attempts to vary the oxygen content in $YBa_2Fe_3O_{8+w}$ show that the structure can also tolerate a small amount of extra oxygens. Some 0.1 per formula unit is achieved at 450°C under $p_{O_2}=15$ MPa [640–642], and only slightly less under ambient-pressure oxidation {$w=0.08$; *P4/mmm*; 391.51(2), 1181.35(9)} [642]. The structural location of the extra oxygens was done by PND on a series of samples where the saturated oxygen content was controlled by a progressing Ca for Y substitution [645]. According to Ref. [645], these oxygen atoms in excess of 8 are present in the Y-layer, imposing split-position crystallographic defects upon the neighbouring oxygen sites. In line with their "interstitial" character, these oxygen ions are easily mobile, and the chemical diffusion coefficient $\tilde{D}$ in the solid is relatively high when these oxygens are involved in the interaction with the surrounding atmosphere [646]:

$$\log_{10}\tilde{D} = -3.28(20) - 2541(211)/T + 0.236(36)\log_{10}p_{O_2} \qquad (29)$$

(expressed in $cm^2\ s^{-1}$, K, and Pa, respectively, from data obtained in the temperature interval of $909 < T < 1250$ K). On the other hand, the presence of the extra oxygen atoms has only a negligible structural effect. It is the replacement of the coordination squares by the octahedra that alters profoundly the charge balance between the two M sites, manifested in

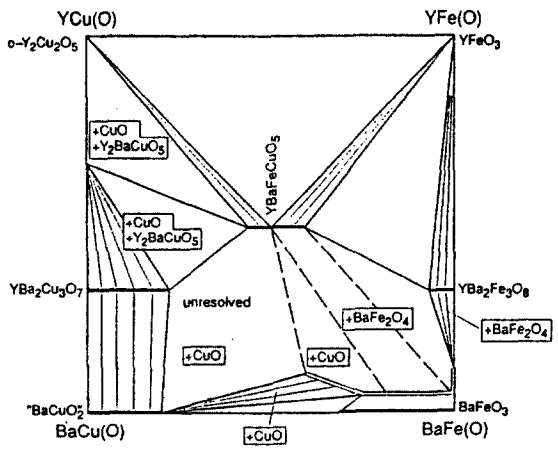

Fig. 51 Subsolidus phase compatibilities in the YCu(O)–BaCu(O)–YFe(O)–BaFe(O) system at 910 to 950°C in oxygen; after Ref. [640]. The $(Ba_{1-y}Y_y)(Fe_{1-z}Y_z)O_3$ solid solution, located above the plane of the diagram, is shown by doubled lines, as seen by PXD

a complete reversal of the two apical bond lengths M–O when going from M=Cu to Fe. This difference is so profound that, despite the otherwise similar unit-cell dimensions, only limited solid solubility occurs between the Cu and Fe variant. These solid solubilities are illustrated in Fig. 51 showing the square section of the tetrahedral phase diagram of the YFe(O)–BaFe(O)–YCu(O)–BaCu(O) subsolidus system at (nearly) isothermal conditions [640], which includes several relevant coexisting phases from both the Cu and Fe system. Considering that Co has the largest homogeneity range of all metals at the Cu site in $YBa_2Cu_3O_{6+w}$, it was not very surprising to find out that Co is also very much compatible with $YBa_2Fe_3O_{8+w}$, being able to replace almost one half of the present Fe atoms [647]. In accordance with the rule that the oxidation state of the transition metals in the mixed-valence oxometalate networks at fixed p_{O_2} is mainly a function of the electropositivity of the cations, also the saturated oxygen content of $YBa_2(Fe_{1-z}Co_z)_3O_{8+w}$ behaves as if the formal valences of both Fe and Co were constant as a function of the substitution level, viz., $\nu_{Fe}\approx 3.05$ and $\nu_{Co}\approx 2.65$. With increasing z, the maximum oxygen content then decreases. Around the limit for the solid solubility for Co, the saturated oxygen content is approximately as low as in the most reduced phase with no Co substitution. The triple-perovskite structure of $REBa_2Fe_3O_{8+w}$ is much less accommodative for various REs than the corresponding cuprate. In fact, it has been obtained only in a narrow region of close RE elements (around the size of Y, Dy and Er). For larger RE atoms, which also introduce more of the extra oxygen atoms (as much as w=0.8 for RE=La), the atomic arrangement gradually acquires the character of the disordered perovskite type, whereas for smaller RE=Yb and Lu the phase in question does not exist [643, 648]. The largest RE, La, can also enter the Ba site in $YBa_2Fe_3O_{8+w}$, but only when a matching amount occurs at the Y site. This situation rapidly brings about the appearance of the disordered cubic perovskite instead of the triple perovskite [649]. This is in interesting contrast with the cuprate where La is able to substitute solely for Ba (see Sec. IV C 3), probably in conjunction with the fact that the unit-cell volume is smaller for the cuprate than for the Fe version.

Y(O)–Ba(O)–M,M'(O). As apparent from the previous paragraph, Co is nearly, but not fully compatible with the 123 triple-perovskite structure. A full replacement by Co is reported under the condition [650] that some barium is simultaneously substituted by potassium {$Y(Ba_{0.75}K_{0.25})_2Co_3O_8$; *P4/mmm*; 386.8(2), 1123.7(9)}. A special kind of M for Cu substitution occurs within the $REBa_2Cu_3O_{6+w}$-type family for large REs. The introduction of M=Nb or Ta here leads to a complete conversion of the Cu–O coordination square chains to sheets of M-centered octahedra [651]. An oxygen content of 8 per formula is thus obtained for the non-superconducting $La(Ba_{0.95}La_{0.05})_2(Cu_{0.1}Ta_{0.9})Cu_2O_8$ phase {*P4/mmm*; 396.58(1), 1203.04(3)}. A zig-zag folding of the transition-metal occupied octahedra is deduced from weak superstructure reflections {*I4/mcm*} observed by neutron diffraction [652]. This indicates that an analogous tilt to that proposed [350, 344] for $YBa_2Cu_3O_7$ may be imagined.

Small REs like Y do not allow such an arrangement of transition metals in the 123 structure and when such preparations are attempted, a different perovskite arrangement is obtained, despite an analogy in stoichiometry, e.g., $YBa_2Cu_2WO_{9-w}$ {$Fm\bar{3}m$; 833.2} [653]. Other substituents may introduce a completely different coordination at one of the Cu sites in $YBa_2Cu_3O_7$, leaving the other untouched. For example, non-superconducting $YBa_2TlCu_2O_7$ {*P4/mmm*; 386.87(1), 1247.3(1)} has a Tl–O monolayer sheet instead of the square chains [654], and is hence not isotypic with $YBa_2Cu_3O_7$. Also in other cases the reasons for the (in)compatibility represent an interplay of bond-valence (ionic size) and electronic band structure arguments. Thus, when Ba is replaced by Sr, other metals can be stabilized substituting for Cu.

Y(O)–Sr(O)–M,M'(O). The presence of the smaller Sr atoms stabilizes some degree of substitution by W as well as Mo and Re in the triple-perovskite structure [655]. Based on

PND structure determinations, it is argued that these high valent transition metals increase the bond valence of Cu, and therefore shorten the Cu–O distances in the cuprate network, by bringing additional oxygen atoms into the structure, which then suits the Sr size better {$YSr_2Cu_{2.8}W_{0.2}O_{7.13}$; *P4/mmm*; 380.36(3), 1151.13(8)} [655]. Also a replacement of a portion of Cu by substantially smaller atoms like Al has a similar effect in stabilizing Sr in the structure (and vice versa) [656, 657]. Such small atoms must have tetrahedral coordination, and this can only be accommodated instead of the copper–oxygen squares in the chains.

This location has been structurally well established for $YSr_2AlCu_2O_7$ {*P4/mmm;* 386.46(1), 1111.39(3)} [658] and for the Ga [659, 660] and Co [661, 662] versions, differing in the details on how the tetrahedral chains propagate in the *a, b* plane. These structures are hence not strictly isotypic with $YBa_2Cu_3O_7$.

VI. Conclusion

Although the chemical information is effectively communicated in the form of phase diagrams, it is clearly seen that only superficial understanding of phase relations and interactions with the atmosphere would be accomplished without the accompanying structural information. In systems like cuprates, where the directional character of the chemical bond is only limited, the composition and stability of the formed oxides depends on efficient filling of space upon maintaining the bond-valence condition for each atom in terms of bond distances and number of bonds. Each structural site thus represents a void of a certain size and shape which can be filled by an atom having bond-valence characteristics within a certain tolerance. The tolerance span can be considerably broad, as demonstrated on the phase-stability trends when the chemically closely related, but size different REs are present.

For the cuprates, the structural information is indispensable for yet another reason. It has become evident that the superconducting property of these materials is closely related to certain structural features – involving the presence of infinite sheets of the octahedral or square-pyramidal cuprate polyanion for a potential hole superconductor and infinite sheets of the square-planar cuprate polyanion for a potential electron superconductor. Behind these structural features, there seems to be another, more primary common denominator. All these cuprates, when superconducting, possess such a copper-oxygen coordination which allows us to imagine the occurrence of a non-bonding, partially filled Cu 3*d* orbital, energetically separated from the other *d* orbitals by the crystal (ligand) field interaction. In this picture, hole superconductivity of a cuprate then occurs when the orbital in question is almost empty, and electron superconductivity when the orbital is almost filled. Both cases result in a diluted occurrence of carriers – paired according to the Hund rule for the non-degenerated orbital. It can be speculated that these bosons are diluted or spaced far enough apart to undergo Bose-Einstein condensation at temperatures corresponding to the observed T_c. Remarkably, such an energetically separated, partially filled orbital may also be imagined in the superconducting bismuthates, vanadates or titanates. Finally, also other superconductors show features which comply with the picture of the dilute occurrence of the non-bonding electron pairs in an "infinite" bond framework. This may involve, e.g., the electron pairs in the alkali metal salts of C_{60}, metallic phosphorus and also in organic superconductors.

In this situation, the chemical information provided by a compilation of phase diagrams, which elucidate trends in stability for various structure types, may represent an important link in the quest for new high-T_c superconductors.

References

1 P. Karen, O. Braaten and A. Kjekshus, Acta Chem. Scand., 46 (1992) 805.
2 E. E. Schumacher, J. Am. Chem. Soc., 48 (1926) 396.

3 R. H. Lamoreaux, D. L. Hildenbrand and L. Brewer, J. Phys. Chem. Ref. Data, 16 (1987) 419.
4 I. F. Guillatt and N. H. Brett, J. Mater. Sci. Lett., 5 (1970) 615.
5 W. G. Burgers, Z. Phys., 80 (1933) 352.
6 K. T. Jacob and V. Varghese, J. Mater. Chem., 5 (1995) 1059.
7 B. V. Abalduev and A. F. Bolchakov, Elektron. Tekh., 4 (1972) 7.
8 V. D. Grebenyuk, I. V. Kavich, A. G. Mikolaichuk and I. T. Romanchuk, Ukr. Fiz. Zh., 12 (1967) 876.
9 E. P. Ostapchenko, Izvest. Akad. Nauk S.S.S.R., Ser. Fiz., 20 (1956) 1105.
10 K. T. Jacob, P. M. Raj and Y. J. Waseda, Phase Equilib., 16 (1995) 113.
11 C. N. Satterfield and T. W. Stein, Ind. Eng. Chem., 46 (1954) 1734.
12 C. Holtermann and P. Laffitte, C. R. Acad. Sci. (Paris), 208 (1939) 517.
13 O. V. Kedrovskii, I. V. Kovtunenko, E. V. Kiseleva and A. A. Bundel, Russ. J. Phys. Chem., 41 (1967) 205.
14 S. C. Abrahams and J. Kalnajs, Acta Crystallogr., 7 (1954) 838.
15 W. Wong-Ng and R. S. Roth, Physica C (Amsterdam), 23 (1994) 97.
16 C. Brosset and N.-G.Vannerberg, Nature (London), 177 (1956) 238.
17 J. D. Bernal, E. Diatlowa, J. Kasarnowsky, S. Reichstein and A. G. Ward, Z. Kristallogr., A 92 (1935) 344.
18 R. A. Gleixner and Y. A. Chang, Metall. Trans., B 16 (1985) 743.
19 S. Tamaru and K. Siomi, Z. Phys. Chem. Stoechiom. Verwandschaftsl., A 159 (1932) 227.
20 H. Chessin and W. C. Hamilton, Acta Crystallogr., 18 (1965) 689.
21 H. Effenberger, K. Mereiter and J. Zemann, Z. Kristallogr., 156 (1981) 233.
22 J. P. R. De Villiers, Am. Mineral., 56 (1971) 758.
23 M. Foëx and J.-P. Traverse, Bull. Soc. Fr. Mineral. Cristallogr., 89 (1966) 184.
24 H. Müller-Buschbaum and H. G. von Schnering, Z. Anorg. Allg. Chem., 340 (1965) 232.
25 R. S. Roth and S. J. Schneider, J. Res. Natl. Bur. Stand., Sect., A 64 (1960) 309.
26 B. H. O'Connor and T. M. Valentine, Acta Crystallogr., B 25 (1969) 2140.
27 D. T. Cromer, J. Phys. Chem. 61 (1957) 753.
28 J. O. Sawyer, B. G. Hyde and L. Eyring, Proc. Chim. Soc. France, Ser., 5 (1965) 1190.
29 G. Brauer and K. A. Gingerich, J. Inorg. Nucl. Chem., 16 (1960) 87.
30 D. J. M. Bevan and J. Kordis, J. Inorg. Nucl. Chem., 26 (1964) 1509.
31 D. J. M. Bevan, J. Inorg. Nucl. Chem., 1 (1955) 49.
32 B. G. Hyde, D. J. M. Bevan and L. Eyring, Phil. Trans. Roy. Soc. London, A 259 (1966) 583.
33 C. L. Sieglaff and L. Eyring, J. Am. Chem. Soc., 79 (1957) 3024.
34 Y. Wilbert, A. Duquesnoy and F. Marion, C. R. Acad. Sci. Paris, 264 (1967) 316.
35 G. Brauer and B. Pfeiffer, J. Less-Common Met., 5 (1963) 171.
36 R. L. N. Sastry, P. N. Mehrotra and C. N. R. Rao, J. Inorg. Nucl. Chem., 28 (1966) 2167.
37 D. M. Gruen, W. C. Koehler and J. J. Katz, J. Am. Chem. Soc., 73 (1951) 1475.
38 D. A. Burnham, L. Eyring and J. Kordis, J. Phys. Chem., 72 (1968) 4424.
39 B. N. Ivanov-Emin and J. N. Medvedev, Zh. Neorg. Khim., 35 (1990) 300.
40 W. Prandtl and G. Rieder, Z. Anorg. Allg. Chem., 238 (1938) 225.
41 S. Ramdas, K. C. Patil and C. N. R. Rao, J. Chem. Soc., A (1970) 64.
42 V. S. Rudenko and A. G. Boganov, Izvest. Akad. Nauk S.S.S.R., Neorg. Mater., 7 (1971) 108.
43 N. C. Baenziger, H. A. Eick, H. S. Schuldt and L. Eyring, J. Am. Chem. Soc., 83 (1961) 2219.
44 J. Kordis and L. Eyring, J. Phys. Chem., 72 (1968) 2030.
45 S. J. Schneider and R. S. Roth, J. Res. Nat. Bur. Stand. Ser., A 64 (1960) 317.
46 C. K. Jørgensen, R. Pappalardo and E. Rittershaus, Z. Naturforsch., A 20 (1965) 54.
47 H. Müller-Buschbaum and C. Teske, Z. Anorg. Allg. Chem., 369 (1969) 255.
48 H. Müller-Buschbaum and P.-H. Graebner, Z. Anorg. Allg. Chem., 386 (1971) 158.
49 J. M. Moreau, Mater. Res. Bull., 3 (1968) 427.
50 S. J. Schneider, R. S. Roth and J. L. Waring, J. Res. Nat. Bur. Stand. Ser., A 65 (1961) 345.
51 G. Brauer and H. Gradinger, Z. Anorg. Allg. Chem., 276 (1954) 209.
52 W. W. Barker and A. F. Wilson, J. Inorg. Nucl. Chem., 30 (1968) 1415.
53 D. J. M. Bevan, W. W. Barker, R. L. Martin and T. C. Parks, Proc. 4th Conf. Rare Earth Res., (Phoenix, Ariz., 1964) p. 441.
54 J. D. McGullough and J. D. Britton, J. Am. Chem. Soc., 74 (1952) 5225.
55 J. D. McGullough, J. Am. Chem. Soc., 72 (1950) 1386.
56 L. Wolf and H. Schwab, J. Prakt. Chem., 24 (1964) 293.
57 F. Petrů, F. Kůtek and J. Šatava, Collect. Czech. Chem. Commun., 31 (1966) 4459.
58 J. O. Sawyer, P. Caro and L. Eyring, Monatsh. Chem., 102 (1972) 333.
59 A. N. Christensen, Acta Chem. Scand., 24 (1970) 2440.

60 J. P. Attfield and G. Férey, J. Solid State Chem., 82 (1989) 132.
61 B. Hallstedt, D. Risold and L. J. Gauckler, J. Phase Equilib., 15 (1994) 483.
62 S. Åsbrink and L.-J. Norrby, Acta Crystallogr., B 26 (1970) 8.
63 F. W. Wrigge and K. Meisel, Z. Anorg. Allg. Chem., 203 (1932) 312.
64 P. Niggli, Z. Kristallogr., 57 (1922) 253.
65 H. S. Roberts and F. H. Smyth, J. Am. Chem. Soc., 43 (1921) 1061.
66 B. T. Collins, W. Desisto, R. Kershaw, K. Dwight and A. Wold, J. Less-Common Met., 156 (1989) 341.
67 J. Gundermann and C. Wagner, Z. Phys. Chem., B 37 (1937) 155.
68 M. Lenglet, K. Kartouni, J. Machefert, J. M. Claude, P. Steinmetz, E. Beauprez, J. Heinrich and N. Gelati, Mater. Res. Bull., 30 (1995) 393.
69 M. O'Keeffe and J.-O. Bovin, Am. Mineral., 63 (1978) 180.
70 P. E. D. Morgan, D. E. Partin, B. L. Chamberland and M. O'Keeffe, J. Solid State Chem., 121 (1996) 33.
71 G. A. Ozin, S. A. Mitchell and J. Garćia-Prieto, J. Am. Chem. Soc., 105 (1983) 6399.
72 Binary Alloy Phase Diagrams, Vol. 1, Ed. by T. B. Massalski, (American Society for Metals, 1986) p. 943.
73 R. Schmid, Metall. Trans., B 14 (1983) 473.
74 A. Ait-Hou, T. Rais, C. Chatillon and M. Allibert, Ann. Chim. Fr., 20 (1995) 345.
75 I. Yazawa, R. Sugise, N. Terada, M. Jo, K. Oka, H. Hayakawa and H. Ihara, Jpn. J. Appl. Phys., Part 2, 29 (1990) L1480.
76 W. Kwestroo, H. A. M. van Hal and C. Langereis, Mater. Res. Bull., 9 (1974) 1631.
77 D. M. de Leeuw, C. A. H. A. Mutsaers, C. Langereis, H. C. A. Smoorenburg and P. J. Rommers, Physica C (Amsterdam), 152 (1988) 39.
78 P. Karen and A. Kjekshus, J. Solid State Chem., 94 (1991) 298.
79 F. J. Gotor, N. Pellerin, P. Odier, E. Cazy, J. P. Bonnet, A. R. Fert and J. Ayache, Physica C (Amsterdam), 247 (1995) 252.
80 L. M. Lopato, Ceramurgia Int., 2 (1976) 18.
81 M. Foëx, Bull. Soc. Chim. France, Ser., 5 (1961) 109.
82 W. Trzebiatowski and R. Horyń, Bull. Acad. Pol. Sci., 13 (1965) 315.
83 J. R. Carter and R. S. Feigelson, J. Am. Ceram. Soc., 47 (1964) 141.
84 V. Longo, D. Minichelli and F. Ricciardiello, Science of Ceramics, 11 (1981) 171.
85 H. Müller-Buschbaum, Z. Anorg. Allg. Chem., 358 (1968) 138.
86 L. M. Lopato, L. I. Lugin and A. V. Shevchenko, Ukr. Khim. Zh., 39 (1973) 142.
87 A.-R. Schulze and H. Müller-Buschbaum, Z. Anorg. Allg. Chem., 471 (1980) 59.
88 H. Müller-Buschbaum and A. Boehlke, Z. Anorg. Allg. Chem., 553 (1987) 212.
89 A.-R. Schulze and H. Müller-Buschbaum, Z. Anorg. Allg. Chem., 461 (1980) 48.
90 A. J. Smith and A. J. E. Welch, Acta Crystallogr., 13 (1960) 653.
91 M. D. Mastromonaco, I. Barbariol and A. Cocco, Ann. Chim. (Rome), 59 (1969) 465.
92 E. Paletta and H. Müller-Buschbaum, J. Inorg. Nucl. Chem., 30 (1968) 1425.
93 W. Wong-Ng and B. Paretzkin, Powder Diff., 6 (1991) 187.
94 P. Karen and A. Kjekshus, (unpublished).
95 W. Zhang and K. Osamura, Mater. Trans., JIM 32 (1991) 1048.
96 G. A. Costa, M. Ferretti, E. A. Franceschi and G. L. Olcese, Thermochim. Acta, 133 (1988) 17.
97 G. M. Kale and K. T. Jacob, Solid State Ionics, 34 (1989) 247.
98 L. M. Lopato, L. I. Lugin and A. V. Shevchenko, Dopov. Akad. Nauk Ukr. S.S.R., Ser. B Ukr. Khim. Zh., 32 (1970) 535.
99 L. M. Lopato, I. M. Maister and A. V. Shevchenko, Izvest. Akad. Nauk S.S.S.R., Ser. Neorg. Mater., 8 (1972) 861.
100 H. Müller-Buschbaum and M. Scheikowski, Z. Anorg. Allg. Chem., 591 (1990) 181.
101 J. P. Guha and D. Kolar, J. Mater. Sci., 6 (1971) 1174.
102 A. J. Jacobson, B. C. Tofield and B. E. F. Fender, Acta Crystallogr., B 28 (1972) 956.
103 E. Banks, S. J. La Placa, W. Kunnmann, L. M. Corliss and J. M. Hastings, Acta Crystallogr., B 28 (1972) 3429.
104 S. A. Hodorowicz, J. Czerwonka and H. A. Eick, J. Solid State Chem., 88 (1990) 391.
105 P. Karen, O. Braaten, H. Fjellvåg and A. Kjekshus, AMSAHTS'90 (NASA Conf. Publ. 3100, 1990) p. 117.
106 L. M. Kovba, L. I. Lykova and E. V. Antipov, Zh. Neorg. Khim., 28 (1983) 724.
107 E. V. Antipov, L. I. Lykova and L. M. Kovba, Zh. Neorg. Khim., 29 (1984) 1624.
108 R. O. Suzuki, P. Bohac and L. J. Gauckler, J. Am. Ceram. Soc., 77 (1994) 41.

109 D. Risold, B. Hallstedt and L. J. Gauckler, J. Am. Ceram. Soc., 78 (1995) 2655.
110 A. M. M. Gadalla and J. White, Trans. Brit. Ceram. Soc., 65 (1966) 181.
111 R. S. Roth, C. J. Rawn, J. J. Ritter and B. P. Burton, J. Am. Ceram. Soc., 72 (1989) 1545.
112 R. S. Roth, N. M. Hwang, C. J. Rawn, B. P. Burton and J. J. Ritter, J. Am. Ceram. Soc., 74 (1991) 2148.
113 C. Tsang, J. K. Meen and D. Elthon, J. Am. Ceram. Soc., 78 (1995) 1863.
114 C. L. Teske and H. Müller-Buschbaum, Z. Anorg. Allg. Chem., 379 (1970) 234.
115 M. Hjorth and J. Hyldtoft, Acta Chem. Scand., 44 (1990) 516.
116 M. T. Weller and D. R. Lines, J. Solid State Chem., 82 (1989) 21.
117 T. Mathews, J. P. Hajra and K. T. Jacob, Chem. Mater., 5 (1993) 1669.
118 C. Krüger, W. Reichelt, A. Almes, U. König, H. Oppermann and H. Scheler, J. Solid State Chem., 96 (1992) 67.
119 T. Siegrist, R. S. Roth, C. J. Rawn and J. J. Ritter, Chem. Mater., 2 (1990) 192.
120 O. Milat, G. Van Tendeloo, S. Amelinckx, T. G. N. Babu and C. Greaves, J. Solid State Chem., 101 (1992) 92.
121 C. L. Teske and H. Müller-Buschbaum, Z. Anorg. Allg. Chem., 371 (1969) 325.
122 R. O. Suzuki, P. Bohac and L. J. Gauckler, J. Am. Ceram. Soc., 75 (1992) 2833.
123 C. B. Alcock and B. Li, J. Am. Ceram. Soc., 73 (1990) 1176.
124 R. S. Roth, C. J. Rawn, B. P. Burton and F. Beech, J. Res. Nat. Bur. Stand., 95 (1990) 291.
125 C. L. Teske and H. Müller-Buschbaum, Z. Anorg. Allg. Chem., 370 (1969) 134.
126 Y. Matsushita, Y. Oyama, M. Hasegawa and H. Takei, J. Solid State Chem., 114 (1994) 289.
127 E. M. McCarron, M. A. Subramanian, J. C. Calabrese and R. L. Harlow, Mater. Res. Bull., 23 (1988) 1355.
128 K. Ukei, T. Shishido and T. Fukuda, Acta Crystallogr., B 50 (1994) 42.
129 C. L. Teske and H. Müller-Buschbaum, Z. Anorg. Allg. Chem., 379 (1970) 113.
130 P. V. P. S. S. Sastry, A. D. Robertson, E. E. Lachowski, A. Coats and A. R. West, J. Mater. Chem., 5 (1995) 1931.
131 Y. Shimakawa, J. D. Jorgensen, J. F. Mitchell, B. A. Hunter, H. Shaked, D. G. Hinks, R. L. Hitterman, Z. Hiroi and M. Takano, Physica C (Amsterdam), 228 (1994) 73.
132 Z. Hiroi, M. Takano, M. Azuma and Y. Takeda, Nature (London), 364 (1993) 315.
133 Y. Y. Wang, H. Zhang, V. P. Dravid, L. D. Marks, P. D. Han and D. A. Payne, Physica C (Amsterdam), 255 (1995) 247.
134 H. Zhang, Y. Y. Wang, L. D. Marks, V. P. Dravid, P. D. Han and D. A. Payne, Physica C (Amsterdam) 255 (1995) 257.
135 R. C. Lobo, C. Greaves and F. J. Berry, J. Solid State Chem., 88 (1990) 513.
136 P. D. Han, L. Chang and D. A. Payne, Physica C (Amsterdam), 228 (1994) 129.
137 X.-J. Wu, P. Laffez, H. Yamauchi and N. Môri, Physica C (Amsterdam), 228 (1994) 292.
138 A. Ono, Physica C (Amsterdam), 198 (1992) 287.
139 B.-H. Chen, D. Walker, B. A. Scott and D. B. Mitzi, J. Solid State Chem., 121 (1996) 498.
140 J. F. Bringley, B. A. Scott, S. J. La Placa, R. F. Boehme, T. M. Shaw, M. V. McElfresh, S. S. Trail and D. E. Cox, Nature (London), 347 (1990) 263.
141 B.-H. Chen, D. Walker, E. Suard, B. A. Scott, B. Mercey, M. Hervieu and B. Raveau, Inorg. Chem., 34 (1995) 2077.
142 M. Takano, Y. Takeda, H. Okada, M. Miyamoto and T. Kusaka, Physica C (Amsterdam), 159 (1989) 375.
143 Z. Hiroi, M. Azuma, M. Takano and Y. Bando, J. Solid State Chem., 95 (1991) 230.
144 T. G. N. Babu, D. J. Fish and C. Greaves, J. Mater. Chem., 1 (1991) 677.
145 Y. Miyazaki, H. Yamane, T. Kajitani, Y. Oku, K. Hiraga, Y. Morii, K. Fuchizaki, S. Funahashi and T. Hirai, Physica C (Amsterdam), 191 (1992) 434.
146 M. Uehara, H. Nakata and J. Akimitsu, Physica C (Amsterdam), 216 (1993) 453.
147 H. Nakata, J. Akimitsu, S. Katano, T. Minami, N. Ogita and M. Udagawa, Physica C (Amsterdam), 255 (1995) 157.
148 K. Yamaura, Z. Hiroi and M. Takano, Physica C (Amsterdam), 229 (1994) 183.
149 G. F. Voronin and S. A. Degterov, J. Solid State Chem., 110 (1994) 50.
150 T. B. Lindemer and E. D. Specht, Physica C (Amsterdam), 255 (1995) 81.
151 W. K. Wong-Ng, K. L. Davis and R. S. Roth, J. Am. Ceram. Soc., 71 (1988) C64.
152 W. Zhang, K. Osamura and S. Ochiai, J. Am. Ceram. Soc., 73 (1990) 1958.
153 D. Mazza, M. Vallino, F. Abbattista and S. Delmastro, Mater. Chem. Phys., 25 (1990) 385.
154 G. Rian, Dissertation NTH Trondheim, IUK-report 1992:65, 1992.
155 R. Kipka and H. Müller-Buschbaum, Z. Naturforsch., B 32 (1977) 121.

156 W. Gutau and H. Müller-Buschbaum, J. Less-Common Met., 152 (1989) L11.
157 E. F. Paulus, G. Miehe, H. Fuess, I. Yehia and V. Löchner, J. Solid State Chem., 90 (1991) 17.
158 E. F. Paulus, G. Wltschek and H. Fuess, Z. Kristallogr., 209 (1994) 586.
159 N. Guskos, V. Likodimos, C. A. Londos, V. Psycharis, C. Mitros, A. Koufodakis, H. Gamari-Seale, W. Windsch and H. Metz, J. Solid State Chem., 119 (1995) 50.
160 M. A. G. Aranda and J. P. Attfield, Ang. Chem. Int. Ed. Engl., 32 (1993) 1454.
161 K. Torkar, H. Krischner and E. Will, Monatsh. Chem., 100 (1969) 825.
162 R. Gottschall and R. Schöllhorn, Solid State Ionics, 59 (1993) 93.
163 A. Bertinotti, J. Hamman, D. Luzet and E.Vincent, Physica C (Amsterdam), 160 (1989) 227.
164 E. L. Brosha, F. H. Garzon, I. D. Raistrick and P. K. Davies, J. Solid State Chem., 122 (1996) 176.
165 N. E. Brese, M. O'Keeffe, R. B. Von Dreele and V. G. Young, Jr., J. Solid State Chem., 83 (1989) 1.
166 J. G. Thompson, T. J. White, R. L. Withers, J. D. Fitz Gerald, P. J. Barlow, and S. J. Collcott, Materials Forum, 14 (1990) 27.
167 J. G. Thompson, J. D. Fitz Gerald, R. L. Withers, P. J. Barlow and J. S. Anderson, Mater. Res. Bull., 24 (1989) 505.
168 O. Chmaissem, Q. Huang, S. N. Putilin, M. Marezio and A. Santoro, Physica C (Amsterdam), 212 (1993) 259.
169 M. Arjomand and D. J. Machin, J. Chem. Soc., Dalton Trans., 11 (1975) 1061.
170 P. Laffez, X. Wu, S. Adachi, H. Yamauchi and N. Môri, Physica C (Amsterdam), 233 (1994) 373.
171 M. Machida, K. Yasnoka, K. Equchi and H. Arai, J. Solid State Chem., 91 (1991) 176.
172 S. Petriček, N. Bukovec, P. Bukovec, J. Solid State Chem., 99 (1992) 58.
173 W. Mingmei, S. Qiang, H. Gang, R. Yufang and W. Hongyiang, J. Solid State Chem., 110 (1994) 389.
174 A. F. Maiorova, S. N. Mudretsova, M. L. Kovba, A. S. Monaenkova and A. A. Popova, Physica C (Amsterdam), 218 (1993) 137.
175 E. L. Brosha, F. H. Garzon and I. D. Raistrick, J. Am. Ceram. Soc., 78 (1995) 1745.
176 H. Chang, Y. Y. Ren, Y. Q. Wang, Y. Y. Xue and C. W. Chu, Physica C (Amsterdam), 228 (1994) 383.
177 G. V. Bazuev and V. N. Krasilnikov, Zh. Neorg. Khim., 36 (1991) 2195.
178 T. Graf, G. Triscone, A. Junod and J. Muller, J. Less-Common Met., 170 (1991) 359.
179 E. George, D. Elthon and J. K. Meen, J. Am. Ceram. Soc., 78 (1995) 3309.
180 L. A. Klinkova, N. V. Barkovskii, D. I. Batova, A. I. Kolyubakin and S. A. Shevchenko, Supercond.: Phys. Chem. Tech., 5 (1992) 1247.
181 C. L. Teske and H. Müller-Buschbaum, Z. Naturforsch., B 27 (1972) 296.
182 F. Abbattista, M. Vallino, C. Brisi and M. Lucco-Borlera, Mater. Res. Bull., 23 (1988) 1509.
183 A. R. Armstrong, H. S. Obhi and P. P. Edwards, J. Solid State Chem., 106 (1993) 120.
184 K. Schulze, P. Majewski, B. Hettich and G. Petzow, Z. Metallk., 81 (1990) 836.
185 C. Krüger, W. Reichelt, A. Almes, U. König, H. Oppermann and H. Scheler, J. Solid State Chem., 96 (1992) 67.
186 M. Heinau, R. Baumann, B. Nick, M. Hartweg and L. Walz, Z. Kristallogr., 209 (1994) 418.
187 T. Siegrist, S. M. Zahurak, D. W. Murphy and R. S. Roth, Nature (London), 334 (1988) 231.
188 S. Kikkawa, N. Kato, N. Taya, M. Tada and F. Kanamaru, J. Am. Ceram. Soc., 78 (1995) 1387.
189 M. Azuma, Z. Hiroi, M. Takano, Y. Bando and Y. Takeda, Nature (London), 356 (1992) 775.
190 M. G. Smith, A. Manthiram, J. Zhou, J. B. Goodenough and J. T. Markert, Nature (London), 351 (1991) 549.
191 A. D. Robertson, P. V. P. S. S. Sastry and A. R. West, J. Eur. Ceram. Soc., 16 (1996) 637.
192 C. Greaves and P. R. Slater, Solid State Commun., 73 (1990) 629.
193 K. A. Kubat-Martin, E. Garcia and D. E. Peterson, Physica C (Amsterdam), 172 (1990) 75.
194 K. A. Kubat-Martin, G. H. Kwei, A. C. Lawson and D. E. Peterson, J. Solid State Chem., 100 (1992) 130.
195 M. Kikuchi, F. Izumi, M. Kikuchi, E. Ohshima, Y. Morii, Y. Shimojo and Y. Syono, Physica C (Amsterdam), 247 (1995) 183.
196 C. Greaves and P. R. Slater, J. Mater. Chem., 1 (1991) 17.
197 M. Kikuchi, E. Ohshima, M. Kikuchi, T. Atou and Y. Syono, Physica C (Amsterdam), 232 (1994) 263.
198 M. Hervieu, B. Mercey, W. Prellier, J. L. Allen, J.-F. Hamet and B. Raveau, J. Mater. Chem., 6 (1996) 165.
199 R. S. Roth, C. J. Rawn, J. D. Whitler, C. K. Chiang and W. K. Wong-Ng, J. Am. Ceram. Soc., 72 (1989) 395.
200 A. Lappas, K. Prassides, A. R. Armstrong and P. P. Edwards, Inorg. Chem., 32 (1993) 383.
201 A. R. Armstrong and P. P. Edwards, J. Solid State Chem., 98 (1992) 432.
202 H. Shibata, K. Kinoshita and T. Yamada, Physica C (Amsterdam), 232 (1994) 181.
203 K. Kinoshita and T. Yamada, Nature (London), 357 (1992) 313.

204 G. M. Kale and K. T. Jacob, Chem. Mater., 1 (1989) 515.
205 K. T. Jacob, T. Mathews and J. P. Harja, Metallurg. Trans., A 24 (1993) 1655.
206 G. M. Kale and D. J. Fray, J. Am. Ceram. Soc., 78 (1995) 1882.
207 R. A. Konetzki and R. Schmid-Fetzer, J. Solid State Chem., 99 (1992) 58.
208 E. Takayama-Muromachi and A. Navrotsky, J. Solid State Chem., 106 (1993) 349.
209 W. Wong-Ng, B. Paretzkin and E. R. Fuller, Jr., J. Solid State Chem., 85 (1990) 117.
210 H. Fjellvåg, P. Karen and A. Kjekshus, Acta Chem. Scand., A 42 (1988) 144.
211 H.-R. Freund and H. Müller-Buschbaum, Z. Naturforsch., B 32 (1977) 609.
212 H.-R. Freund and H. Müller-Buschbaum, Z. Naturforsch., B 32 (1977) 1123.
213 J. Aride, S. Flandrois, M. Taibi, A. Boukhari, M. Drillon and J. L. Soubeyroux, Solid State Commun., 72 (1989) 459.
214 J. L. García-Muñoz and J. Rodríguez-Carvajal, Physics Letters, A 149 (1990) 319.
215 A. M. Gadalla and P. J. Kongkachuichay, Mater. Res., 6 (1991) 450.
216 E. L. Brosha, F. H. Garzon and I. D. Raistrick, J. Am. Ceram. Soc., 77 (1994) 1139.
217 H. Fjellvåg, P. Karen, A. Kjekshus, P. Kofstad and T. Norby, Acta Chem. Scand., A 42 (1988) 178.
218 R. J. Cava, T. Siegrist, B. Hessen, J. J. Krajewski, W. F. Peck, B. Batlogg, H. Takagi, J. V. Waszczak, L. F. Schneemeyer and H. W. Zandbergen, J. Solid State Chem., 94 (1991) 170.
219 J. M. S. Skakle and A. R. West, J. Mater. Chem., 5 (1995) 765.
220 J. M. S. Skakle and A. R. West, J. Am. Ceram. Soc., 77 (1994) C2199.
221 B. Grande, H. Müller-Buschbaum and M. Schweizer, Z. Anorg. Allg. Chem., 428 (1977) 120.
222 H. Müller-Buschbaum and W. Wollschläger, Z. Anorg. Allg. Chem., 414 (1975) 76.
223 D. E. Cox, A. I. Goldman, M. A. Subramanian, J. Gopalakrishnan and A. W. Sleight, Phys. Rev. B: Condens. Matter, 40 (1989) 6998.
224 K. A. K. Martin, Z. Fisk and R. R. Ryan, Acta Crystallogr., C 44 (1988) 1518.
225 A. C. W. P. James, S. M. Zahurak and D. W. Murphy, Nature (London), 338 (1989) 240.
226 T. Tokura, H. Takagi and S. Uchida, Nature (London), 337 (1989) 345.
227 J. L. Jorda and M. T. S. Cohen-Adad, J. Less-Common Met., 171 (1991) 127.
228 W. Wong-Ng, L. P. Cook, B. Paretzkin, M. D. Hill and J. K. Stalick, J. Am. Ceram. Soc., 77 (1994) 2354.
229 A. A. Fotiev, G. E. Shter, A. S. Kosmynin, I. K. Garkuchin, V. L. Balachov and A. S. Trunin, Sverkhprovodimost Fiz. Khim. Tekh., 3 (1990) 1071.
230 J. M. Longo and P. M. Raccah, J. Solid State Chem., 6 (1973) 526.
231 B. Dąbrowski, D. G. Hinks, J. D. Jorgensen and D. R. Richards, Mater. Res. Soc. Symp. Proc., 100 (1989) 69.
232 J. D. Jorgensen, H.-B. Schüttler, D. G. Hinks, D. W. Capone, H. K. Zhang, M. B. Brodsky and D. J. Scalapino, Phys. Rev. Lett., 58 (1987) 1024.
233 J. G. Bednorz and K. A. Müller, Z. Phys. B: Condens. Matter, 64 (1986) 189.
234 S. W. Cheong, J. D. Thompson and Z. Fisk, Physica C (Amsterdam), 158 (1989) 109.
235 M. R. Chandrachood, D. E. Morris and A. P. B. Sinha, Physica C (Amsterdam), 171 (1990) 187.
236 A. W. Webb, E. F. Skelton, S. B. Qadri, E. R. Carpenter, Jr., M. S. Osofsky, R. J. Soulen and V. Le-Tourneau, Physica C (Amsterdam), 162 (1989) 899.
237 A. W. Webb, E. F. Skelton, S. B. Quadri and E. R. Carpenter, J. Solid State Chem., 102 (1993) 519.
238 S. J. La Placa, J. F. Bringley, B. A. Scott and D. E. Cox, J. Solid State Chem., 118 (1995) 170.
239 S. J. La Placa, J. F. Bringley, B. A. Scott and D. E. Cox, Acta Crystallogr. C 49 (1993) 1415.
240 M. F. Hundley, J. D. Thompson, S. W. Cheong, Z. Fisk and J. E. Schirber, Phys. Rev. B: Condens. Matter, 41 (1990) 4062.
241 C. Chaillout, J. Chenavas, S. W. Cheong, Z. Fisk, M. Marezio, B. Morosin and J. E. Schirber, Physica C (Amsterdam), 170 (1990) 87.
242 P. Zolliker, D. E. Cox, J. B. Parise, E. M. McCarron III and W. E. Farneth, Phys. Rev. B: Condens. Matter, 42 (1990) 6332.
243 K. F. McCarty, J. E. Schirber, S. W. Cheong and Z. Fisk, Phys. Rev. B: Condens. Matter, 43 (1991) 7883.
244 C. Chaillout, S. W. Cheong, Z. Fisk, M. S. Lehmann, M. Marezio, B. Morosin and J. E. Schirber, Physica Scripta, T 29 (1989) 97.
245 H. Wilhelm, C. Cros, F. Arrouy and G. Demazeau, C. R. Acad. Sci. (Paris), 322 (1996) 437.
246 H. Okada, M. Takano and Y. Takeda, Physica C (Amsterdam), 166 (1990) 111.
247 B. Chen, D. Walker, E. Y. Suard and B. A. Scott, Chem. Mater., 7 (1995) 355.
248 H. Haas and E. Kordes, Z. Kristallogr., 129 (1969) 259.
249 B. U. Köhler and M. Jansen, Z. Anorg. Allg. Chem., 543 (1986) 73.
250 A. P. Ramirez, R. Jager-Waldau and T. Siegrist, Z. Phys. B: Condens. Matter, 64 (1986) 189.

251 J.-P. Doumerc, A. Ammar, A. Wichainchai, M. Pouchard and P. Hagenmuller, J. Phys. Chem. Solids, 8 (1987) 37.
252 M. Trari, J. Toepfer, J.-P. Doumerc, M. Pouchard, A. Ammar and P. Hagenmuller, J. Solid State Chem., 111 (1994) 104.
253 A. Caneiro, D. Serafini, J. P. Abriata and J. Andrade Gamboa, J. Solid State Commun., 75 (1990) 915.
254 J. F. Bringley, S. S. Trail and B. A. Scott, J. Solid State Chem., 86 (1990) 310.
255 J. F. Bringley, S. S. Trail and B. A. Scott, J. Solid State Chem., 88 (1990) 590.
256 P. Lightfoot, S. Pei, J. D. Jorgensen, X.-X. Tang, A. Manthiram and J. B. Goodenough, Physica C (Amsterdam), 169 (1990) 15.
257 M. F. Hundley, J. D. Thompson, S.-W. Cheong, Z. Fisk, R. B. Schwarz and J. E. Schirber, Phys. Rev. B: Condens. Matter, 40 (1989) 5251.
258 K. Sawa, S. Suzuki, M. Watanabe, J. Akimitsu, H. Matsubara, H. Watabe, S. Uchida, K. Kokusho, H. Asano, F. Izumi and E. Takayama-Muromachi, Nature (London), 337 (1989) 347.
259 Z. Fisk, J. D. Thompson, M. F. Hundley, R. B. Schwarz, G. H. Kwei, J. E. Schirber, S.-W. Cheong, A. S. Cooper, P. Bordet and M. Marezio, J. Less-Common Met., 168 (1991) 31.
260 Y. Tokura, H. Takagi and S. Uchida, Nature (London), 337 (1989) 345.
261 M. Hiratani, Y. Takeda, S. Saitoh and K. Miyauchi, Jpn. J. Appl. Phys., Part 2, 28 (1989) L769.
262 E. Takayama-Muromachi, F. Izumi, Y. Uchida, K. Kato and H. Asano, Physica C (Amsterdam), 159 (1989) 634.
263 T. Kajitani, K. Hiraga, S. Hosoya, T. Fukuda, K. Oh-ishi, M. Kikuchi, Y. Syono, S. Tomiyoshi, M. Takahashi and Y. Muto, Physica C (Amsterdam), 169 (1990) 227.
264 N. Y. Ayoub, C. C. Almasan, E. A. Early, J. T. Markert, C. L. Seaman and M. B. Maple, Physica C (Amsterdam), 170 (1990) 211.
265 K. Oka and H. Unoki, Jpn. J. Appl. Phys., Part 2, 29 (1990) L909.
266 A. N. Maljuk, G. A. Emelchenko and A. V. Kosenko, J. Alloys Compd., 234 (1996) 52.
267 P. K. Davies, E. Caignol and T. King, J. Am. Ceram. Soc., 74 (1991) 569.
268 Q. Zhong, Y. Zhang, X. Chen, G. Rao and J. Liang, J. Alloys Compd., 210 (1994) 261.
269 N. Nguyen, L. Er-Rakho, C. Michel, J. Choisnet and B. Raveau, Mat. Res. Bull., 15 (1980) 891.
270 A. Fuertes, X. Obradors, J. M. Navarro, P. Gomez-Romero, N. Casañ-Pastor, F. Pérez, J. Fontcuberta, C. Miravitlles, J. Rodríguez-Carvajal and B. Martínez, Physica C (Amsterdam), 170 (1990) 153.
271 K. Doverspike, J.-H. Liu, K. Dwight and A. Wold, J. Solid State Chem., 82 (1989) 30.
272 P. Lightfoot, S. Pei, J. D. Jorgensen, X.-X. Tang, A. Manthiram and J. B. Goodenough, Physica C (Amsterdam), 169 (1990) 464.
273 V. Caignaert, N., Nguyen and B. Raveau, Mat. Res. Bull., 25 (1990) 199.
274 R. J. Cava, B. Batlogg, R. B. van Dover, J. J. Krajewski, J. V., Waszczak, R. M. Fleming, W. F. Peck, Jr., L. W. Rupp, Jr., P. Marsh, A. C. W. P. James and L. F. Schneemeyer, Nature (London), 345 (1990) 602.
275 K. Kinoshita, F. Izumi, T. Yamada and H. Asano, Phys. Rev. B: Condens. Matter, 45 (1992) 5558.
276 M. Hiratani, S. Saito, M. Suga and T. Sowa, Solid State Commun., 75 (1990) 425.
277 D. M. De Leeuw, C. A. H. A. Mutsaers, G. P. J. Geelen. H. C. A. Smoorenburg and C. Langereis, Physica C (Amsterdam), 152 (1988) 508.
278 K. T. Jacob and Y. Waseda, J. Phase Equilib., 15 (1994) 401.
279 D. M. De Leeuw, J. Less-Common Met., 150 (1989) 95.
280 D. M. De Leeuw, C. A. H. A. Mutsaers, G. P. J. Geelen and C. Langereis, J. Solid State Chem., 80 (1989) 276.
281 L. Er-Rakho, C. Michel and B. Raveau, J. Solid State Chem., 73 (1988) 514.
282 T. C. Huang, J. B. Torrance, A. I. Nazzal and Y. Tokura, Powder Diffr., 4 (1989) 152.
283 N. Nguyen, F. Studer and B. Raveau, J. Phys. Chem. Solids, 44 (1983) 389.
284 R. Moret, J. P. Pouget and G. Collin, Europhys. Lett., 4 (1987) 365.
285 P. L. Gai and E. M. McCarron III, Science, 247 (1990) 553.
286 D. Haskel, E. A. Stern, D. G. Hinks, A. W. Mitchell, J. D. Jorgensen and J. I. Budnick, Phys. Rev. Lett., 76 (1996) 439.
287 H. J. Scheel and F. Licci, Thermochim. Acta, 174 (1991) 115.
288 J. Y. Lee, J. S. Kim, J. S. Swinnea and H. Steinfink, J. Solid State Chem., 84 (1990) 335.
289 Y. Tokura, J. B. Torrance, A. I. Nazzal, T. C. Huang and C. Ortiz, J. Am. Chem. Soc., 109 (1987) 7555.
290 K. Otzschi, A. Hayashi, Y. Fujiwara and Y. Ueda, J. Solid State Chem., 105 (1993) 573.
291 K. Otzschi and Y. Ueda, J. Solid State Chem., 107 (1993) 149.
292 K. Otzschi, K. Koga and Y. Ueda, J. Solid State Chem., 115 (1995) 490.

293 W. T. Fu, Q. Xu, A. A. Verheijen, H. W. Von Ruitenbeek, H. W. Zandbergen and L. J. de Jongh, Solid State Commun., 73 (1990) 291.
294 C. Michel and B. Raveau, Rev. Chim. Miner., 21 (1984) 407.
295 E. A. Hayri and J. Z. Larese, Physica C (Amsterdam), 170 (1990) 239.
296 J. R. Grasmeder and M. T. Weller, J. Solid State Chem., 85 (1990) 88.
297 N. Nguyen, J. Choisnet and B. Raveau, Mat. Res. Bull., 17 (1982) 567.
298 M. Hervieu, V. Caignaert, C. Michel, R. Retoux and B. Raveau, Microsc. Microanal. Microstruct., 1 (1990) 109.
299 S. E. Dann and M. T. Weller, J. Solid State Chem., 115 (1995) 499.
300 V. Caignaert, R. Retoux, M. Hervieu, C. Michel and B. Raveau, J. Solid State Chem., 91 (1991) 41.
301 V. Caignaert, R. Retoux, C. Michel, M. Hervieu and B. Raveau, Physica C (Amsterdam), 167 (1990) 483.
302 B. Okai, Jpn. J. Appl. Phys., Part 2, 29 (1990) L2180.
303 S. Darracq, S. G. Kang, J. H. Choy and G. Demazeau, J. Solid State Chem., 114 (1995) 88.
304 N. Ikeda, Z. Hiroi, M. Azuma, M. Takano and Y. Bando, Physica C (Amsterdam), 210 (1993) 367.
305 G. M. Kuzmicheva, V. V. Luparev and E. P. Khlybov, Zh. Neorg. Khim., 41 (1996) 181.
306 E. Takayama-Muromachi, Y. Uchida, M. Kobayashi and K. Kato, Physica C (Amsterdam), 158 (1989) 449.
307 J. Akimitsu, S. Suzuki, M. Watanabe and H. Sawa, Jpn. J. Appl. Phys., Part 2, 27 (1988) L1859.
308 F. Izumi, E. Takayama-Muromachi, A. Fujimori, T. Kamiyama, H. Asano, J. Akimitsu and H. Sawa, Physica C (Amsterdam), 158 (1989) 440.
309 Z. Tan, J. I. Budnick, W. Q. Chen and D. L. Brewe, Phys. Rev. B: Condens. Matter, 42 (1990) 4808.
310 T. Wada, A. Ichinose, H. Yamauchi and S. Tanaka, Physica C (Amsterdam), 171 (1990) 344.
311 H. Fjellvåg, P. Karen and A. Kjekshus, Acta Chem. Scand., A 41 (1987) 283.
312 F. Abbattista, M. Vallino and D. Mazza, Mater. Chem. Phys., 21 (1989) 521.
313 R. S. Roth, C. J. Rawn, F. Beech, J. D. Whitler and J. O. Anderson, Ceram. Supercond. 2, Res. Update Ed. M. F. Yan, (American Ceramic Society, 1988) p. 13.
314 R. S. Roth, K. L. Davis and J. R. Dennis, Adv. Ceram. Mater., 2 (1987) 303.
315 H. Steinfink, J. S. Swinnea, Z. T. Sui, H. M. Hsu and J. B. Goodenough, J. Am. Chem. Soc., 109 (1987) 3348.
316 K. G. Frase, E. G. Liniger and D. R. Clarke, J. Am. Ceram. Soc., 70 (1987) C204.
317 G. Wang, S.-J. Hwu, S. N. Song, J. B. Ketterson, L. D. Marks, K. R. Poeppelmeier and T. O. Mason, Adv. Ceram. Mat., 2 (1987) 313.
318 K. G. Frase and D. R. Clarke, Adv. Ceram. Mat., 2 (1987) 295.
319 K. Y. Yang, H. Homma, R. Lee, R. Bhadra, M. Grimsditch, S. D. Bader, J. P. Locquet, Y. Bruynseraede and I. K. Schuller, Appl. Phys. Lett., 53 (1988) 808.
320 T. Graf, J. L. Jorda and J. Muller, J. Less-Common Met., 146 (1989) 49.
321 I. A. Saltykova, N. N. Baranova, V. P. Barchatov, I. N. Dubrovina and V. F. Balakirev, Sverkhprovodimost Fiz. Khim. Tekh., 3 (1990) 1250.
322 S. N. Koscheeva, V. A. Fotiev, A. Fotiev and A. Zubkov, Izv. Akad. Nauk. S.S.S.R., Neorg. Mater., 26 (1990) 1491.
323 V. F. Shamrai, Y. V. Efimov, M. E. Saveleva, G. M. Leitus, E. A. Myasnikova, T. M. Frolova and A. M. Postnikov, Supercond. Phys. Chem. Tech., 5 (1992) 1647.
324 E. Hodorowicz, S. A. Hodorowicz and H. A. Eick, Physica C (Amsterdam), 158 (1989) 127.
325 E. Hodorowicz, S. A. Hodorowicz and H. A. Eick, J. Alloys Compd., 181 (1992) 445.
326 C. Michel and B. Raveau, J. Solid State Chem., 43 (1982) 73.
327 S. Sato and I. Nakada, Acta Crystallogr., C 45 (1989) 523.
328 S. Pei, A. P. Paulikas, B. W. Veal and J. D. Jorgensen, Acta Crystallogr., C 46 (1990) 1986.
329 T. Aselage and K. Keefer, J. Mater. Res., 3 (1988) 1279.
330 K. Nakahigashi, K. Yoshiara, M. Kogachi, S. Nakanishi, H. Sasakura, S. Minamigawa, N. Fukuoka and A. Yanase, Jpn. J. Appl. Phys., Part 2, 27 (1988) L747.
331 E. N. Izakovich, N. A. Zheltova, Y. M. Korolev, Z. D. Sokolovskaya, V. N. Spector and M. L. Khidekel, Phys. Status Solidi, 116 (1989) K13.
332 M. Vallino, D. Mazza and F. Abbattista, J. Less-Common Met., 170 (1991) 83.
333 D. M. De Leeuw, C. A. H. A. Mutsaers, R. A. Steeman, E. Frikkee and H. W. Zandbergen, Physica C (Amsterdam), 158 (1989) 391.
334 F. Abbattista, M. Vallino, M., Lucco Bolera and C. Brisi, Mater. Chem. Phys., 20 (1988) 191.
335 P. Karen, H. Fjellvåg, O. Braaten, A. Kjekshus and H. Bratsberg, Acta Chem. Scand., 44 (1990) 994.
336 P. H. Hor, R. L. Meng, Y. Q. Wang, L. Gao, Z. J. Huang, J. Bechtold, K. Forster and C. W. Chu, Phys. Rev. Lett., 58 (1987) 1891.

337 J. M. S. Skakle and A. R. West, J. Mater. Chem., 4 (1994) 1745.
338 A. W. Hewat, J. J. Capponi, C. Chaillout, M. Marezio and E. A. Hewat, Solid State Commun. 64 (1987) 301.
339 M. F. Garbauskas, R. W. Green, R. H. Arendt and J. S. Kasper, Inorg. Chem., 27 (1988) 871.
340 J. D. Jorgensen, B. W. Veal, A. P. Paulikas, L. J. Nowicki, G. W. Crabtree, H. Claus and W. K. Kwok, Phys. Rev. B: Condens. Matter, 41 (1990) 1863.
341 H. Casalta, P. Schleger, P. Harris, B. Lebech, N. H. Andresen, R. Liang, P. Dosanjh and W. N. Hardy, Physica C (Amsterdam), 258 (1996) 321.
342 R. J. Cava, A. W. Hewat, E. A. Hewat, B. Batlogg, M. Marezio, K. M. Rabe, J. J. Krajewski, W. F. Peck, Jr. and L. W. Rupp, Jr., Physica C (Amsterdam), 165 (1990) 419.
343 M. A. Beno, L. Soderholm, D. W. Capone II, D. G. Hinks, J. D. Jorgensen, J. D. Grace, I. K. Schuller, C. U. Segre and K. Zhang, Appl. Phys. Lett., 51 (1987) 57.
344 M. François, A. Junod, K. Yvon, A. W. Hewat, J. J. Capponi, P. Strobel, M. Marezio and P. Fischer, Solid State Commun., 66 (1988) 1117.
345 J. D. Jorgensen, S. Pei, P. Lightfoot, D. G. Hinks, B. W. Veal, B. Dąbrowski, A. P. Paulikas and R. Kleb, Physica C (Amsterdam), 171 (1990) 93.
346 H. A. Ludwig, W. H. Fietz and H. Wühl, Physica C (Amsterdam), 197 (1992) 113.
347 N. H. Andersen, B. Lebech and H. F. Poulsen, Physica C (Amsterdam), 172 (1990) 31.
348 T. Graf, G. Triscone and J. Muller, J. Less Common Met., 159 (1990) 349.
349 J. Mizusaki, H. Tagawa, K. Hayakawa and K. Hirano, J. Am. Ceram. Soc., 78 (1995) 1781.
350 W. Wong-Ng, F. W. Gayle, D. L. Kaiser, S. F. Watkins and F. R. Fronczek, Phys. Rev. B: Condens. Matter, 41 (1990) 4220.
351 M. Guillaume, P. Allenspach, J. Mesot, B. Roessli, U. Staub, P. Fischer and A. Furrer, Z. Phys. B: Condens. Matter, 90 (1993) 13.
352 P. Meuffels, R. Naeven and H. Wenzl, Physica C (Amsterdam), 161 (1989) 539.
353 H. Shaked, J. D. Jorgensen, J. Faber, Jr., D. G. Hinks and B. Dąbrowski, Phys. Rev. B: Condens. Matter, 39 (1989) 7363.
354 R. J. Cava, B. Batlogg, C. H. Chen, E. A. Rietman, S. M. Zahurak and D. Werder, Nature (London), 329 (1987) 423.
355 A. Ourmazd and J. C. H. Spence, Nature (London), 329 (1987) 425.
356 T. Ichihashi, S. Iijima, Y. Kubo and J. Tabuchi, Jpn. J. Appl. Phys., Part 2, 27 (1988) L1187.
357 Y. P. Lin, J. E. Greedan, A. H. O'Reilly, J. N. Reimers, C. V. Stager and M. L. Post, J. Solid State Chem., 84 (1990) 226.
358 C. J. Hou, A. Manthiram, L. Rabenberg and J. B. Goodenough, J. Mater. Res., 5 (1990) 9.
359 M. A. Alario-Franco, C. Chaillout, J. J. Capponi, J. Chenavas and M. Marezio, J. Less-Common Met., 150 (1989) 117.
360 A. Simon, K. Trübenbach and H. Borrmann, J. Solid State Chem., 106 (1993) 128.
361 R. Sonntag, D. Hohlwein, T. Brückel and G. Collin, Phys. Rev. Lett., 66 (1991) 1497.
362 P. Schleger, H. F. Hadfield, H. Casalta, N. H. Andresen, H. F. Poulsen, M. Zimmermann, J. R. Schneider, R. Liang, P. Dosanjh and W. N. Hardy, Phys. Rev. Lett., 74 (1995) 1446.
363 J. D. Jorgensen, S. Pei, P. Lightfoot, H. Shi, A. P. Paulikas and B. W. Veal, Physica C (Amsterdam), 167 (1990) 571.
364 R. J. Cava, B. Batlogg, C. H. Chen, E. A. Rietman, S. M. Zahurak and D. Werder, Phys. Rev. B: Condens. Matter, 36 (1987) 5719.
365 Y. Nakazawa, M. Ishikawa, T. Takabatake, K. Koga and K. Terakura, Jpn. J. Appl. Phys., Part 2, 26 (1987) L796.
366 H. Verweij, Solid State Commun., 67 (1988) 109.
367 G. Ceder, M. Asta, W. C. Carter, M. Kraitchman, D. de Fontaine, M. E. Mann and M. Sluiter, Phys. Rev. B: Condens. Matter, 41 (1990) 8698.
368 M. Asta, D. de Fontaine, G. Ceder, E. Salomons and M. Kraitchman, J. Less-Common Met., 168 (1991) 39.
369 C. Vettier, P. Burlet, J. Y. Henry, M. J. Jurgens, G. Lapertot, L. P. Regnault and J. Rossat-Mignod, Physica Scripta, T29 (1989) 110.
370 N. H. Andersen, B. Lebech and H. F. Poulsen, J. Less-Common Met., 164 (1990) 124.
371 W. Zhang and K. Osamura, Physica C (Amsterdam), 190 (1992) 396.
372 P. Bordet, J. L. Hodeau, R. Argoud, J. Muller, M. Marezio, J. C. Martinez, J. J. Prejean, J. Karpinski, E. Kaldis, S. Rusiecki and B. Bucher, Physica C (Amsterdam), 162 (1989) 524.
373 E. Kaldis, P. Fischer, A. W. Hewat, E. A. Hewat, J. Karpinski and S. Rusiecki, Physica C (Amsterdam), 159 (1989) 668.

374 J. Karpinski, E. Kaldis, S. Rusiecki, E. Jilek, P. Fischer, P. Bordet, C. Chaillout, J. Chenavas, J. L. Hodeau and M. Marezio, J. Less-Common. Met., 150 (1989) 129.
375 J. Karpinski, E. Kaldis, E. Jilek, S. Rusiecki and B. Bucher, Nature (London), 336 (1988) 660.
376 P. Karen, A. Kjekshus and A. F. Andresen, Acta Chem. Scand., 96 (1992) 1059.
377 P. Karen and A. Kjekshus, J. Am. Ceram. Soc., 77 (1994) 547.
378 R. J. Cava, J. J. Krajewski, W. F. Peck, Jr., B. Batlogg and L. W. Rupp, Jr., Physica C (Amsterdam), 159 (1989) 372.
379 S. Jin, H. M. O'Bryan, P. K. Gallagher, T. H. Tiefel, R. J. Cava, R. A. Fastnacht and G. W. Kammlott, Physica C (Amsterdam), 165 (1990) 415.
380 Z. Zhou and A. Navrotsky, J. Mater. Res., 8 (1993) 3023.
381 M. A. Señaris-Rodriguez, A. M. Chippindale, A. Várez, E. Morán and M. A. Alario-Franco, Physica C (Amsterdam), 172 (1991) 477.
382 G. F. Voronin, Zh. Neorg. Khim., 39 (1994) 1776.
383 P. Bordet, C. Chaillout, J. Chenavas, J. L. Hodeau, M. Marezio, J. Karpinski and E. Kaldis, Nature (London), 334 (1988) 596.
384 J. L. Tallon, D. M. Pooke, R. G. Buckley, M. R. Presland and F. J. Blunt, Phys. Rev. B: Condens. Matter, 41 (1990) 7220.
385 J. Karpinski, S. Rusiecki, B. Bucher, E. Kaldis and E. Jilek, Physica C (Amsterdam), 161 (1989) 618.
386 J. Karpinski, S. Rusiecki, E. Kaldis, B. Bucher and E. Jilek, Physica C (Amsterdam), 160 (1989) 449.
387 D. E. Morris, N. G. Asmar, J. H. Nickel, R. L. Sid and J. Y. T. Wei, Physica C (Amsterdam), 159 (1989) 287.
388 J. Karpinski, S. Rusiecki, E. Kaldis and E. Jilek, J. Less-Common. Met., 164 (1990) 3.
389 G. F. Voronin and S. A. Degterov, Physica C (Amsterdam), 176 (1991) 387.
390 F. H. Garzon, I. D. Raistrick, D. S. Ginley and J. W. Halloran, J. Mater. Res., 6 (1991) 885.
391 Z. Zhou and A. Navrotsky, J. Mater. Res., 7 (1992) 2920.
392 G. K. Moiseev, N. A. Vatolin, S. I. Zaizeva, N. I. Ilyinych, D. S. Taagareishvili, G. G. Gvelesiani, I. B. Baratashvili and J. Šesták, Thermochim. Acta, 198 (1992) 267.
393 J. Šesták, G. K. Moiseev and D. S. Tzagareishvili, Jpn. J. Appl. Phys., 33 (1994) 97.
394 G. K. Moiseev, N. A. Vatolin and J. Šesták, Thermochim. Acta, 237 (1994) 391.
395 G. K. Moiseev, N. A. Vatolin and J. Šesták, Thermochim. Acta, 237 (1994) 401.
396 G. K. Moiseev, N. A. Vatolin and J. Šesták, Thermochim. Acta, 237 (1994) 409.
397 R. K. Williams, D. M. Kroeger, P. M. Martin, J. R. Mayotte, E. D. Specht and J. Brynestad, J. Appl. Phys., 76 (1994) 3673.
398 K. Borowiec and K. Kolbrecka, J. Solid State Chem., 92 (1991) 170.
399 J. P. Lawanier, J. K. Meen and D. Elthon, J. Am. Ceram. Soc., 79 (1996) 533.
400 S. A. Hodorowicz, A. Lasocha, W. Lasocha and H. A. Eick, J. Solid State Chem., 75 (1988) 270.
401 C. N. Pieczulewski, J. E. McAdams and T. O. Mason, J. Am. Ceram. Soc., 73 (1990) 3088.
402 K. Zhang, B. Dąbrowski, C. U. Segre, D. G. Hinks, I. K. Schuller, J. D. Jorgensen and M. Slaski, J. Phys. C: Solid State Phys., 20 (1987) L935.
403 J. M. S. Skakle and A. R. West, Physica C (Amsterdam), 220 (1994) 187.
404 T. Plackowski, C. Sułkovski, Z. Bukowski, D. Włosewicz and K. Rogacki, Physica C (Amsterdam), 254 (1995) 331.
405 P. Karen, H. Fjellvåg and A. Kjekshus, J. Solid State Chem., 97 (1992) 257.
406 S. Li, E. A. Hayri, K. V. Ramanujachary and M. Greenblatt, Phys. Rev. B: Condens. Matter, 38 (1988) 2450.
407 T. B. Lindemer, E. D. Specht, C. S. MacDougall, G. M. Taylor and S. L. Pye, Physica C (Amsterdam), 216 (1993) 99.
408 T. B. Lindemer, E. D. Specht, P. M. Martin and M. L. Flitcroft, Physica C (Amsterdam), 255 (1995) 65.
409 D. E. Morris, J. H. Nickel, J. Y. T. Wei, N. G. Asmar, J. S. Scott, U. M. Scheven, C. T. Hultgren, A. G. Markelz, J. E. Post, P. J. Heaney, D. R. Veblen and R. M. Hazen, Phys. Rev. B: Condens. Matter, 39 (1989) 7347.
410 S. Adachi, H. Adachi, K. Setsune and K. Wasa, Physica C (Amsterdam), 175 (1991) 523.
411 Y. Yaegashi, S. Adachi, T. Wada, S. Takano and H. Yamauchi, Physica C (Amsterdam), 190 (1992) 433.
412 N. Seiji, S. Adachi and H. Yamauchi, Physica C (Amsterdam), 227 (1994) 377.
413 J. Valo, R. Matero, M. Leskelä, M. Karppinen, L. Niinistö and J. Lindén, J. Mater. Chem., 5 (1995) 875.
414 D. E. Morris, N. G. Asmar, J. Y. T. Wei, J. H. Nickel, R. L. Sid and J. S. Scott, Phys. Rev. B: Condens. Matter, 40 (1989) 11406.

415 F. Abbattista, D. Mazza and M. Vallino, Eur. J. Solid State Inorg. Chem., 28 (1991) 649.
416 S. I. Yoo and R. W. McCallum, Physica C (Amsterdam), 210 (1993) 147.
417 C. Michel, L. Er-Rakho and B. Raveau, J. Solid State Chem., 39 (1981) 161.
418 F. Mizuno, H. Masuda, I. Hirabayashi, S. Tanaka, M. Hasegawa and U. Mizutani, Nature (London), 345 (1990) 788.
419 J. Stalick and W. Wong-Ng, Mater. Lett., 9 (1990) 401.
420 F. Abbattista, M. Vallino and D. Mazza, Mater. Chem. Phys., 24 (1990) 363.
421 F. Abbattista, C. Brisi, S. Delmastro, M. Lucco-Bolera, D. Mazza and M. Vallino, Mater. Chem. Phys., 24 (1989) 147.
422 B. Domenges, F. Abbattista, C. Michel, M. Vallino, L. Barbey, N. Nguyen and B. Raveau, J. Solid State Chem., 106 (1993) 271.
423 M. Park, M. J. Kramer, K. W. Dennis and R. W. McCallum, Physica C (Amsterdam), 259 (1996) 43.
424 D. Klibanow, K. Sujata and T. O. Mason, J. Am. Ceram. Soc., 71 (1988) C-267.
425 C. Michel, L. Er-Rakho, M. Hervieu, J. Pannetier and B. Raveau, J. Solid State Chem., 68 (1987) 143.
426 P. K. Davies and C. M. Katzan, J. Solid State Chem., 88 (1990) 368.
427 N. Rangavittal, G. N. Subbana, T. N. Guru Row and C. N. R. Rao, J. Solid State Chem., 114 (1995) 95.
428 E. Thiele and P. K. Davies, J. Am. Ceram. Soc., 74 (1991) 1011.
429 V. Neukirch, C. T. Simmons, P. Sladeczek, C. Laubschat, O. Strebel, G. Kaindl and D. D. Sarma, Europhys. Lett., 5 (1988) 567.
430 C. Thomsen, R. Liu, A. Wittlin, L. Genzel, M. Cardona, W. König, M. V. Cabañas and E. García, Solid State Commun., 65 (1988) 219.
431 K. Noto, H. Morita, K. Watanabe, T. Murakami, Y. Koyanagi, I. Yoshi, I. Sato, H. Sugawara, N. Kobyashi, H. Fujimori and Y. Muto, Physica B (Amsterdam), 148 (1987) 239.
432 A. Oota, Y. Sasaki, Y. Kiyoshima, M. Ohkubo and T. Hioki, Jpn. J. Appl. Phys., Part 2, 26 (1987) L2091.
433 P. Millet, R. Enjalbert, J. Galy, C. Faulmann, P. Cassoux, H. Rakoto and S. Askénazy, C. R. Acad. Sci., Ser. 2, 306 (1988) 407.
434 A. K. Raychandhuri, K. Sreedhar, K. P. Rajeev, R. A. Mohan Ram, P. A. Ganguly and C. N. R. Rao, Philos. Mag. Lett., 56 (1987) 29.
435 P. Karen, H. Fjellvåg, A. Kjekshus and A. F. Andresen, J. Solid State Chem., 93 (1991) 163.
436 C. U. Segre, B. Dąbrowski, D. G. Hinks, K. Zhang, J. D. Jorgensen, M. A. Beno and I. K. Schuller, Nature (London), 329 (1987) 227.
437 K. Takita, H. Katoh, H. Akinaga, M. Nishino, T. Ishigaki and H. Asano, Jpn. J. Appl. Phys., Part 2, 27 (1988) L57.
438 J. M. Newsam, A. J. Jacobson, D. P. Goshorn, J. T. Lewandowski, D. B. Mitzi, A. Kapitulnik, D. Xie and W. B. Yelon, Solid State Ionics, 32/33 (1989) 1064.
439 T. Sakurai, T. Wada, N. Suziki, S. Koriyama, T. Miyatake, H. Yamauchi, N. Koshizuka and S. Tanaka, Phys. Rev. B: Condens. Matter, 42 (1990) 8030.
440 D. E. Morris, P. K. Narwankar, A. P. B. Sinha, K. Takano and V. Shum, Appl. Phys. Lett. (USA), 57 (1990) 715.
441 H. Sawa, K. Obara, J. Akimitsu, Y. Matsui and S. Horiuchi, J. Phys. Soc. Jpn., 58 (1989) 2252.
442 K. Tsuda, M. Tanaka and J. Akimitsu, Jpn. J. Appl. Phys., Part 2, 28 (1989) L1552.
443 H. Nobumasa, K. Shimizu, Y. Kitano, M. Tanaka and T. Kawai, Jpn. J. Appl. Phys., Part 2, 28 (1989) L1948.
444 M. V. Patrakeev, I. A. Leonidov, A. A. Lakhtin, V. L. Kozhevnikov, J. Solid State Chem., 120 (1995) 146.
445 T. Wada, A. Ichinose, Y. Yaegashi, H. Yamauchi and S. Tanaka, Phys. Rev. B: Condens. Matter, 41 (1990) 1984.
446 A. Ichinose, T. Wada, Y. Yaegashi, H. Yamauchi and S. Tanaka, Jpn. J. Appl. Phys., Part 2, 29 (1990) L426.
447 T. Wada, T. Kaneko, A. Ichinose, Y. Yaegashi, S. Ikegawa, H. Yamauchi and S. Tanaka, Jpn. J. Appl. Phys., Part 2, 29 (1990) L43.
448 T. Watanabe, K. Kinoshita, H. Shibata, A. Matsuda, Y. Asano and T. Yamada, Jpn. J. Appl. Phys., Part 2, 27 (1988) L1245.
449 R. J. Cava, H. W. Zandbergen, R. B. Van Dover, J. J. Krajewski, T. Siegrist, W. F. Peck, R. S. Roth and R. J. Felder, J. Solid State Chem., 109 (1994) 345.
450 R. J. Cava, A. Santoro, J. J. Krajewski, R. M. Fleming, J. V. Waszczak, W. F. Peck, Jr. and P. Marsh, Physica C (Amsterdam), 172 (1990) 138.
451 J. Huang and W. Sleight, Physica C (Amsterdam), 169 (1990) 169.

452 D. E. Morris, P. K. Narwankar and A. P. B. Sinha, Physica C (Amsterdam), 169 (1990) 7.
453 A. Manthiram, S.-J. Lee and J. B. Goodenough, J. Solid State Chem., 73 (1988) 278.
454 C. Gledel, J.-F. Marucco and B. Touzelin, Physica C (Amsterdam), 165 (1990) 437.
455 J. B. Parise and E. M. McCarron III, J. Solid State Chem., 83 (1989) 188.
456 E. M. McCarron III, M. K. Crawford and J. B. Parise, J. Solid State Chem., 78 (1989) 192.
457 R. S. Liu, J. R. Cooper, J. W. Loram, W. Zhou, W. Lo, P. P. Edwards, W. Y. Liang and L. S. Chen, Solid State Commun., 76 (1990) 679.
458 T. Wada, N. Suzuki, A. Ichinose, Y. Yaegashi, H. Yamauchi and S. Tanaka, Jpn. J. Appl. Phys., Part 2, 29 (1990) L915.
459 T. Miyatake, S. Gotoh, N. Koshizuka and S. Tanaka, Nature (London), 341 (1989) 41.
460 I. Mangelschots, M. Mali, J. Roos, H. Zimmermann, D. Brinkmann, S. Rusiecki, J. Karpinski, E. Kaldis and E. Jilek, Physica C (Amsterdam), 172 (1990) 57.
461 I. Mangelschots, M. Mali, J. Roos, H. Zimmermann, D. Brinkmann, J. Karpinski, E. Kaldis and S. Rusiecki, J. Less-Common Met., 164 (1990) 78.
462 W. T. Fu, H. W. Zandbergen, C. J. Van der Beek and L. J. de Jongh, Physica C (Amsterdam), 156 (1988) 133.
463 D. M. de Leeuw, C. A. H. A. Mutsaers, H. A. M. Van Hal, H. Verweij, A. H. Carim and H. C. A. Smoorenburg, Physica C (Amsterdam), 156 (1988) 126.
464 D. W. Murphy, S. Sunshine, R. B. Van Dover, R. J. Cava, B. Batlogg, S. M. Zahurak and L. F. Schneemeyer, Phys. Rev. Lett., 58 (1987) 1888.
465 J. M. S. Skakle and A. R. West, Physica C (Amsterdam), 227 (1994) 336.
466 A. H. Carim, A. F. de Jong and D. M. de Leeuw, Phys. Rev. B: Condens. Matter, 38 (1988) 7009.
467 H. W. Zandbergen, W. T. Fu and L. J. de Jongh, Physica C (Amsterdam), 156 (1988) 307.
468 J. M. S. Skakle, A. Tempelton, E. E. Lachowski and A. R. West, Physica C (Amsterdam), 260 (1996) 137.
469 F. Keller-Berest, S. Metgert, G. Collin, P. Monod and M. Ribault, Physica C (Amsterdam), 161 (1989) 150.
470 J. M. S. Skakle and A. R. West, Physica C (Amsterdam), 261 (1996) 105.
471 P. Karen, H. Fjellvåg, A. Kjekshus and A. F. Andresen, J. Solid State Chem., 92 (1991) 57.
472 J. M. S. Skakle and A. R. West, Physica C (Amsterdam), 241 (1995) 191.
473 D. B. Currie, M. T. Weller, S. Rowles and D. H.Gregory, Mat. Res. Bull., 25 (1990) 1279.
474 H. Fjellvåg, P. Karen, A. Kjekshus and J. K. Grepstad, Acta Chem. Scand., 42 (1988) 171.
475 T. M. Shaw, D. Dimos, P. E. Batson, A. G. Schrott, D. R. Clarke and P. R. Duncombe, J. Mater. Res., 5 (1990) 1176.
476 T. B. Lindemer, C. B. Hubbard and J. Brynestad, Physica C (Amsterdam), 167 (1990) 312.
477 M. A. Rodriguez, R. L. Snyder, J. J. Simmins, Y. M. Guo, R. A. Condrate, Sr., F. J. Rotella and J. D. Jorgensen, J. Appl. Cryst., 28 (1995) 429.
478 M. A. Rodriguez, J. J. Simmins and R. L. Snyder, J. Mater. Res., 8 (1993) 415.
479 C. Greaves and P. R. Slater, Physica C (Amsterdam), 175 (1991) 172.
480 E. Hodorowicz, S. A. Hodorowicz and H. A. Eick, Physica C (Amsterdam), 198 (1992) 19.
481 P. Karen, A. Kjekshus, Q. Huang, V. Karen, A. D. Mighell and A. Santoro, Physica C (Amsterdam), (submitted).
482 Z. Iqbal, F. Reidinger, A. Bose, N. Cipollini, T. J. Taylor, H. Eckhardt, B. L. Ramakrishna and E. W. Ong, Nature (London), 331 (1988) 326.
483 A. M. Umarji, P. Somasundaram, L. Ganapathi and C. N. R. Rao, Solid State Commun. 66 (1988) 177.
484 Y. Myiazaki, H. Yamane, N. Ohnishi, Y. Kajitani, K. Hiraga, Y. Morii, S. Funahashi and T. Hirai, Physica C (Amsterdam), 198 (1992) 7.
485 Y. Myiazaki, H. Yamane and T. Hirai, Physica C (Amsterdam), 198 (1992) 53.
486 B. Domengès, M. Hervieu and B. Raveau, Physica C (Amsterdam), 207 (1993) 65.
487 B. Domengès, Ph., Boullay, M. Hervieu and B. Raveau, J. Solid State Chem., 108 (1994) 219.
488 B. Raveau, C. Michel, B. Mercey, J. F. Hamet and M. Hervieu, J. Alloys Compd., 229 (1995) 134.
489 A. Maignan, M. Hervieu, C. Michel and B. Raveau, Physica C (Amsterdam), 208 (1993) 116.
490 J. Q. Li, H. Chen and Z. X. Zhao, Physica C (Amsterdam), 233 (1994) 40.
491 R. Nagarajan, S. Ayyappan and C. N. R. Rao, Physica C (Amsterdam), 220 (1994) 373.
492 T. Krekels, O. Milat, G. Van Tendeloo, J. Van Landuyt and S. Amelinckx, Physica C (Amsterdam), 210 (1993) 439.
493 F. J. Gotor, P. Odier, M. Gervais, J. Choisnet and Ph. Monod, Physica C (Amsterdam), 218 (1993) 429.
494 J. Wang, I. Monot, M. Hervieu, J. Provost and G. Desgardin, Supercond. Sci. Technol., 9 (1996) 69.
495 M. Maciejewski, A. Baiker, K. Conder, C. Krüger, J. Karpinski and E. Kaldis, Physica C (Amsterdam), 227 (1994) 343.

496 B. Gudmundsson, H. Wang, R. A. Neiser, B. Katz and H. Herman, J. Appl. Phys., 67 (1990) 2653.
497 E. K. Chang, E. F. Ezell and M. J. Kirschner, Supercond. Sci. Technol., 3 (1990) 391.
498 T. V. Dlyachkova, N. I. Kadyrova, N. V. Talashmanova, S. I. Alyamovskii, Yu. G. Zainulin, Zh. Neorg. Khim., 36 (1991) 1091.
499 A. Ono and S. Horiuchi, Physica C (Amsterdam), 247 (1995) 319.
500 M. J. Cima, J. S. Schneider, S. C. Peterson and W. Coblenz, Appl. Phys. Lett., 53 (1988) 710.
501 T. Komatsu, O. Tanaka, K. Matusita, M. Takata and T. Yamashita, Jpn. J. Appl. Phys., Part 2, 27 (1988) L1025.
502 G. K. Moiseev, S. I. Zaitseva, J. Šesták and N. A. Vatolin, Thermochim. Acta, 216 (1993) 301.
503 C. H. Raeder and D. B. Knorr, J. Am. Ceram. Soc., 73 (1990) 2407.
504 K. Yokota, T. Kura, M. Ochi and S. Katayama, J. Mater. Res., 5 (1990) 2790.
505 J. G. Thompson, B. G. Hyde, R. L. Withers, J. S. Anderson, J. D. Fitzgerald, J. Bitmead, M. S. Paterson and A. M. Stewart, Mater. Res. Bull., 22 (1987) 1715.
506 S. A. Montzka, B. M. Hybertson, R. M. Barkley and R. E. Sievers, J. Mater. Res., 6 (1991) 891.
507 Y. Gao, K. L. Merkle, C. Zhang, U. Balachandran and R. B. Poeppel, J. Mater. Res., 5 (1990) 1363.
508 I. Barin and O. Knacke, Thermochemical Properties of Inorganic Substances (Springer Verlag, 1973), pp. 77, 79, 163, 174, 181, 711.
509 I. Barin, O. Knacke and O. Kubashevski, Thermochemical Properties of Inorganic Substances, Supplement (Springer Verlag, 1977), p. 679.
510 K. Borowiec, J. Przyluski and K. Kolbrecka, J. Am. Ceram. Soc., 74 (1991) 2007.
511 P. K. Gallagher, G. S. Grader and H. M. O'Bryan, Mater. Res. Bull., 23 (1988) 1491.
512 G. Selvduray, C. Zhang, U. Balachandran, Y. Gao, K. L. Merkle, H. Shi and R. B. Poeppel, J. Mater. Res., 7 (1992) 283.
513 P. K. Gallagher, Thermochim. Acta, 174 (1991) 85.
514 T. B. Lindemer, F. A. Washburn, C. S. MacDougall, R. Feenstra and O. B. Cavin, Physica C (Amsterdam), 178 (1991) 93.
515 Y. Idemoto and K. Fueki, Jpn. J. Appl. Phys., Part 1, 29 (1989) 2729.
516 A. P. Clarke, R. B. Schwarz and J. D. Thompson, J. Less-Common Met., 168 (1991) 1.
517 P. G. Wahlbeck, D. L. Myers and J. C. Ho, Physica C (Amsterdam), 161 (1989) 175.
518 T. Sata, K. Sakai and S. Tashiro, J. Am. Ceram. Soc., 74 (1991) 1445.
519 R. Bormann and J. Nölting, Appl. Phys. Lett., 54 (1989) 2148.
520 J. Nowotny, M. Rekas and W. Weppner, J. Am. Ceram. Soc., 73 (1990) 1040.
521 O. Porat, I. Riess and H. L. Tuller, Physica C (Amsterdam), 192 (1992) 60.
522 J.-S. Kim and D. R. Gaskell, J. Am. Ceram. Soc., 77 (1994) 753.
523 R. Beyers and B. T. Ahn, Annu. Rev. Mater. Sci., 21 (1991) 335.
524 J. L. MacManus-Driscoll, J. C. Bravman and R. B. Beyers, Physica C (Amsterdam), 241 (1995) 401.
525 B. T. Ahn, T. M. Gür, R. Huggins, R. Beyers and E. M. Engler, Mater. Res. Soc. Symp. Proc., 99 (1988) 171.
526 B. T. Ahn, V. Y. Lee, R. Beyers, T. M. Gür and R. A. Huggins, Physica C (Amsterdam), 167 (1990) 529.
527 S. Kawabata, H. Hoshizaki, N. Kawahara, H. Enami, T. Shinohara and T. Imura, Jpn. J. Appl. Phys., Part 2, 29 (1990) L1490.
528 G. A. Mikirticheva, V. I. Schitova, L. Yu. Grabovenko, D. I. Romanov and R. G. Grebenschikov, Zh. Neorg. Khim., 36 (1991) 562.
529 J. Šesták, J. Kamarád, P. Holba, A. Tříska, E. Pollert and M. Nevřiva, Thermochim. Acta, 174 (1991) 99.
530 F. Licci, P. Tissot and H. J. Scheel, J. Less-Common Met., 150 (1989) 201.
531 A. C. Kosmynin, G. E. Shter, I. K. Garkushin, A. S. Trunin, V. A. Balashov and A. A. Fotiev, Sverkhprovodimost Fiz. Khim. Tekh., 3 (1990) 1870.
532 W. Wong-Ng and L. P. Cook, J. Am. Ceram. Soc., 77 (1994) 1883.
533 N. Nevřiva, P. Holba, S. Durčok, D. Zemanová, E. Pollert and A. Tříska, Physica C (Amsterdam), 157 (1989) 334.
534 B.-J. Lee and D. N. Lee, J. Am. Ceram. Soc., 72 (1989) 314.
535 P. K. Gallagher, Adv. Ceram. Mater., 2 (1987) 632.
536 P. Strobel, J. J. Capponi, M. Marezio and P. Monod, Solid State Commun., 64 (1987) 513.
537 S. Yamaguchi, K. Terabe, A. Saito, S. Yahagi and Y. Iguchi, Jpn. J. Appl. Phys., 27 (1988) L179.
538 K. Kishio, J. Shimoyama, T. Hasegawa, K. Kitazawa and K. Fueki, Jpn. J. Appl. Phys., 26 (1987) L1228.
539 K. Kishio, K. Suzuki, T. Hasegawa, T. Yamamoto, K. Kitazawa and K. Fueki, J. Solid State Chem., 82 (1989) 192.

540 R. Liang and T. Nakamura, Jpn. J. Appl. Phys., 27 (1988) L1277.
541 M. V. Patrakeev, I. A. Leonidov and V. L. Kozhevnikov, Solid State Ionics, 82 (1995) 5.
542 E. Pörschke, P. Meuffels and H. Wenzl, J. Phys. Chem. Solids, 53 (1992) 73.
543 H. M. O'Bryan, P. K. Gallagher, R. A. Laudise, A. J. Caporaso and R. C. Sherwood, J. Am. Ceram. Soc., 72 (1989) 1298.
544 J. Karpinski, E. Kaldis and S. Rusiecki, J. Less-Common Met., 150 (1989) 207.
545 J. Maier and H. L. Tuller, Phys. Rev. B: Condens. Matter, 47 (1993) 8105.
546 D. M. Smyth, in: Selected Topics in High Temperature Chemistry, Defect Chemistry of Solids, Ed. Ø. Johannesen and A. G. Anderson, Elsevier 1989, p. 1.
547 E. K. Chang, D. J. L. Hong, A. Mehta and D. M. Smyth, Mater. Letters, 6 (1988) 251.
548 J. Maier, P. Murugaraj and G. Pfundtner, Solid State Ionics, 40/41 (1990) 802.
549 H.-I. Yoo and S.-M. Lee, J. Am. Ceram. Soc., 77 (1994) 3131.
550 M.-Y. Su, S. E. Dorris and T. O. Mason, J. Solid State Chem., 75 (1988) 381.
551 G. Schwitzgebel and St. Junk, Ber. Bunsenges. Phys. Chem., 93 (1989) 1356.
552 J. Nowotny and M. Rekas, J. Am. Ceram. Soc., 73 (1990) 1048.
553 J. Nowotny and M. Rekas, J. Am. Ceram. Soc., 73 (1990) 1054.
554 A. Lanckbeen, C. Legros, J. F. Marucco and R. Deltour, Physica C (Amsterdam), 221 (1994) 53.
555 W. R. McKinnon, M. L. Post, L. S. Selwyn and G. Pleizier, Phys. Rev. B: Condens. Matter, 38 (1988) 6543.
556 A. P. Mozhaev and S. V. Chernayev, J. Mater. Chem., 4 (1994) 1107.
557 T. B. Tang and W. Lo, Physica C (Amsterdam), 174 (1991) 463.
558 L. T. Shi and K. N. Tu, Appl. Phys. Lett., 55 (1989) 1351.
559 F. Cellucci, D. Gozzi and M. Tomellini, J. Mater. Chem., 4 (1994) 579.
560 Y. Song, X.-D. Chen and J. R. Gaines, J. Mater. Res., 5 (1990) 27.
561 K. N. Tu, N. C. Yeh, S. I. Park and C. C. Tsuei, Phys. Rev. B: Condens. Matter, 39 (1989) 304.
562 H. F. Poulsen, N. H. Andersen and B. Lebech, Physica C (Amsterdam), 173 (1991) 387.
563 J. M. D. Coey and X. Z. Wang, J. Solid State Chem., 77 (1988) 204.
564 N. Miura, H. Suzuta, Y. Teraoka and N. Yamazoe, Jpn. J. Appl. Phys., 27 (1988) L337.
565 A. Pękalski and M. Ausloos, Physica C (Amsterdam), 226 (1994) 188.
566 S. J. Rothman, J. L. Routbort and J. E. Baker, Phys. Rev. B: Condens. Matter, 40 (1989) 8852.
567 X. Turrillas, J. A. Kilner, I. Kontoulis and B. C. H. Steele, J. Less-Common Met., 151 (1989) 229.
568 S. J. Rothman, J. L. Routbort, U. Welp and J. E. Baker, Phys. Rev. B: Condens. Matter, 44 (1991) 2326.
569 J. L. Tallon and M. P. Staines, J. Appl. Phys., 68 (1990) 3998.
570 W. Carrillo-Cabrera, H.-D. Wiemhöfer and W. Gopel, Solid State Ionics, 32/33 (1989) 1172.
571 D. J. Vischjager, P. J. Van der Put, J. Schram and J. Schoonman, Solid State Ionics, 27 (1988) 199.
572 J.-S. Lee and H.-I. Yoo, J. Electrochem. Soc., 142 (1995) 1169.
573 J. G. Fletcher, A. R. West and J. T. S. Irvine, J. Electrochem. Soc., 142 (1995) 2650.
574 J.-H. Park, P. Kostic and J. P. Singh, Mater. Lett., 6 (1988) 393.
575 J. Maier, P. Murugaraj, G. Pfundtner and W. Sitte, Ber. Bunsenges. Phys. Chem., 93 (1989) 1350.
576 M. V. Patrakeev, I. A. Leonidov, V. L. Kozhevnikov, V. I. Tsildikovskii, A. K. Demin and A. V. Nikolaev, Solid State Ionics, 66 (1993) 61.
577 R. C. Evans, An Introduction to Crystal Chemistry, Cambridge 1964, p. 273.
578 T. Norby, Solid State Ionics, 40/41 (1990) 857.
579 H. Iwahara, H. ISSI Lett., 3 (1992) 11.
580 D. P. Sutija, T. Norby and P. Björnbom, Solid State Ionics, 77 (1995) 167.
581 C. Y. Yang, X.-Q. Yang, S. M. Heald, J. J. Reilly, T. Skotheim, A. R. Moodenbaugh and M. Suenaga, Phys. Rev. B: Condens. Matter, 36 (1987) 8798.
582 J. P. Burger, M. Nicolas, J. N. Daou, P. Vajda, L. Dumoulin and J. Lesueur, Z. Phys. Chem., 163 (1989) 733.
583 J. R. Johnson, M. Suenaga, P. Thompson and J. J. Reilly, Z. Phys. Chem., 163 (1989) 721.
584 Y. Ikuma, M. Yoshimura and S. Kabe, J. Mater. Res., 5 (1990) 17.
585 K. Kobayashi, J. Am. Ceram. Soc., 73 (1990) 146.
586 D. Porath, A. Grayevsky, N. Kaplan, D. Shaltiel, U. Yaron and E. Walker, J. Alloys Compd., 204 (1994) 79.
587 G. Dortmann, J. Erxmayer, S. Blässer, J. Steiger, T. Paatsch, A. Weidinger, H. Karl and B. Stritzker, Phys. Rev. B: Condens. Matter, 49 (1994) 600.
588 I. Garrote, E. Morán, M. A. Alario-Franco, J. M. Rojo and J. Sanz, J. Mater. Chem., 5 (1995) 1171.
589 D. Fruchart, J. L. Soubeyroux, D. Tran Qui, C. Pique, C. Rillo, F. Lera, V. Orera, J. Flokstra and D. H. A. Blank, J. Less-Common Met., 157 (1990) 233.

590 I. Harrington, C. Korn, S. D. Goren, H. Shaked and G. Kimmel, Physica C (Amsterdam), 226 (1994) 255.
591 T. Kebukawa, Y. Kumaki, K. Fujiwara, Y. Tatsumi, H. Taimatsu and H. Kaneko, Jpn. J. Appl. Phys., Part 2, 33 (1994) L507.
592 C. Niedermayer, H. Glückler, R. Simon, A. Golnik, M. Rauer, E. Recknagel, A. Weidinger, J. I. Budnick, W. Paulus and R. Schöllhorn, Phys. Rev. B: Condens. Matter, 40 (1989) 11386.
593 H. Glückler, U. Binninger, C. Niedermayer, E. Recknagel and A. Weidinger, Z. Phys. Chem., 179 (1993) 389.
594 Y. M. Baikov, ISSI Lett., 6 (1995) 1.
595 S. Prakash and J. P. Burger, Z. Phys. Chem., 181 (1993) 159.
596 M. Cherry, M. S. Islam, J. D. Gale and C. R. A. Catlow, J. Phys. Chem., 99 (1995) 14614.
597 J. R. LaGraff, E. C. Behrman, J. A. T. Taylor, F. J. Rotella, J. D. Jorgensen, L. Q. Wang and P. G. Mattocks, Phys. Rev. B: Condens. Matter, 39 (1989) 347.
598 A. K. Tyagi, S. J. Patwe, U. R. K. Rao and R. M. Iyer, Solid State Commun., 65 (1988) 1149.
599 H. H. Wang, A. M. Kini, H.-C. I. Kao, E. H. Appelman, A. R. Thompson, R. E. Botto, K. D. Carlson, J. M. Williams, M. Y. Chen, J. A. Schlueter, B. D. Gates, S. L. Hallenbeck and A. M. Despotes, Inorg. Chem., 27 (1988) 5.
600 C. Perrin, O. Peña, M. Sergent, P. Christensen, G. Fonteneau and J. Lucas, Supercond. Sci. Technol., 2 (1989) 35.
601 J. L. MacManus, D. J. Fray and J. E. Evetts, Physica C (Amsterdam), 184 (1991) 172.
602 M. Mokhtari, C. Perrin, M. Sergent, E. Furet, J.-F. Halet, J.-Y. Saillard, E. Ressouche and P. Burlet, Solid State Commun., 93 (1995) 487.
603 B. Morosin, E. L. Venturini, J. E. Schirber, R. G. Dunn and P. P. Newcomer, Physica C (Amsterdam), 241 (1995) 181.
604 M. Al-Mamouri, P. P. Edwards, C. Greaves, P. R. Slater and M. Sląski, J. Mater. Chem., 5 (1995) 913.
605 K. V. Ramanujachary, M. Greaney, R. L. Fuller and M. Greenblatt, J. Solid State Chem., 93 (1991) 263.
606 Y. Zenitani, K. Inari, S. Sahoda, M. Uehara, J. Akimitsu, N. Kubota and M. Ayabe, Physica C (Amsterdam), 248 (1995) 167.
607 T. Kawashima, Y. Matsui and E. Takayama-Muromachi, Physica C (Amsterdam), 257 (1996) 313.
608 L. Soderholm, G. L. Goodman, U. Welp, C. W. Williams and J. Bolender, Physica C (Amsterdam), 161 (1989) 252.
609 M. Andersson, Z. Hegedűs, M. Nygren and Ö. Rapp, Physica C (Amsterdam), 160 (1989) 65.
610 J. W. Chen, C. F. Chen, T. C. Chang and Y. D. Yao, Physica C (Amsterdam), 165 (1990) 287.
611 M. Ausloos, C. Laurent, H. W. Vanderschueren, A. Rulmont and P. Tarte, Solid State Commun., 68 (1988) 539.
612 J. L. Tallon, D. M. Pooke, M. P. Staines, M. E. Bowden, N. E. Flower, R. G. Buckley, M. R. Presland and R. L. Davis, Physica C (Amsterdam), 171 (1990) 61.
613 W. T. Fu, H. W. Zandbergen, W. G. Haije and L. J. de Jongh, Physica C (Amsterdam), 159 (1989) 210.
614 H. W. Zandbergen, W. T. Fu and J. M. Van Ruitenbeek, Physica C (Amsterdam), 166 (1990) 502.
615 P. H. Andresen, H., Fjellvåg, P. Karen and A. Kjekshus, Acta Chem. Scand., 45 (1991) 698.
616 B. Ullmann, K. Heinemann, H. U. Krebs, H. C. Freyhardt and E. Schwarzmann, Physica C (Amsterdam), 153–155 (1988) 872.
617 R. Kiemel, W. Schäfer, S. Kemmler-Sack, G. Kruschel and B. Elschner, J. Less. Common Met., 143 (1988) L11.
618 M. Qian, E. A. Stern, Y. Ma, R. Ingalls, M. Sarikaya, B. Thiel, R. Kurosky, C. Han, L. Hutter and I. Aksay, Phys. Rev. B: Condens. Matter, 39 (1989) 9192.
619 Y. Maeno, T. Nojima, Y. Aoki, M. Kato, K. Hoshino, A. Minami and T. Fujita, Jpn. J. Appl. Phys., Part 2, 26 (1987) L774.
620 J. M. Tarascon, L. H. Greene, P. Barrboux, W. R. McKinnon, G. W. Hull, T. P. Orlando, K. A. Delin, S. Foner and E. J. McNiff, Jr., Phys. Rev. B: Condens. Matter, 36 (1987) 8393.
621 T. Takabatake and M. Ishikawa, Solid State Commun., 66 (1988) 413.
622 G. Xiao, M. Z. Cieplak, A. Gavrin, F. H. Streitz, A. Bakhshai and C. L. Chien, Phys. Rev. Letters, 60 (1988) 1446.
623 P. B. Kirby, M. R. Harrison, W. G. Freeman, I. Samuel and M. J. Haines, Phys. Rev. B: Condens. Matter, 36 (1987) 8315.
624 T. Siegrist, L. F. Schneemeyer, J. V. Waszczak, N. P. Singh, R. L. Opila, B. Batlogg, L. W. Rupp and D. W. Murphy, Phys. Rev. B: Condens. Matter, 36 (1987) 8365.
625 Y. Xu, R. L. Sabatini, A. R. Moodenbaugh and M. Suenaga, Phys. Rev. B: Condens. Matter, 38 (1988) 7084.

626 A. F. Hepp, J. R. Gaier, J. J. Pouch and P. D. Hambourger, J. Solid State Chem., 74 (1988) 433.
627 M. Z. Cieplak, G. Xiao, C. L. Chien, A. Bakshai, D. Artymovicz, W. Bryden, J. K. Stalick and J. J. Rhyne, Phys. Rev. B: Condens. Matter, 42 (1990) 6200.
628 H. Renevier, J. L. Hodeau, T. Fournier, P. Bordet and M. Marezio, Physica C (Amsterdam), 172 (1990) 183.
629 G. Ferey, A. Le Bail, Y. Lalignant, M. Hervieu, B. Raveau, A. Sulpice and R. Tournier, J. Solid. State Chem., 73 (1988) 610.
630 M. Hiratani, Y. Ito, K. Miyauchi and T. Kudo, Jpn. J. Appl. Phys., Part 2, 26 (1987) L1997.
631 P. Bordet, J. L. Hodeau, P. Strobel, M. Marezio and A. Santoro, Solid State Commun., 66 (1988) 435.
632 T. Kajitani, K. Kusaba, M. Kikuchi, Y. Syono and M. Hirabyashi, Jpn. J. Appl. Phys., Part 2, 27 (1988) L354.
633 P. F. Miceli, J. M. Tarascon, L. H. Greene, P. Barboux, F. J. Rotella and J. D. Jorgensen, Phys. Rev. B: Condens. Matter, 37 (1988) 5932.
634 H. Renevier, J. L. Hodeau, P. Bordet, J. J. Capponi, M. Marezio, F. Baudelet, H. Tolentino, G. Tourillon, E. Dartige, A. Fontaine, J. C. Martinez and J. J. Prejean, Physica C (Amsterdam), 162–164 (1989) 51.
635 Z. Hiroi, M. Takano, Y. Takeda, R. Kanno and Y. Bando, Jpn. J. Appl. Phys., Part 2, 27 (1988) L580.
636 S. Katsuyama, Y. Ueda and K. Kosuge, Matter. Res. Bull., 24 (1989) 603.
637 S. Katsuyama, Y. Ueda and K. Kosuge, Physica C (Amsterdam), 165 (1990) 404.
638 I. Felner, I. Nowik, B. Brosh, D. Hechel and E. R. Bauminger, Phys. Rev. B: Condens. Matter, 43 (1991) 8737.
639 Q. Huang, P. Karen, V. L. Karen, A. Kjekshus, J. W. Lynn, A. D. Mighell, N. Rosov and A. Santoro, Phys. Rev. B: Condens. Matter, 45 (1992) 9611.
640 P. Karen, P. H. Andresen and A. Kjekshus, J. Solid State Chem., 101 (1992) 48.
641 P. Karen and A. Kjekshus, J. Solid State Chem., 112 (1994) 73.
642 P. Karen, Q. Huang, V. L. Karen, A. D. Mighell, J. W. Lynn, N. Rosov, I. Natali Sora, A. Santoro and A. Kjekshus, (in preparation).
643 V. Karen, A. Kjekshus, Q. Huang, J. Lynn, P. Karen, A. Mighell and A. Santoro, Proc., Amer. Crystallogr. Assoc., Annual Meeting, Montreal, Canada, July 23-28, 1995, W179.
644 Y. K. Atanassova, V. G. Hadjiev, P. Karen and A. Kjekshus, Phys. Rev. B: Condens. Matter, 50 (1994) 586.
645 I. Natali Sora, Q. Huang, J. W. Lynn, N. Rosov, P. Karen, A. Kjekshus, V. L. Karen, A. D. Mighell and A. Santoro, Phys. Rev. B: Condens. Matter, 49 (1994) 3465.
646 P. Karen, Solid State Ionics, (in preparation).
647 Q. Huang, P. Karen, V. L. Karen, A. Kjekshus, J. W. Lynn, A. D. Mighell, N. Rosov and A. Santoro, (in preparation).
648 P. Karen, A. Kjekshus, Q. Huang, J. W. Lynn, N. Rosov, I. Natali Sora, V. L. Karen, A. D. Mighell and A. Santoro, Phys. Rev. B: Condens. Matter, (submitted).
649 Q. Huang, P. Karen, V. L. Karen, A. Kjekshus, J. W. Lynn, A. D., Mighell, N. Rosov and A. Santoro, (in preparation).
650 S. Geremia, G. Nardin, R. Mosca, L. Randaccio and E. Zangrando, Solid State Commun., 72 (1989) 333.
651 C. Greaves and P. R. Slater, Physica C (Amsterdam), 161 (1989) 245.
652 M.-J. Rey, P. Dehaudt, J. Joubert and A. W. Hewat, Physica C (Amsterdam), 167 (1990) 162.
653 U. Yaron, D. Kowal, J. Felner and M. Einav, Physica C (Amsterdam), 168 (1990) 546.
654 T. Manako, Y. Shimakawa, Y. Kubo, T. Satoh and H. Igarashi, Physica C (Amsterdam), 156 (1988) 315.
655 R. L. Harlow, G. H. Kwei, R. Suryanarayanan and M. A. Subramanian, Physica C (Amsterdam), 257 (1996) 125.
656 M. Stavola, D. M. Krol, L. F. Schneemeyer, S. A. Sunshine, J. V. Waszczak and S. G. Kosinski, Phys. Rev. B: Condens. Matter, 39 (1989) 287.
657 S. A. Sunshine, L. F. Schneemeyer, T. Siegrist, D. C. Douglass, J. V. Waszczak, R. J. Cava, E. M. György and D. W. Murphy, Chem. Mater., 1 (1989) 331.
658 Q. Huang, S. A. Sunshine, R. J. Cava and A. Santoro, J. Solid State Chem., 102 (1993) 534.
659 J. T. Vaughey, J. P. Thiel, E. F. Hasty, D. A. Groenke, B. Dąbrowski, D. G. Hinks and A. W. Mitchell, Chem. Mater., 3 (1991) 935.
660 J. P. Zhang, D. A. Groenke, B. Dąbrowski, K. R. Poeppelmeier and L. D. Marks, Physica C (Amsterdam), 227 (1994) 259.
661 Q. Huang, R. J. Cava, A. Santoro, J. J. Krajewski and W. F. Peck, Physica C (Amsterdam), 193 (1992) 196.
662 T. Krekels, O. Milat, G. Van Tendeloo, S. Amelinckx, T. G. N. Babu, A. J. Wright and C. Greaves, J. Solid State Chem., 105 (1993) 313.